University of Nevada, Reno

A Forecast Procedure for Dry Thunderstorms

A thesis submitted in partial fulfillment of the
requirements for the degree of Master of Science in
Atmospheric Science

by

Nicholas J. Nauslar

Dr. Timothy J. Brown/Thesis Advisor

December, 2010

THE GRADUATE SCHOOL

University of Nevada, Reno
Statewide · Worldwide

We recommend that the thesis
prepared under our supervision by

NICHOLAS J. NAUSLAR

entitled

A Forecast Procedure For Dry Thunderstorms

be accepted in partial fulfillment of the
requirements for the degree of

MASTER OF SCIENCE

Timothy J. Brown, Ph. D., Advisor

Michael L. Kaplan, Ph. D., Committee Member

Narasimhan K Larkin, Ph. D., Committee Member

Frederick C. Harris, Jr., Ph. D., Graduate School Representative

Marsha H. Read, Ph. D., Associate Dean, Graduate School

December, 2010

ABSTRACT

Dry thunderstorm (traditionally less than 2.5 mm or 0.1" of rainfall) forecasting has long been a forecast problem for the western United States. Dry thunderstorms are responsible for starting thousands of wildland fires every year. In the largest lightning outbreaks (or busts in the wildland fire-meteorological community), hundreds of fires may be started in a 24- to 36-hour period. These extreme events put a huge strain on fire suppression efforts. Many of these fires may go unstaffed due to the lack of available fire personnel simply because of the large number of fire starts. Forecasting these events in advance, even just 24-48 hours, could help fire agencies plan resources in preparation of a large outbreak. Fires are much more likely to be controlled during the early stages, and therefore cost much less to suppress.

Due to the seemingly innocuous conditions preceding dry thunderstorm development across the western United States (west of the Rocky Mountains), forecasting dry thunderstorm events can prove challenging and inconsistent. To improve dry thunderstorm forecasting, the National Weather Service (NWS) Reno Weather Forecast Office (WFO) developed WA04 (Wallmann 2004, 2010), a conceptual model of dry thunderstorms that includes the pressure of the dynamic tropopause, jet streak dynamics, equivalent potential temperature, and upper level lapse rates in conjunction with the High Level Total Totals. This thesis supplements WA04 by adding moist isentropic analysis and enhancing the jet streak analysis to help a Dry Thunderstorm Procedure (DTP). Moist isentropic analysis resolves

moisture and instability better than analyzing constant pressure maps, thus making it ideal to find the pockets of instability and plumes of moisture that spawn dry thunderstorms. The enhanced jet streak analysis in DTP more completely resolves upward motion and divergence aloft that might not be distinguished using constant pressure maps or traditional quasi-geostrophic theory.

The goal of this research is to build upon previous work by examining six case studies using WA04 while enhancing the procedure by adding moist isentropic analysis and augmenting the jet streak analysis. By examining the procedure and investigating the case studies, an operational checklist is developed to accurately depict the potential for dry thunderstorms across the western United Sates. This procedure and checklist is designed to be applied operationally in NWS WFO's and Geographical Area Coordination Center's (GACC) Predictive Services offices throughout the western United States to ascertain daily potential for dry thunderstorms.

DTP was applied to six dry lightning events within the past five years across all regions of the western United States. Dates of the investigated events included 25-27 June 2006, 20-21 August 2006, 16-18 July 2007, 20-21 June 2008, 1 August 2009, and 20-21 August 2009. These events show the diversity of dry thunderstorms in terms of development, location, and timing. The procedure proved useful in determining the potential for dry thunderstorm development 36-48 hours before initiation of the event. This thesis summarizes these case studies, describes

the dry lightning forecast procedure, and depicts a goldilocks environment of moisture and instability conducive for dry thunderstorms.

ACKNOWLEDGEMENTS

thunderstorm procedure, and we have worked closely over the last two years to not only investigate but also improve upon the procedure. A big thanks to Laura Edwards who has provided lots of advice and input throughout my graduate degree. It was always helpful and thoughtful, and I appreciate it greatly. Hauss Reinbold and Kevin Goebbert probably deserve a portion of my M.S. due to all their help with my seemingly infinite computer programming issues. Their selflessness and patience were a godsend.

DRI and especially the Atmospheric Sciences Division provided a great environment and support. All of the professors and staff were excellent and I learned a lot. A very special thanks goes to all the graduate students at DRI, but especially the atmospheric science graduate students. Ben Hatchett, KC King, Andy Joros, Cassie Hansen, and Bo Tan just to name a few helped me in many ways to complete not only my course work but my research too. The studying, critiquing, and the fun we had made this experience that much better.

All the people in Colorado I worked with over the last two summers provided me great experience learning about fire fighting and management. The Upper Colorado River Management Unit and Rocky Mountain Predictive Services were unbelievable to me by providing avenues to forecast operationally, dispatch, and fight fires while learning how the whole system works. Everyone there but especially Don Scronek made Grand Junction and pretty much all of western Colorado a home away from home.

Finally, I would love to thank my family and friends. My friends here in Reno whether on the basketball court, ski runs, or attending our weekly Wednesday meeting, provided me an outlet, support, and great times since I moved to Reno. You've help made Reno my home. My family, especially my Mom, Dad, Cola, Tony, Sophie, Olivia, and Wyatt have provided me with unconditional love support my whole life. Without them, I wouldn't be where or who I am today. I love you guys.

TABLE OF CONENTS

LIST OF FIGURES

LIST OF APPENDIX FIGURES

1. Introduction

Dry lightning (receiving less than 0.1 in. of rainfall or CG strikes outside main rain core) events or busts create numerous fire starts in the western United States, which stress local and regional initial attack resources. A lightning bust refers to a storm system producing thousands of lightning strikes over an area or region. Most of the significant dry lightning events occur in the western United States between June and September (Figure 1). From 2001-2008 lightning ignited a yearly average of 11,912 fires totaling nearly 4.5 million acres burned (See Appendix A1 & A2). This accounts for approximately 65 percent of total acres burned per year (data.gov, 2010). Fighting wildfires costs an average of $1 billion in addition to the millions of dollars of property loss (National Interagency Coordination Center (NICC)). The cost monetarily can pale in comparison to the fatalities and injuries incurred by firefighters and the public each year.

Better forecasting of dry lightning events could lead to more efficient and productive fire management and resource allocation. If fire managers and government officials had 24 to 48 hours of lead-time, more efficient steps could be taken to prepare for multiple fire starts, and thus reduce the cost and risk by having adequate resources nearby to keep fires from becoming problematic. If dry fuels and extreme fire weather, such as low relative humidity (RH) and high winds exist, then fires could still grow large and become tough to contain. However, even with extreme fire conditions due to dry fuels and hot, dry, and windy weather, proper

preparation could mitigate some of the costs of fighting fires in terms of money and safety.

Figure 1: Map of western United States: Pacific Coast to Rocky Mountains. (http://stevekluge.com/geoscience/images/physiography.jpg)

Many of these lightning busts occur with a trough approaching the western United States that phases with monsoonal moisture entrained from the south. Monsoonal moisture can be defined as an influx of moisture advected northward, westward and/or eastward originating from the Gulfs of California and/or Mexico during the North American warm season. These busts generate problems not only for fire managers, but to forecasters as well. It can be difficult to diagnose the location of high-based convection or to delineate dry and wet storms. Due to surface or lower tropospheric thunderstorm indices (Totals Totals (TT), Convective Available Potential Energy (CAPE), K Index, Lifted Index (LI), etc.) not revealing the

true potential of most of these busts, many events go under forecasted or even unforecasted. To better ascertain dry lightning potential, a collaborative effort developed a procedure incorporating some non-traditional thunderstorm parameters and analyses (Nauslar *et al.* 2009).

1.1 Description of Procedure

The dry thunderstorm procedure (DTP) includes moist isentropic analysis, upper tropospheric lapse rates (ULLR), high-level total totals (HLTT) (Milne 2004), jet streak dynamics, and dynamic tropopause (DT) analysis. Moist isentropic analysis entails the inspection of vertical cross-sections with equivalent potential temperature θ_E and mixing ratio or relative humidity plotted to determine instability and moisture plumes. Contoured upper level lapse rate values indicate the dry thunderstorm formation threshold of 7.5°C km^{-1} (Wallmann 2004). HLTT values of $\geq$ 28°C represent an environment conducive for high-based convection (Milne 2004). These thresholds are based on empirical evidence and can be explained physically. The influence and location of an upper level jet determine divergence aloft, which aides the vertical development of the storms. Finally, the analysis of the dynamic tropopause location and more importantly the transition or gradient of it in conjunction with the other parameters determines the potential for dry thunderstorm formation (Nauslar *et al.* 2009).

1.2 Literature Review

Other papers have aimed to predict dry thunderstorms by determining the importance of mid-level instability and low-level dewpoint depressions (Rorig and Ferguson 1999, 2002; Rorig *et al.* 2006). Rorig *et al.* 2006 aimed to predict dry thunderstorms via an algorithm when convection was expected by implementing thresholds based on moisture and instability components. Rorig and Ferguson 1999 and Crimmins 2005 show a short climatology of synoptic patterns for critical fire conditions in Pacific Northwest and the Southwest United States.

Rorig and Ferguson (1999) used 30 years (1948-77) of thunderstorm occurrence and precipitation observations along with lightning data from 1986-96. They classified convective days as dry or wet by using dewpoint depression at 850 hPa and the temperature difference between 850 and 500 hPa. Rorig and Ferguson (1999; 2000) noted past research concerning lightning and fire starts. Fuquay *et al.* (1979) developed the lightning activity level (LAL) index, which aims to estimate the number of lightning-caused fire ignitions. This index uses cloud-to-ground (CG) lightning strikes, radar echoes showing coverage of precipitation, intensity of rainfall, and storm size and duration over a given area to diagnose which parameter best determines the LAL for the day. Fuquay (1980; 1982), Meisner *et al.* (1993), and Reap (1986) all investigated the relationship between CG lightning, fire starts, precipitation, and radar echoes. Lack of correlation and data hampered efforts to conclusively predict fire ignitions due to thunderstorms in the western United States. Rorig and Ferguson (1999) noted that dry thunderstorms develop with a

high base of moisture and are decidedly unstable. They aimed to distinguish between not only wet and dry storms, but also a larger picture of wet and dry synoptic patterns in the Pacific Northwest. The study yielded two important conclusions: 1) days with a highly unstable and dry lower atmosphere (also conducive for dry, gusty conditions receptive to fire ignition and spread) and 2) a synoptic pattern with the core of the trough off the Pacific coast (in conjunction with 850-500 hPa temperature difference of approximately ≥ 30°C and 850 hPa dewpoint depression of ≥13-14°C yielded dry lightning.

Rorig and Ferguson (2002) took their findings and applied them to the 2000 fire season noting that lightning starts 60% of the fires on public lands in Washington, Idaho, Oregon, Wyoming, Nevada, Montana, California, and Utah, and ignitions rely on multiple factors including lightning, fuel moisture, RH, and fire suppression efforts. They found a noticeable disparity in the 850-500 hPa temperature difference, and the 850 hPa dewpoint depression occurred between fire and non-fire days when lightning occurred. Five to seven degrees Celsius of 850-500 hPa temperature difference and two to four degrees Celsius of 850 hPa dewpoint depression separated fire from non-fire days. Larger values for both parameters led to a greater probability of not only dry lightning, but fire starts as well.

Rorig *et al.* (2007) used their previous results in developing an algorithm to predict dry lightning. Applying the 850-500 hPa temperature difference and the 850 hPa dewpoint depression from previous papers, they studied over a dozen

different upper air stations across the western United States. Implementing the two past parameters along with the 700-500 hPa temperature difference, the research showed statistically relevant forecasts for lightning caused fires using the 5th generation mesoscale model (MM5). Additionally, they computed the algorithm using sigma levels of 0.9 and 0.48 to help account for terrain. An analysis of the results showed 40% of fires occurred when the probability of dry lightning was 90% or higher, and 58% of fires observed occurred when the probability exceeded 75%. A product was developed from the research and can be found at AirFire (AirFire, 2010).

Reap (1986) examined CG lightning in the western United States. He took radar data obtained from the operational video integrator and processor (VIP), which parses the radar echo dBZ values into six levels (VIP1-VIP6). 87% of all CG lightning struck at echo values below VIP3 (below 41 dBZ), which constitutes the standard for delineating thunderstorms in the eastern United States. However, an increase of 40-50% of lightning strike frequency transpired with VIP4 or greater values. In addition, cloud-top temperatures below -35°C showed a steep increase in lightning frequency noting a 70% frequency at -63°C. Anecdotal evidence suggests higher elevations receive more frequent lightning strikes than lower elevations, and the timing of the maxima occurs in the afternoon hours for higher elevation strikes compared to the evening and overnight hours for lower elevations.

Thunderstorm electrification fuels the lightning strikes produced from these storms. The main charging zone (location of the negative charge) in the cloud

resides between the -10°C and -20°C temperature levels. The positive charge inhabits a larger region above the negative charge area (Wallace and Hobbs 2006). The beginning of the electrification commences after a large amount of graupel or hailstones occurs. The ice (rimer) falls through the cloud and becomes negatively charged due to collisions of smaller particles. This helps form the negative charge zone. Updrafts then carry the positive charges upward after the rebound from the rimer finalizing the electrification of the cloud. Lightning then occurs when the electric field intensity surpasses the threshold the atmosphere can maintain (Wallace and Hobbs 2006).

When this happens, the stepped leader moves incrementally 50m downward every 1 μs. Research has shown that the stepped leader originates as a discharge between a small pocket of positive charge at the bottom the cloud and the main charging zone. As the stepped leader moves downward it induces positive charges on the ground, and when it is 10-100m from the ground, a discharge moves up from the ground to meet it (Wallace and Hobbs 2006). After contact is made, a large amount of electrons flow to the ground and a visible lightning stroke propagates upward in a continuous manner from the ground to the cloud along the stepped leader's path. The lightning strike carries an average of 30,000 amps and removes 20 coulombs or more of charge in a cloud. The thunderstorm must replenish the charge before another strike can occur, which can happen in as little as 10 s (Wallace and Hobbs 2006).

Fuquay (1980; 1982) looked at the relationship between flash polarity and lightning ignition. Correlations between positive and negative strikes and ignition suggested no substantial relationship. Positive strikes register five to ten times more current and voltage while making up less than 10% of all lightning strikes, but he found no data that suggested positive strikes are more efficient in starting fires. Baughman and Fuquay (1970) investigated hail and lightning occurrence in mountain thunderstorms of western Montana. Only about 15-20% of summer thunderstorms in this region yielded hail, and Montana summer thunderstorms compare modestly in size and intensity to thunderstorms of the eastern United States. Results showed that storms with hailstorms produced more lightning than those without. Additionally, thunderstorms spawned more lightning strikes as the hail size increased.

Bright *et al.* (2004) extend the work of Baughman and Fuquay and note the work of Houze (1993), MacGorman and Rust (1998), which state ice particles must be present in the mixed phase region (-10 to -40°C) of a convective cloud for storm electrification. The updraft must be strong enough to replenish supercooled liquid water and elevate graupel above the charge reversal temperature zone (-15 to -20°C). A certain level of instability must be attained within this region to accomplish the feat. CAPE provides a quantitative measure of instability, but the amount of CAPE needed to ensure the upward movement remains speculative. To ensure the proper lifting and mixing for storm electrification, 100 to 200 Jkg^{-1} of CAPE should

be sufficient along with an updraft speed of 6-7 ms^{-1}. Bright *et al.* (2004) developed

the Cloud Physics Thunder Parameter (CPTP):

$$CPTP = \frac{(-19°C - T_{EL})(CAPE_{-20} - K)}{K},$$

where T_{EL} is the equilibrium temperature, CAPE$_{-20}$ is the CAPE between 0°C and -

20°C, and K a constant set to 100 Jkg[-1]. The lifting condensation level (LCL) must be

below -10°C to guarantee supercooled water, and T_{EL} must be below -20°C to make

certain the cloud top will be above the charge reversal temperature zone. A

percentage of CPTP ≥ 1 within the Short Range Ensemble Forecast (SREF) then is

calculated and delineated on a map.

Bothwell (2005; 2009) developed statistical techniques to predict dry

lightning and thunderstorms. Using lightning climatology, Bothwell took over 200

candidate predictors within model data to predict lightning. Logistic regression

helped developed the Perfect Prog (Prognosis) Forecast (PPF) (Bothwell 2002)

equations for ≥1, ≥10, and ≥100 CG flashes. Eighteen regions and three seasons

were developed for use across the United States. These forecasts helped for the Dry

Thunderstorm Potential Index (DTPI), which is run every three hours as an

experimental product on the Storm Prediction Center (SPC) website.

Wallmann (2004; 2010) delineate a dry lightning forecast procedure (WA04;

WA10), which includes the use of the dynamic tropopause, jet streak dynamics, 850-

700 hPa layer equivalent potential temperature (θ_E), upper level lapse rates (500-

300 hPa), and HLTT. Using these parameters, moisture plumes and mid- to upper-

troposphere moisture plumes and instability can be located, which are vital to decipher whether or not high-based convection will occur. This procedure successfully predicted in retrospect the Nevada August 2001 and northern California 2008 dry lightning busts, which produced over 11,000 strikes and 600 fires combined. This procedure provided the basis for the dry thunderstorm procedure (DTP) produced in this thesis.

1.3 Hypothesis

It is hypothesized that not just one synoptic pattern can spur dry lightning busts given the diverse synoptic patterns for dry thunderstorm formation. Also, monsoonal moisture juxtaposed with instability departed away from the main core of a vigorous trough is a common theme for the varied synoptic patterns. This suffices as a thread that weaves together the DTP to successfully diagnose an outbreak of dry thunderstorms throughout the western United States.

To test this hypothesis in this study, six dry lightning events are investigated while using the DTP to determine if it can predict these events 24-48 hours out using operational Global Forecast System (GFS) and North American Model (NAM) data. Approximately ten events were chosen over the last ten years, but due to data limitations only six were chosen. The six events chosen are: 25-26 June 2006, 21-22 August 2006, 16-17 July 2007, 20-21 June 2008, 1 August 2009, and 20-21 August 2009. All of these events occur across different regions of the western United States including the Great Basin, northern California, Pacific Northwest, and northern

Rockies. In addition to the different regions in which these events occur, a diversity of timing and synoptic patterns also reveals the encompassing validity of the DTP. Each one of the dry lightning busts also ignited anywhere from dozens to hundreds of fires, and caused a major strain on local, regional, and national resources. Plots of each parameter within the procedure, lightning strike maps, three-hour precipitation and national situational (sit) reports will demonstrate the severity of each episode and the ability of the procedure. The DTP was developed and implemented not to supplant, but to build upon and work with current dry lightning work to better help prepare and estimate the impact on the fire community while aiding operational meteorologists with a difficult and unique forecasting challenge.

2. Data and Methods
2.1. Data

Several sources of data provided the foundation of the plots created to illustrate the DTP capacity for outlining the potential for dry lightning events. Dozens of GFS and NAM model runs were obtained from the NOAA Operational Model Archive and Distribution System (NOMADS). The National Climatic Data Center (NCDC), National Centers for Environmental Prediction (NCEP), and Geophysical Fluid Dynamics Laboratory (GFDL) in a collaborative effort developed NOMADS archiving operational model data over the last three to six years.

The research implemented GFS and NAM data due to their operational nature. The DTP is meant to use data readily available to forecasters to exhibit dry thunderstorm potential 24 to 48 hours in advance. The Rapid Update Cycle (RUC) model was not used since it only forecasts 12 hours out. The GFS works on a 40 km grid and provides forecasts every 6 hours out to 48 hours, and then every 12 hours to 180 hours (some parameters available to 384 hours). The NAM works on a 12 km grid and provides forecasts every 6 hours to 48, and then every 12 hours to 84 hours. The GFS and NAM each possess 00 UTC, 06 UTC, 12 UTC, and 18 UTC initialized runs, which were implemented up to 48 hours preceding each event. Figure 1 depicts the western U.S. region of interest for this study.

The General Meteorology Package (GEMPAK) and Advanced Weather Interactive Processing System (AWIPS) plotted the data after converting the NOMADS' gridded binary files (GRIB). Both systems can plot in a variety of ways and with many different variables. This allows flexibility in developing products to help

ascertain certain meteorological conditions. GEMPAK and AWIPS both allow making many different maps in a short amount of time, which lets researchers try an assortment of combinations of meteorological variables with both planar and vertical views as desired. The fluidity of the systems allowed creating the best plots for each event no matter the region or timing.

Constant pressure maps at 250, 500, 600, and 700 hPa with geopotential heights, winds, and relative humidities from the North American Regional Reanalysis (NARR) data were plotted to show some traditional analysis maps. NARR data, which is on a 32 km grid, blends observational and model simulated data from the NAM as a part of the reanalysis. This aided in illustrating the synoptic setup before and during each event. The maps also provide validation along with the zero forecast hour GFS and NAM runs to the plots examined 24 to 48 hours before. In addition to the NARR constant pressure maps, three-hour precipitation maps throughout each event were created from NARR data to exhibit the storms' rainfall. This verified dry thunderstorms and when an event developed into wetting thunderstorms. Atmospheric soundings obtained from the University of Wyoming provided more support for the synoptic and mesoscale setup for each event. The soundings detail the lifespan of the event in the relative area of the event. Some of the soundings were positioned in the midst of the event, but in many instances the timing and the location were slightly outside the apex of the event.

The Program for Climate, Ecosystem, and Fire Applications (CEFA) provided lightning strike data from the National Lightning Detection Network (NLDN).

Twelve hour lightning data were plotted from 00 UTC to 12 UTC and 12 UTC to 00 UTC for each day during the event using NCAR Command Language (NCL). The plots visually show where the strikes occur, and provide the ability to count the number of strikes per time period. The reason for splitting the day up into two separate maps helps show a more detailed picture of lightning strikes that match with the timing and location of the DTP plots.

2.2. Methods: Dry Thunderstorm Procedure

Building on WA10, the DTP seeks to ascertain an understanding of a unique forecasting problem through multiple analyses. Each one of the analysis tools is used to identify instability and the potential for high-based thunderstorm development. Some traditional thunderstorm or instability indices have been modified to deal with the high-based nature of the investigated storms, while other forecasting methods are used in a different manner than is customary (i.e., HLTT, moist isentropic analysis). Each part of the procedure plays a role in determining not only the potential, but also the severity of each dry lightning event.

WA10 did not incorporate moist isentropic analysis, and this analysis constitutes the largest change to WA10 to form the DTP. Moist isentropic analysis has long been used to determine instability and moisture transport especially for winter weather. The vertical structure of instability and moisture represent the two biggest difficulties in forecasting dry lightning, and thus moist isentropic analysis became a logical addition to WA10 and an integral part of DTP. For moist isentropic

analysis, moist isentropes slope down towards warm air and up towards cold air due to the inverse pressure and temperature relationship. On a synoptic scale, without diabatic processes, moist isentropic surfaces offer greater continuity with the depiction of three-dimensional motions including three-dimensional transport of moisture. Horizontal movement along moist isentropic surfaces also includes an adiabatic vertical motion component often disregarded and not depicted on constant height or pressure surfaces (Moore 2002). Moist isentropic surfaces tend to be steeper as well across the same thermal gradient than constant height or pressure surfaces. In short, moist isentropic analysis can more readily diagnose instability and moisture, which helps in locating the potential dry thunderstorm areas.

GEMPAK plotted equivalent potential temperature $(\theta_E$, Kelvin (K)) with mixing ratio (g kg^{-1}) and θ_E with relative humidity (RH, %) to implement the moist isentropic analysis. These plots will show the potential instability $((d\theta_E/dz)<0)$ and moisture collocated to form the thunderstorms. No moisture benchmarks were set to deem whether enough or too much moisture existed for dry thunderstorms. An increase in RH or θ_E above lower values of each was desired, but not necessarily mandatory. The main utility of the moist isentropic plots demonstrated potential instability and moisture in the mid- to upper-levels, and usually the collocation of both. These plots proved very useful in illustrating the location and why thunderstorms developed in the case studies.

Jet streak dynamics help provide vertical motion forcing aloft in each of the case studies by virtue of their ageostrophic circulations. 250 hPa winds and heights were plotted with NARR data along with GEMPAK plots that contour velocity divergence in units of s^{-1} x 10^{-5} along side wind barbs in knots at 250 hPa. Research on two and four cell balanced jet streak ageostrophic circulation patterns has shown substantial upward vertical motion in the divergent regions of the jet streak. Transverse circulations set up in the entrance and exit regions of the straight jet streak, which aid in the analysis construction of divergent regions, and therefore the development of dry thunderstorms resulting from ascent and dynamical destabilization of a layer (Uccellini and Johnson 1979).

In a two-cell jet, the downstream cell or the exit region of the jet becomes divergent due to the curvature-induced ageostrophic wind (V_{AG}) response/circulation. The four-cell pattern of vertical motions accompanying jet streaks which has left and right entrance and left and right exit regions are divergent in the right forward and left rearward quadrants. Transverse ageostrophic circulations set up in the entrance and exit regions. In the entrance region, the V_{AG} component moves parcels to the left of the entrance region helping divergence form in the right entrance while inducing convergence in the left entrance region (Uccellini and Johnson 1979). A direct circulation sets up in the entrance region with sinking motion in the left entrance region and rising motion in the right entrance region. In the exit region, V_{AG} is directed towards the right exit region, creating divergence in the left exit region and convergence in the right exit

region. An indirect circulation sets up, where sinking motion occurs on right side of the exit region and rising motion on the left side of the exit region (Uccellini and Johnson 1979).

These divergent regions can change, especially when flow becomes unbalanced or breaks from traditional jet streak and quasi-geostrophic theory. Convection can cause this imbalance, and thus change the divergent regions within the jet structure and completely alter the transverse circulations. When this occurs mesoscale jetlets can form creating highly diffluent areas that can support explosive convection (Kaplan *et al.* 1998).

Dynamic tropopause analysis represents another method to supplant and improve upon traditional synoptic forecast tools. Constant pressure maps and vorticity maps do not always resolve short waves or subsynoptic fronts or their magnitude, especially in the summer (Wallmann 2010). Dynamic tropopause maps depict the pressure of the tropopause, which illustrate short waves and disturbances embedded in the flow that otherwise may go unnoticed. Hirschberg and Fristch 1991 demonstrated the importance of the tropopause undulations in the formation of extratropical cyclones. Dynamic tropopause maps also help depict warm season convection due to weaker short waves being more discernible through tropopause undulations. Its success with warm season convection is that it delineates upward motion in the mid to upper part of the atmosphere making it an appropriate choice for the DTP (Wallmann 2010).

For dry thunderstorms, a gradient of tropopause pressure, and not just areas with a lower tropopause, represent potential for development of high-based thunderstorms. Often the most conducive patterns of upward vertical motion will lie just ahead and along a stronger gradient of tropopause pressure. In many ways it acts as an upper-level front thus replicating the same upward motion locations as a front in the lower levels of the atmosphere. Plotting the pressure of the dynamic tropopause on the 1.5 potential vorticity (PV) unit surface using AWIPS demonstrates the characteristics of the atmosphere and helps diagnose areas of transition in velocity/divergence, and thus upward motion. WA10 implemented the use of the dynamic tropopause very well, and it proved vital in help discerning not only where upward motion occurred, but why upward motion occurred as well.

WA10 utilized upper level lapse rates (ULLR) to determine instability aloft. The ULLR examines the 500-300 hPa layer since many of the cloud bases throughout the western United States, especially in the Intermountain West, have cloud bases above 700 hPa and even above 600 hPa on a regular basis. Additionally, due to the higher elevations in the Intermountain West, 700 hPa can reside within the planetary boundary layer. Hot and dry conditions can create a well-mixed layer from the surface through 700 hPa, thus skewing the actual instability associated with thunderstorm potential. ULLR values of ≥ 7.5 °C km^{-1} can sustain dry thunderstorm development based on operational and observational evidence. This threshold value has physical validity since with adequate low- or mid-level moisture, lapse rate values of 8.0 °C km^{-1} are sufficient for thunderstorm

development (Wallmann 2010). The threshold also lies within the dry adiabatic lapse rate of 9.8 °C km^{-1} and the moist adiabatic lapse rate approximated at 6.5 °C km^{-1}. Other research has also pointed to increased lapse rates in the 3-6 km MSL layer in the mid- to upper-troposphere has helped increase moist isentropic slope and supported short wave development (Staley 1988; 1991). As a result, frontogenetical circulations result helping form the dθ_E/dz<0 layers, strengthening an upper level jet, and increasing the gradient of dynamic tropopause slope environment seen in most dry thunderstorm cases.

Milne (2004) developed the High Level Total Totals Index (HLTT) from the traditional Total Totals Index (TT). Both measure the potential for thunderstorm development and coverage. The HLTT can be computed by this equation:

$$700T + 700T_D + (500T * 2) = HLTT$$

Milne showed in depth analyses via case studies and statistics that a threshold of 28 °C can serve as the bottom threshold for thunderstorm development with more promising results above 30 °C. However, thunderstorms can still form with lower HLTT especially if the moisture and instability exist in layers above 700 hPa. Similar to using TT, HLTT should not be used as a stand-alone product to ascertain instability or thunderstorm potential. Moisture plumes and streams in conjunction with instability can often reside above the 700 hPa and 700-500 hPa layers. If this happens, HLTT can underestimate the convective potential, and conversely if abundant moisture resides at and below 700 hPa, it will overestimate the potential for dry thunderstorms. Wallmann (2004: 2010) does specify that HLTT can be an

integral tool, especially when used with ULLR to determine high probabilities of dry

thunderstorms.

3. Analysis and Results

Six cases over the past four years were chosen to demonstrate the legitimacy of the DTP in an effort to test the hypothesis. Each case met the criteria of dry lightning strikes that ignited dozens to hundreds of fires, which strained the fire community's resources. Additionally, some of the other cases were not forecasted, which helped provide the impetus for creating the DTP along with the fire management concerns. National situation reports, precipitation maps, and plotted lightning strikes provide evidence that dry lightning ignited not only many fires, but also problematic fire complexes. Many of the lightning tracks started numerous fires in a particular area, which can confuse fire reporting and complicate fire management due to the close proximity of multiple fires. One primary nocturnal and one primary afternoon event are chronicled along with four other dry lightning busts that occurred in at least one afternoon and overnight period.

3.1 Case Study: 20-21 August 2009
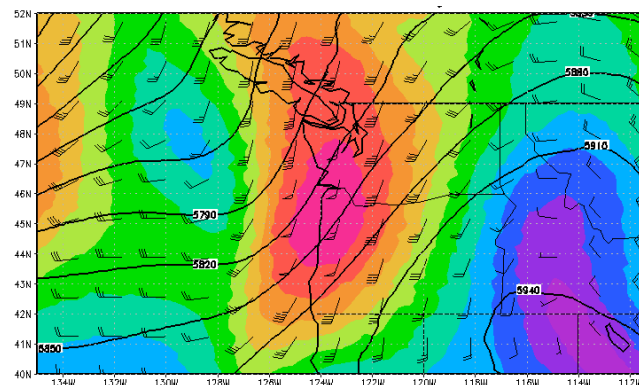
Figure 2: NARR 00 UTC 21 August 2009 500 hPa winds (barbs and filled, knots) and height (contoured, dm)

A vigorous trough approached the Pacific Northwest on August 20, 2009. The main core of the trough stayed off the coast, but a shortwave moved onshore around 00 UTC 21 August 2009 (Figure 2). This short wave helped trigger and aided the development of dry thunderstorms across eastern Washington overnight. The pattern replicated one of the dry synoptic patterns in Rorig and Ferguson (1999). However, as the event transpired, it morphed into one of the wet synoptic patterns. Over 2,000 lightning strikes resulted with the first storms beginning between 04 and 05 UTC (Figure 3)(See Appendix A3). The storms, initially dry, continued to build and form further east spilling over into the Idaho panhandle. The first few hours of storm development possessed dry thunderstorms, but gradually transitioned to wetting thunderstorms into eastern Washington and northern Idaho. The storms sparked multiple fires, which became problematic enough to dispatch two incident management teams to coordinate fire-fighting efforts in the area (Nauslar *et al.* 2009).
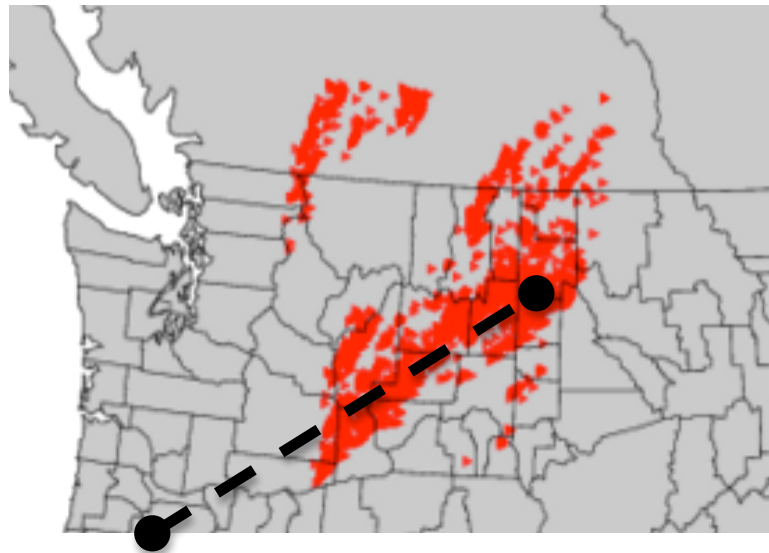
Figure 3: Lightning strikes from 00-12 UTC 21 August 2009. Dotted line represents cross-section Salem, OR (SLE) to Spokane, WA (OTX).
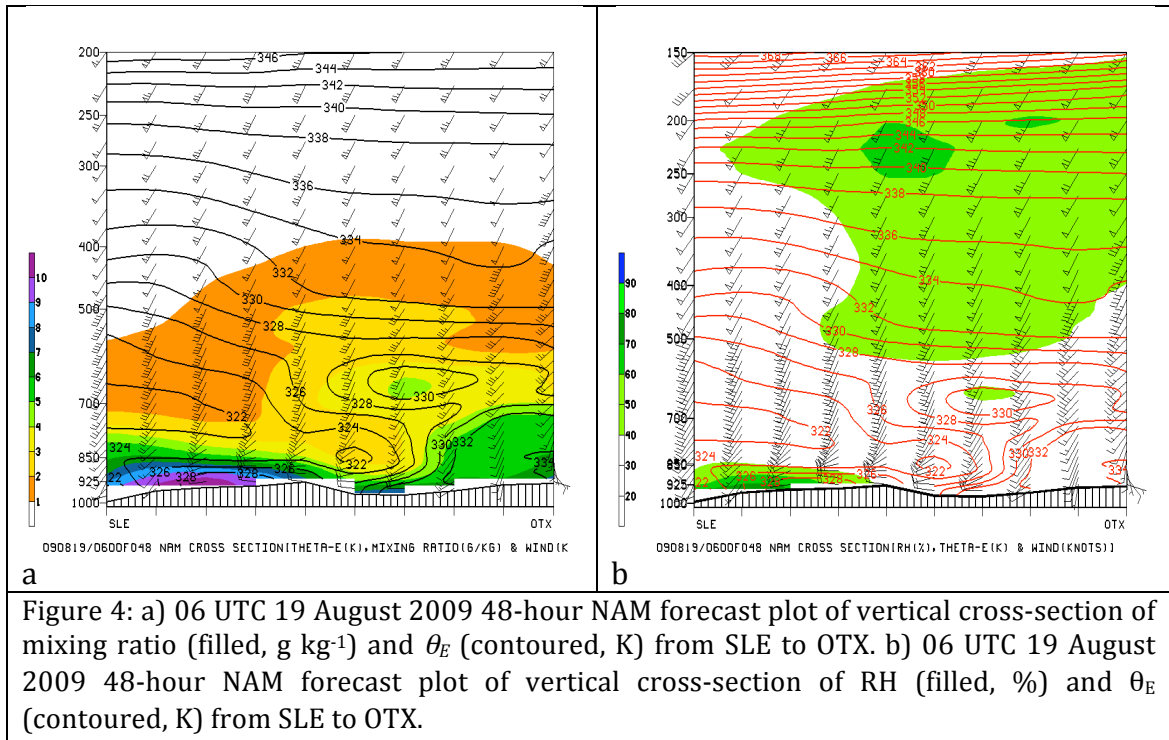
Figure 4: a) 06 UTC 19 August 2009 48-hour NAM forecast plot of vertical cross-section of mixing ratio (filled, g kg⁻¹) and θ_E (contoured, K) from SLE to OTX. b) 06 UTC 19 August 2009 48-hour NAM forecast plot of vertical cross-section of RH (filled, %) and θ_E (contoured, K) from SLE to OTX.

Examining several NAM and GFS model runs, both models depicted the potential for dry lightning 42 to 48 hours in advance. The time frame of the event encompassed 00 UTC to 12 UTC 21 August 2009. The model simulations initialized at these times 42 to 48 hours out illustrated the potential for high-based thunderstorms. The moist isentropic cross-section plots from Salem, OR (SLE) and Quillayute, WA (UIL) to Spokane, WA (OTX) show the moist isentropic structure desired for identifying potential instability (dθ_E/dz<0). Additionally, RH values below 40% exist underneath the layer of instability (Figure 4). Figure 4a demonstrates the elevated mixing ratio value co-located with the instability over central and eastern Washington. This collocation of instability and slight increase in moisture perfectly exemplifies the desired structure and signal for dry thunderstorms (Figures 4a-b). By 12 UTC August 21, the instability strengthens and

widens in breath, but the lower levels moisten, thus reducing the likelihood for dry thunderstorms.

The cause of these thermodynamical adjustments can be traced to a smaller jet streak associated with the short wave, which moves across Washington at 06 UTC 19 August (See Appendix A4, A5, & A6). Figures A4 and A5 exhibit the divergence aloft associated with the jet streak. The jet exhibits divergence consistent with both the two and four cell jet streak models, which promotes upward vertical motion over Washington and especially eastern Washington (See Appendix A4 & A5). As the smaller jet streak passes over eastern Washington, convection initiated. Convective support aloft in the form of increased potential instability and elevated moisture as noted in Figures 4a-b helped trigger and sustain thunderstorms for several hours overnight. The storm tracks followed the divergence aloft throughout the event. The NAM 250 hPa plot of divergence (See Appendix A5) does not allow one to locate the origin of the convection, but remains relatively close to the origin, while the GFS 250 hPa plot (See Appendix A4) delineates correctly where the high-based thunderstorms started over eastern Washington. The GFS dynamic tropopause did not correlate with thunderstorm development as well, but a gradient and noticeable depression in the tropopause did materialize across in central and northern Washington (See Appendix A7). The NAM dynamic tropopause forecasts show an excellent swath of lower tropopause pressure with an increased downstream gradient of tropopause pressure corresponding to the location of the dry lightning (See Appendix A8).

Figures A9 and A10 (See Appendix) show the NAM and GFS correctly located, and predicted the time the 7.5°C km^{-1} upper-level lapse rate threshold identified for the DTP. The 7.5°C km^{-1} contour starts right at the spot where convection commenced in east-central Washington. The elevated ULLR comes as no surprise when analyzing the cross-section plots in Figures 4a-b. The greatest amount of instability resides between 700-500 hPa, thus contributing to the ULLR benchmark. Reaching this benchmark also supports the instability noticed in the moist isentropic cross-section, dynamic tropopause, and 250 hPa plots since elevated lapse rates help tilt the isentropes creating baroclinic zones aloft, thus tightening the gradient of the dynamic tropopause pressure and increasing the variation of upward motion caused by divergence aloft (Staley 1988, 1991). The ULLR actually achieved the benchmark across the eastern half of the state during the afternoon hours and stayed elevated through 06 UTC 21 August 2009. Values of reduced static stability started to weaken when the base of the storms lowered throughout the event with the best lapse rates lying below the 700-500 hPa layer.

HLTT GFS and NAM plots generally outline the area of thunderstorm formation, although the GFS does a slightly better job (See Appendix A11 & A12). A gap exists between two pockets of elevated HLTT over far southeastern Washington and far northeastern Washington. Figure A11 has less of a gap between the two maxima, but it still exists. The gap resides over the area where the dry thunderstorms form and probably exists due to the moisture residing just above the 700 hPa level out of the HLTT dewpoint calculation. This would explain the slightly

lower values in the area. HLTT probably represents the weakest procedural tool as evidenced for this case, but it still roughly outlines elevated totals near the short wave outside the main core of the approaching trough.

This nocturnal event demonstrates that not all dry thunderstorm forcing happens with the aid of daytime heating. Elevated instability and moisture can just as easily trigger thunderstorm development. The DTP exhibited how all of the components come together in a small region where the dry lightning occurred. While each component of the forecast paradigm might not have been exceptional, the minimum thresholds were met and signals were seen in the same area 48 hours in advance, thus proving the validity of the DTP for 20-21 August 2009 case study.

3.2 Case Study: 1 August 2009

A strong trough approached the California coast on 1 August 2009. A ridge centered over the Sierra Nevada mountain range held moisture in place just east of the mountains throughout the western Great Basin and Arizona in the preceding days (Figures 5a-b). As the leading edge of the negatively tilted Pacific system edged onshore, it helped bring a more southerly and southeasterly flow in the lee side of the Sierra Nevada. This helped tap the building moisture pool aloft since mountains blocked the lower level winds of the approaching system, thus keeping the lower atmosphere drier (Figure 5c). The blocked lower flow and strong trough affecting the upper levels over western Nevada to southern Oregon help set up an environment conducive for dry lightning. This environment yielded over 6500

lightning strikes and approximately 200 fires on the lee side of the Sierra Nevada and southern Cascades (Figure 5d). As the event progressed into southern and central Oregon and as the atmosphere moistened, wetting thunderstorms developed lessening the initial fire numbers in Oregon (Nauslar *et al.* 2009). However, during the first several hours thousands of lightning strikes occurred with minimal precipitation leading to hundreds of fires including three complexes of fires in northern California.

Figure 5: a) NARR 18 UTC 31 July 2009 500 hPa winds (barbs and filled, knots) and height (contoured, dm). b) NARR 18 UTC 31 July 2009 600 hPa RH (filled). c) NARR 18 UTC 31 July 2009 700 hPa winds (barbs and filled, knots) and height (contoured, dm). d) Lightning strikes from 00-12 UTC 1 August 2009. Dotted Line: RNO-MFR cross-section.
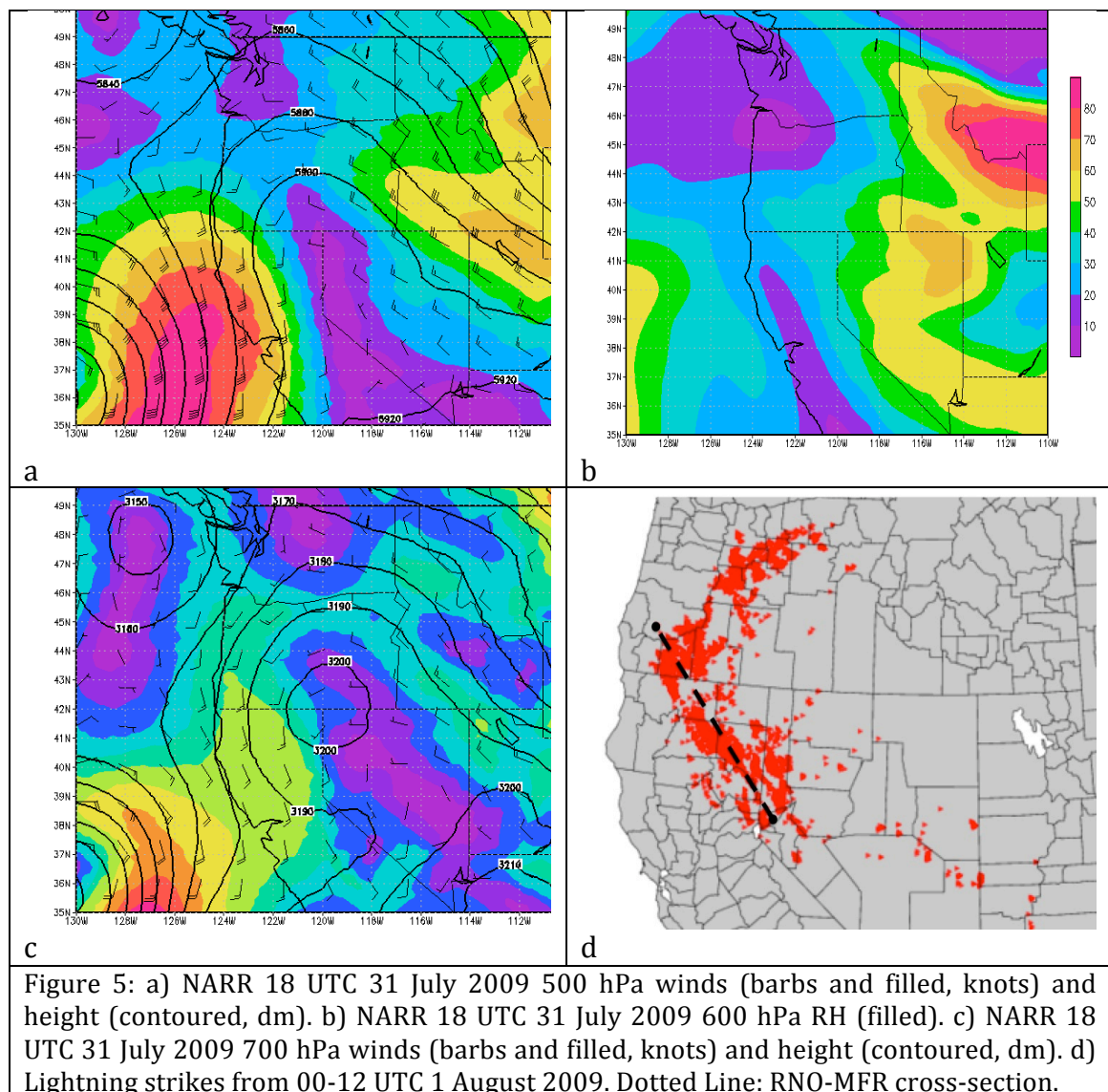
As the storms started to develop during the afternoon of 1 August 2009 in western Nevada, the upper level jet streak started to produce divergence aloft. Figures 6a and 6b depict 2-5 x 10^{-5} s^{-1} of divergence aloft along the lee side corridor of the Sierra Nevada and southern Cascades through western Nevada and northern California. While the main core of the jet had not reached this region, the influence of the approaching jet perturbed the wind field aloft inducing diffluence by turning the winds more southeasterly due to the negative tilt of the system. Figures 6a and 6b demonstrate the spreading of the wind barbs, which is a classic signal for diffluence over northern California in particular. This in turn induces upward vertical motion and perturbs the mass field as divergence forms. The consequences of the approaching jet preconditioned the atmosphere to become conducive for vertical motion resulting in adiabatic expansion, destabilization and possible thunderstorm development. Figures 6a and 6b illustrate the correct location and strength of the dry thunderstorm potential 48 hours ahead of the event as inferred from the velocity divergence. Both the NAM and GFS correctly forecasted the 250 hPa winds and divergence with the NAM better depicting the impressive divergence aloft.

The southeast to northwest cross-sections in Figures 6c-d, A13, and A14 (See Appendix A13 & A14) extending from Reno, NV (RNO) to Medford, OR (MFR) and SLE depict the moisture being transported up the lee side of the Sierra Nevada and Cascade Mountains above 700 hPa. The flow has a distinct velocity/directional discontinuity at 700 hPa, thus reinforcing the likelihood of the validity of the lower

atmospheric flow blocking theory due to the mountains. Figures 6c-d, A13, and A14 aptly demonstrate the potential instability throughout the cross-sections. Figures 19 and 20 illustrate a zone of potential instability in the 400-500 hPa layer in northwestern Nevada stretching to northern California. Figures 6c and 6d reveal two pockets of potential instability in the same areas, but now stretching into southern Oregon approaching MFR. The summer season monsoonal moisture along with the jet-induced instability via adiabatic expansion helped create explosive upright convection throughout the region. The moisture not only provides fuel for thunderstorm formation, but also helps destabilize the atmosphere by decreasing the threshold for lapse rates for convective initiation consistent with increasing convective available potential energy (CAPE). As the atmosphere becomes saturated, it follows the moist adiabat on the skew-t diagram, which if the environmental lapse rate exceeds the moist adiabatic lapse rate (MALR), volatile upright convection develops.

Figures 6c-d, A13, and A14 also show relatively drier lower levels with RH values below 30% throughout the region as the mixing ratio remains slightly elevated ranging from 4-7g kg^{-1}. Figure A15 (See Appendix) shows accumulated precipitation, but western Nevada and northern California saw little to no precipitation. The majority of the precipitation fell in southern and central Oregon as the event progressed. The elevated RH and mixing ratio values located closer to Salem (SLE) and Medford (MFR) indicate why more precipitation would reach the ground than in northern California and western Nevada.
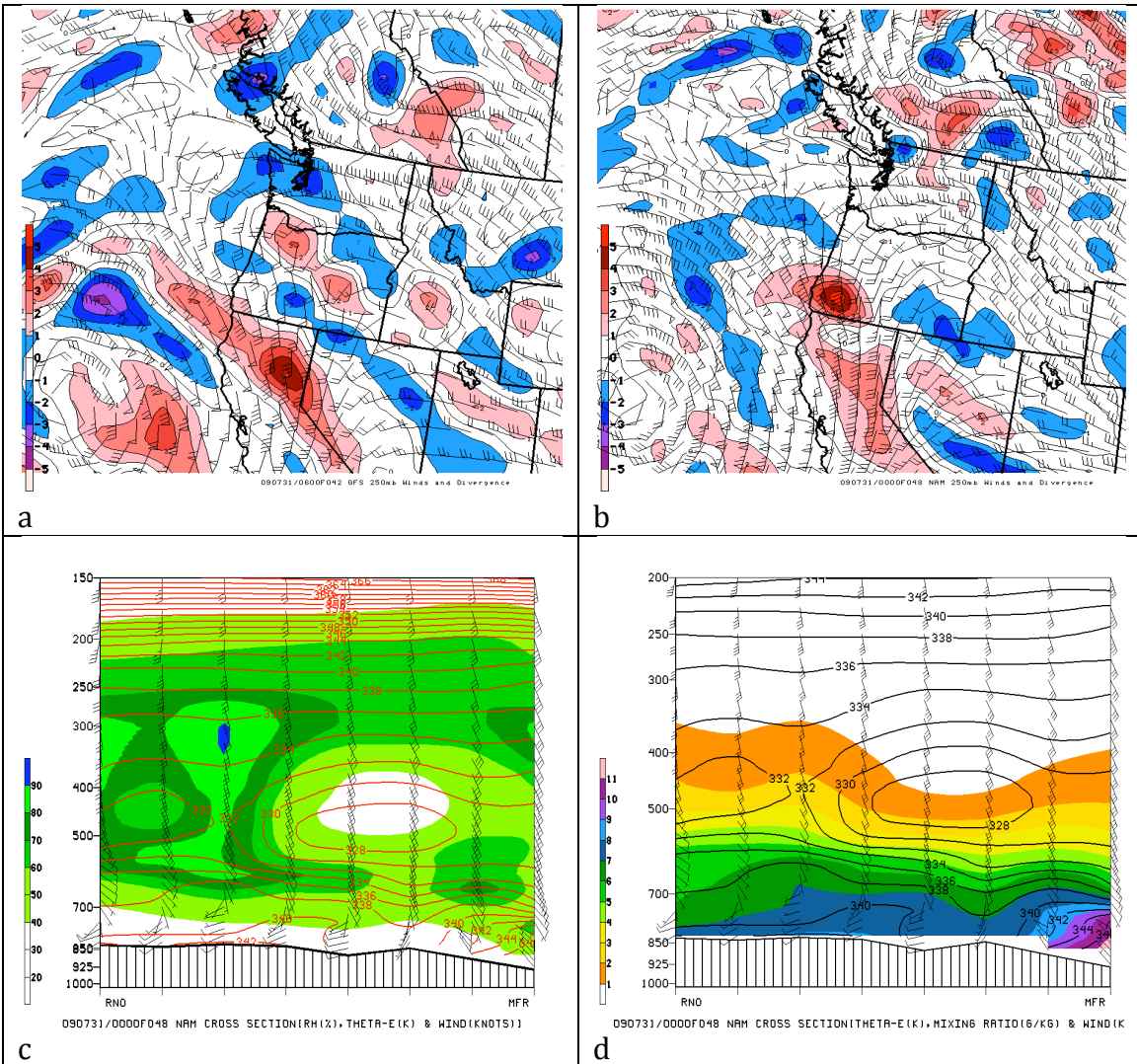
Figure 6: a) 06 UTC 31 July 2009 48-hour forecast plot of GFS 250 hPa Winds (knots) and Divergence (s^{-1} x 10^{-5}). b) 00 UTC 31 July 2009 48-hour forecast plot of NAM 250 hPa Winds (knots) and Divergence (s^{-1} x 10^{-5}). c) 00 UTC 31 July 2009 48-hour NAM forecast plot of vertical cross-section of RH (filled, %) and θ_E (contoured, K) from RNO to MFR. d) 00 UTC 31 July 2009 48-hour NAM forecast plot of vertical cross-section of mixing ratio (filled, g kg^{-1}) and θ_E (contoured, K) from RNO to MFR.

The GFS ULLR meets and exceeds the 7.5°C km^{-1} target set for the DTP. With the impressive divergence aloft this comes as no surprise as instability should increase where ascent is generated. The swath of 7.75-8.0°C km^{-1} ULLR falls directly in line with the coverage of the storms, and overlays with the other parameters very

favorably across the northern Nevada, California, and southern Oregon (See Appendix A16 & A17). Examining the earlier cross-sections, the greatest pockets of instability occur within the 500-300 hPa layer, which would help explain the higher ULLR in Figures A16 and A17 over central Oregon and northeastern California. Figure A17 shows the ULLR meeting the benchmark, but the NAM did not come to this solution until the 36-hour forecast. All of the other ingredients present themselves at the 48-hour forecast. The lag for the NAM ULLR continues to be puzzling considering the NAM cross-sections show substantial instability in the 500-300 hPa layer. However, even with this delay, the NAM simulation still shows the correct location of the instability for the proper timing of the event. Noting the other ingredients strength and collocation should compensate for one model's conservative estimate of one component, therefore demonstrating the strength of the DTP.

The impressive lapse rates, unstable isentropic plots, and the divergence aloft all point to a solid gradient of tropopause pressure approaching the area of interest (See Appendix A18 & A19). Figures A18 and A19 show the approaching system moving towards the Pacific coast on 00 UTC 31 July, although the tropopause pressure gradient does not meet the magnitude anticipated when based on the previously analyzed products. However, the edge of the tropopause pressure gradient impinges on the area of observed convection, which complies with the greatest support for vertical motion lying just ahead of the tropopause pressure gradient. Both the GFS and NAM show the diffluence in the winds along the leeside

corridor of the Sierra Nevada and Cascade mountain ranges and the gradient, although the NAM has a small cutoff feature/perturbation in tropopause pressure just ahead of the system in northwest Nevada, while the GFS pressure contours merely expand over the same area. This could be due to the higher resolution of the NAM, but both still describe a similar picture of tropopause dynamics 48 hours in advance.
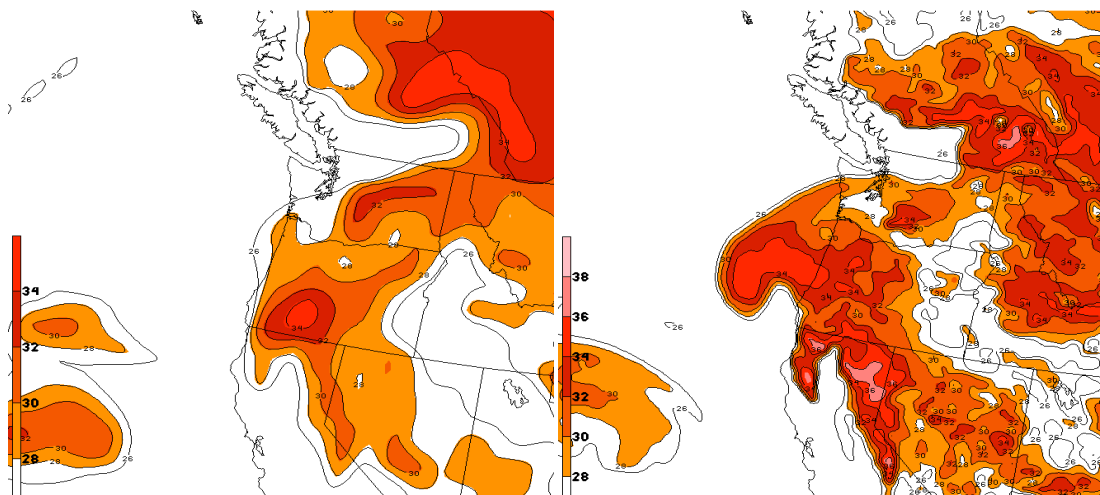
Figure 7: 00 UTC 31 July 2009 48-hour GFS forecast of HLTT (contoured & filled, °C).

Figure 8: 00 UTC 31 July 2009 48-hour NAM forecast of HLTT (contoured & filled, °C).

Figures 7 and 8 accurately portray the location and potential for high-based convection based on static stability considerations. Values larger than 30°C line the corridor of interest in the GFS forecast, and the NAM shows values over 36°C in northeastern California. The presence of the moisture at 700 hPa, especially in the NAM along with the instability residing within the upper part of the 700-500 hPa layer, act to elevate the HLTT. The corridor east of the Cascade mountain range possesses the highest values of HLTT as the instability spills over and the moisture

flows along the Sierra Nevada and southern Cascades. Milne's (2004) table for HLTT explains that values exceeding 31°C exhibits an atmosphere conducive to develop scattered to numerous thunderstorms, which correctly describes the environment on 1 August 2009.

The observed convection accompanying this case study started early in the afternoon on 1 August 2009 and continued into the night as the event moved further northwest into central Oregon. However, thunderstorms (especially dry thunderstorms) diminished overnight with most of the dry lightning occurring in the afternoon and evening hours through western Nevada and northern California. All of the DTP components collocated and sufficed in strength to predict a dry lightning bust for this afternoon and evening event. The earlier cross-sections portrayed the moistening of the lower levels when moving into Oregon demonstrating at least qualitatively the DTP's ability to distinguish between dry and wet thunderstorm formation.

3.3 Case Study: 20-21 June 2008

One of the most notorious dry lightning busts of all time transpired 20-21 June 2008 across northern California. Predominantly dry thunderstorms produced over 5,000 lightning strikes, which ranked in the top 5 of lightning strikes during a 24-hour time period in northern California (See Appendix A20). The lightning ignited 602 fires by 00 UTC June 22 throughout northern California, which overwhelmed the local and regional fire management. Five Incident Management

Teams (IMT) were dispatched to help deal with the larger and more complex fires. Twelve firefighters lost their lives, and the monetary cost of fighting the fires nearly reached $300 million (Wallmann 2010). An approaching system started producing convection offshore in the preceding 24 hours prior to the commencement of the event.

Figure 9: a) 06 UTC 19 June 2008 48-hour GFS forecast plot of vertical cross-section of RH (filled, %) and θ_E (contoured, K) from OAK to MFR. b) 06 UTC 19 June 2008 48-hour GFS forecast plot of vertical cross-section of mixing ratio (filled, g kg^{-1}) and θ_E (contoured, K) from OAK to MFR. c) 00 UTC 19 June 2008 48-hour NAM forecast plot of vertical cross-section of RH (filled, %) and θ_E (contoured, K) from OAK to MFR. d) 00 UTC 19 June 2008 48-hour NAM forecast plot of vertical cross-section of mixing ratio (filled, g kg^{-1}) and θ_E (contoured, K) from OAK to MFR.

Examining the cross-sections from Oakland, CA (OAK) to MFR, noticeable instability and increased moisture around 700 hPa occurs just offshore through northern California (Figures 9a-d). The instability moving onshore likely contributed to the initiation of the offshore convection providing a clue of the potential for thunderstorm development. Figures 9a-d show drier lower levels relative to the increased moisture above 750 hPa across northern California. The stream of moisture was transported from northeast of Hawaii imitating a transport regime similar to a pineapple express that the California coast experiences during the winter. Additionally, moisture from thunderstorms circulating around a ridge near Baja California and the Sierra Madre Occidental converged with the Pacific stream of moisture offshore. A quasi-atmospheric river of moisture formed between 750-600 hPa aiding the high-based convection (Kaplan 2009). A noticeable increase of RH and mixing ratio existed in the 750-600 hPa layer, which collocated with areas of potential instability that riddle the cross-sections in the 750-500 hPa layer beginning just offshore and moving over northern California. This increase of moisture and potential instability provides a perfect vertical illustration of an environment primed for high-based convection.

With the offshore convection and the lifting occurring in the eastern Pacific off the coast of California, latent heat release occurred. Latent heat release has been known to produce mesoscale pressure perturbations that accelerate jet structures and further exacerbate upward motions (Hamilton 1998). This is due to momentum accompanying the jet encountering a strong mass perturbation, thus being deflected

by the local pressure perturbation resulting from latent heating. Imbalance within the jet occurs via the nonlinear balance equation terms resulting in an imbalance between the advection of kinetic energy and the pressure gradient force. This organizes a series of adjustments in the exit region of a jet. Parcels turn to the left instead of the right due to the imbalanced adjustments. The divergent tendency now resides on a timescale not of quasi-geostrophic motion (Ro>>1.0, <<1/f), which induces an ageostrophic wind component directed to the left of the large-scale wind and height fields. The mass adjustment is embodied in the advection of total momentum not equaling geostropic momentum advection, thus inducing a highly divergent subsynoptic jetlet (Hamilton 1998). Figures 10a-b illustrate the divergent region impinging onto the coast just west of the San Francisco Bay. One can distinguish this from the larger area of divergence to the west and northwest that was associated with the main core of the system lying just west-southwest of the northern California coast. The latent heat in the synoptic scale jet's exit region induces the pressure gradient force, which forms this jetlet, which then induces confluence upstream and diffluence downstream. This area of imbalance gives rise to parcel vertical and horizontal accelerations. This occurs in part due to the diabatic isallobaric wind on isentropic surfaces where mutual wind/mass adjustments occur due to latent heat release causing thickness/pressure changes which disrupts momentum within the flow-causing imbalance and the subsequent jetlet (Kaplan 1998).

Figure 10: a) 06 UTC 19 June 2008 48-hour forecast plot of GFS 250 hPa Winds (knots) and Divergence (s^{-1} x 10^{-5}). b) 06 UTC 19 June 2008 48-hour forecast plot of NAM 250 hPa Winds (knots) and Divergence (s^{-1} x 10^{-5}). c) NARR 18 UTC 20 June 2008 250 hPa winds (barbs and filled, knots) and height (contoured, dm). d) NARR 00 UTC 21 June 2008 250 hPa winds (barbs and filled, knots) and height (contoured, dm).
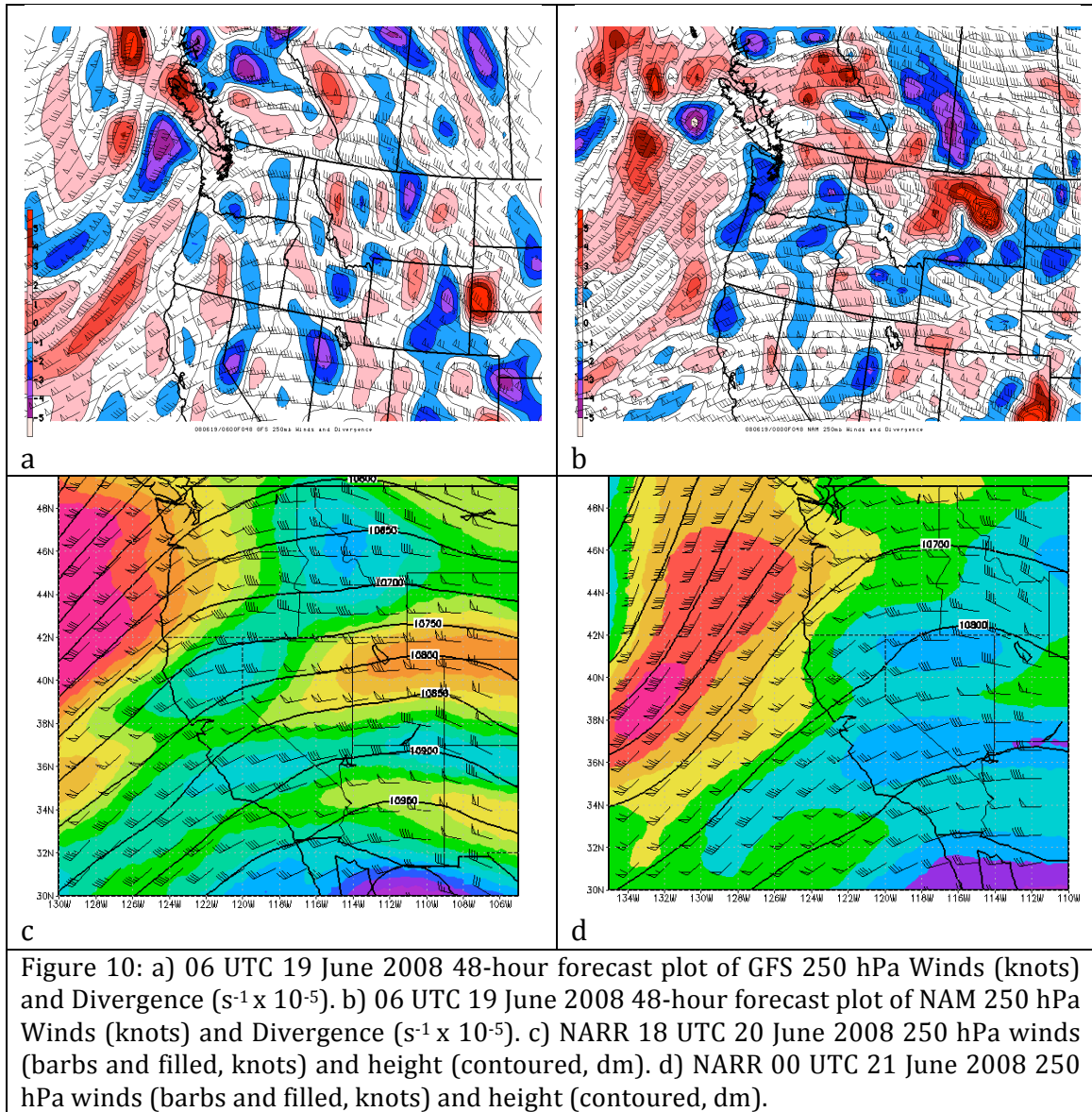
This process occurs off the coast of California during the preceding hours to the dry lightning event. Convection and lifting helped release latent heat setting off the series of processes to form the important jetlet. The jetlet can be seen as an appendage of the larger polar jet on its right forward flank exceeding 40 kts and approaching the coast within the 600-250 hPa layer during 18 UTC June 20 to 00

UTC June 21 before the larger scale flow becomes more dominant and adjusts (Figures 10c-d). This puts the lifespan of the jetlet consistently with other jetlets (3-12 hours) (Hamilton 1998). This does not appear to be the subtropical jet due to the height at which the region of enhanced flow resides. The blending of theoretical models from Kaplan (1998) and Hamilton (1998), in which diabatic forcing induces imbalanced flow and subsequently locally enhanced divergent flow, appears to be applicable for this lightning outbreak. Figures A21 and A22 (See Appendix) show a weak undulation in the tropopause in the same vicinity as the flow of moisture and dry thunderstorm formation across northern California. The gradient of tropopause pressure outlines the southeast boundary of the approaching system, which falls in line with signals seen in other cases. This feature provided some additional lift/instability, and possibly resulted from the offshore convection and subsequent highly divergent jetlet.

Figures A23 and A24 (See Appendix) depict a consistent static stability perturbation structure to the preceding dynamic tropopause, cross-sections, and 250 hPa divergence plots. All follow the same southwest to northeast stream-like form approaching and entering northern California. The HLTT easily reach the minimum thresholds and offer more evidence of the offshore convection as the threshold is met well off the coast. With the best moisture and instability residing in the 700-500 hPa layer, the lofty HLTT makes sense due to its equation focusing on that layer. The ULLR values on both the NAM and GFS runs meet the threshold although the GFS depiction more accurately portrays the highly unstable

atmosphere over the region (See Appendix A25 & A26). Figure A25 shows values exceeding 8°C km^{-1} and all of northern California reaching the 7.5°C km^{-1}. The ample moisture and instability reinforce each other and the effects of this positive feedback manifest in the HLTT, ULLR, and cross-section plots.

This complex and immense event had origins ranging from Hawaii to the Gulf of Mexico. Two moisture sources flowed above the surface in between constant pressure layers due to the upward vertical motion and transport. The unique collection of isentropic and vertical motion plots within the DTP help diagnose this event 48 hours before it occurred. This event also stresses the importance of looking upstream in the preceding 24 hours even if it is in the observation sparse Pacific Ocean. The cross-section plots really show the amount of moisture and instability between the 750-500 hPa levels and how convection can alter balanced flow meteorology. The unbalanced flow from the latent heat release helped perturb the mass and wind fields thus forming the jetlet, which supported and enhanced the convection as it came onshore. The strength of the DTP lies with the fact that it employs information at multiple levels, and aims to identify certain moisture and instability signals, which the forecasting of this event requires.

3.4 Case Study: 16-17 July 2007

Thunderstorms began forming early in the morning on 16 July 2007 in eastern Nevada. The storms quickly produced lightning, which then spread in coverage across all of northern Nevada, Idaho, and western Montana over the next

36 hours. The storms stayed relatively dry over Nevada and Idaho, but became wetter with time as they approached Montana. Examining the national situation reports, thousands of lightning strikes ignited over 150 fires including more than 25 large fires thus forcing the Western and Eastern Great Basin GACC's to the highest preparedness level possible (five) (Figure 11a). A thermal trough and shortwave at 500 hPa moved over the area between 12-18 UTC 16 July 2007 helping trigger the convection (Figure 11b). This shortwave along with monsoonal moisture aloft helped compensate for the relatively weak nature of the jet streak support to develop and sustain widespread dry thunderstorm formation.

A shortwave not as well depicted in conventional height fields as in the dynamic tropopause maps moved through Nevada early on 16 July 2007. Figures 11c and 11d demonstrate the shortwave sweeping through the area just before this time, as the pressure perturbation is quite evident on the dynamic tropopause as well as a wind shear zone. The placement of the shortwave between the GFS and NAM might be slightly off, but the timing and magnitude coincide. These figures do not represent the 48-hour forecast, but the best depiction of the shortwave available. These figures do a better job of showing the shortwave during the most intense period of the event and not necessarily the beginning. However, the shortwave does appear in the longer-range forecasts ending at the beginning of the event. Figures 11c and 11d depict the most apparent shortwave in any of the case studies, and due to its strength makes up for a couple of the other DTP's parameters that lack during the onset and even the peak of this event.

Figure 11: a) Lightning strike plot from 12 UTC 16 July to 00 UTC 17 July 2007. Dotted Line: RNO-TFX & LKN-BOI cross-sections. b) NARR 12 UTC 16 July 2007 500 hPa winds (barbs and filled, knots) and height (contoured, dm). c) 15 July 2007 36-hour GFS forecast of dynamic tropopause pressure (contoured & filled, hPa) and winds (knots) plotted on 1.5 potential vorticity surface. d) 12 UTC 15 July 2007 36-hour NAM forecast of dynamic tropopause pressure (contoured & filled, hPa) and winds (knots) plotted on 1.5 potential vorticity surface.

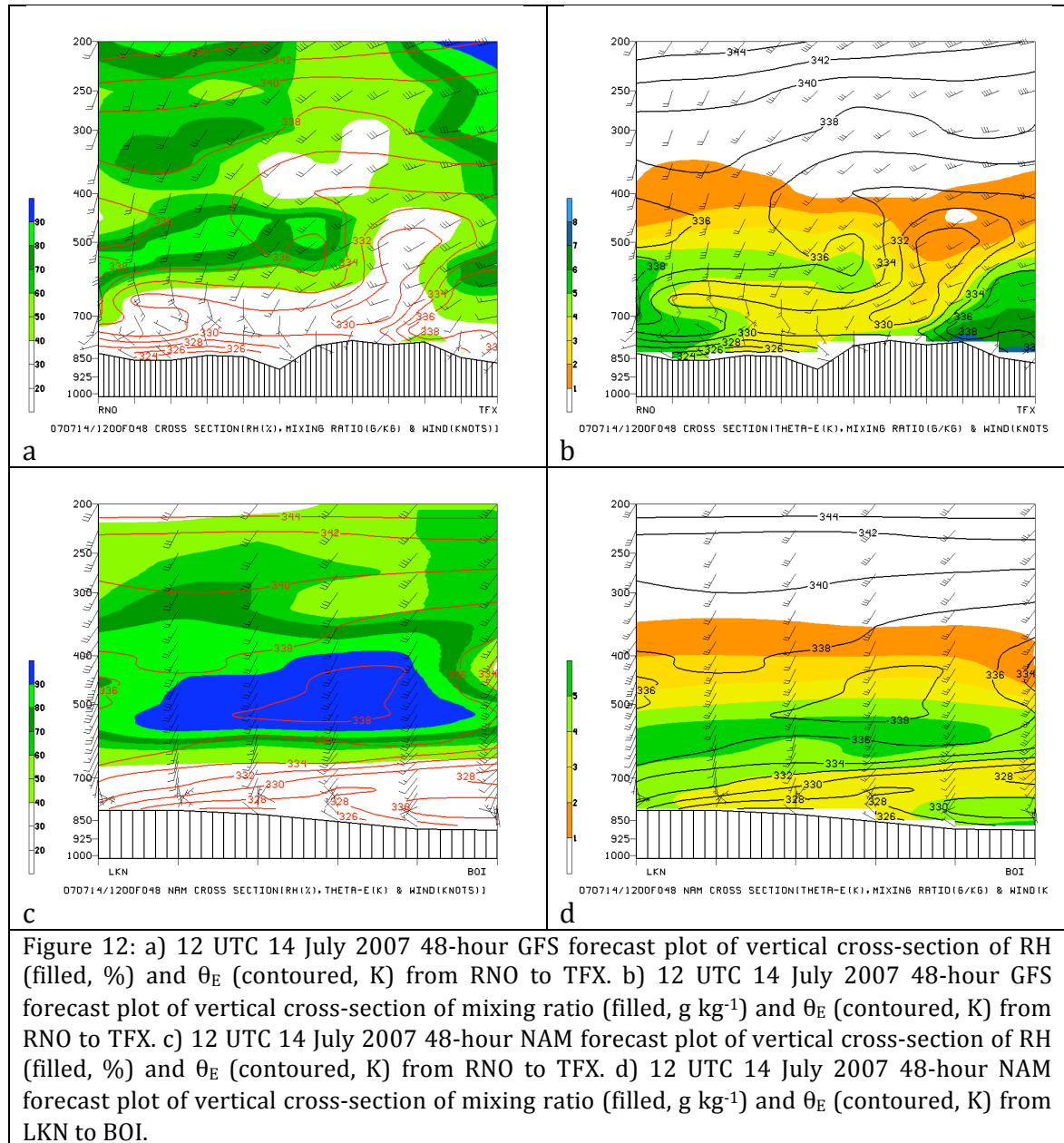The vertical thermodynamic and moisture cross-sections exhibit the highly unstable atmosphere across the western Great Basin and into Idaho as diagnosed by the nearly vertical moist isentropic surfaces. Pockets of instability aloft coincide with a monsoonal push of moisture. Figures 12, A27, and A28 (See Appendix A27 & A28) depict this collocation of instability and moisture. The best collocation of the

instability and moisture resides over northeastern Nevada into southern Utah when examining the cross-sections. Figures 12c and 12d display the best collocation of moisture and potential instability with drier lower levels within the vertical structure of the atmosphere from Elko, NV (LKN) to Boise, ID (BOI). The 48-hour forecasts from the NAM and GFS both identify northeastern Nevada and southern Idaho as an area for with high potential for dry thunderstorm formation. The instability occurs from the shortwave moving through the intermountain region and the moisture stream advecting from the south-southwest to the north-northeast, i.e., from central Nevada to western Idaho. Figures 12, A27, and A28 also show the elevated moisture content over the drier lower atmosphere of Nevada. This occurs in the early morning hours when RH and moisture recovery tends to happen, but the monsoonal water vapor remains confined to above 700 hPa. The atmosphere residing over Nevada throughout 16 July 2007 becomes nearly ideal for dry thunderstorm development. The cross-sections throughout the entire 36 hours of the event illustrate the instability and moisture collocated above a drier lower troposphere. The event also shows the so-called Goldilocks environment for dry lightning, where further south, the monsoon has penetrated the lower levels, while Pacific moisture settled in Montana with Nevada and Idaho lying in between.

The HLTT as expected indicated increased potential and coverage for high-based thunderstorms. With most of the instability and moisture residing in the 700-500 hPa layer, significantly elevated values of HLTT are expected (See Appendix A29 & A30). (See Appendix) A29 shows the GFS 48-hour forecast indicating

enhanced HLTT including a swath of 32°C near the location and time of dry

thunderstorm formation across eastern Nevada. The GFS continued to spread values

Figure 12: a) 12 UTC 14 July 2007 48-hour GFS forecast plot of vertical cross-section of RH (filled, %) and θ_E (contoured, K) from RNO to TFX. b) 12 UTC 14 July 2007 48-hour GFS forecast plot of vertical cross-section of mixing ratio (filled, g kg^{-1}) and θ_E (contoured, K) from RNO to TFX. c) 12 UTC 14 July 2007 48-hour NAM forecast plot of vertical cross-section of RH (filled, %) and θ_E (contoured, K) from RNO to TFX. d) 12 UTC 14 July 2007 48-hour NAM forecast plot of vertical cross-section of mixing ratio (filled, g kg^{-1}) and θ_E (contoured, K) from LKN to BOI.

of HLTT within the region bordered by 30-36°C across Nevada and into Idaho over

the next 36 hours coincident with the broadening development of dry

thunderstorms. The NAM and GFS do accurately delineate an area conducive for the

high-based convection, but the NAM (See Appendix A30) underestimates the coverage and magnitude. Scattered values of 28°C cover eastern Nevada intermittently at 12 UTC 16 July 2007 from the 48-hour forecast. Not until a 36-hour forecast verifying at the same time does the NAM generate HLTT that cover most of the area of convection and values reaching above 30°C (See Appendix A31). The lack of coverage at 48 hours is difficult to understand since the NAM simulates the instability and moisture in the 700-500 hPa layer, which the HLTT calculation comes from. However, it does generally provide guidance, which indicates the potential at 48 hours for elevated convection; however, more accurately depicts the favorable atmospheric environment at 36 hours.

The two parameters that did not strongly support the 48-hour forecast of dry thunderstorm formation were the 250 hPa divergence and ULLR. The 250 hPa GFS 48-hour forecast does simulate some divergence in eastern Nevada at the beginning of thunderstorm formation (See Appendix A32). However, the NAM does not show coherent divergence across northern or eastern Nevada until the 36-hour forecast verifying at 12 UTC 16 July 2007 (See Appendix 33) at this particular level. The NAM does not tend to correct this error until a 48-hour forecast verifying at 00 UTC 17 July 2007 when the peak of the event occurs. Examining the synoptic environment, the absence of a strong and unambiguously coherent upper level jet streak is noted at the level of analysis, which helps explain the small amount and erratic pattern of divergence across the case study area at 250 hPa. It is possible that the pressure level analysis of divergence might be less sensitive than an analysis on isentropic

surfaces such as gleaned from the dynamic tropopause figure. The GFS ULLR 48-hour forecast shows a swath of 7.5°C km^{-1} values through the approximate area of dry thunderstorms early on 16 July 2007 (See Appendix A34). It relatively collocates with the other parameters in Nevada. The NAM forecast never truly shows the 7.5°C km^{-1} threshold explicitly over the area of dry lightning. It propagates in from the south and west later in the event, but does serve as a good predictor for this particular dry lightning bust. The reasoning for the weak divergence and ULLR values could be due to the bulk of the instability lying below 400 hPa and predominantly around 500 hPa as noted in the thermodynamic cross-section plots.

An immense dry lightning event that affected northern Nevada and southern Idaho produced thousands of lightning strikes igniting hundreds of fires including more than 20 large fires. The event lasted more than 36 hours with thunderstorms developing along a mostly northward vector during the time period when they entered Idaho and progressed to western Montana. However, the storms closer to and over Montana had wetting rains while the majority of Nevada and Idaho storms remained drier. This event began in the early morning hours as the shortwave impinged on central Nevada. As the instability induced from the shortwave encountered residual mid-level monsoonal moisture in the Great Basin, high-based thunderstorms developed. The relative lack of upper-level jet support only enhanced the importance of the shortwave trough structure and monsoonal moisture at mid-levels as noted by the cross-sections, HLTT, and dynamic
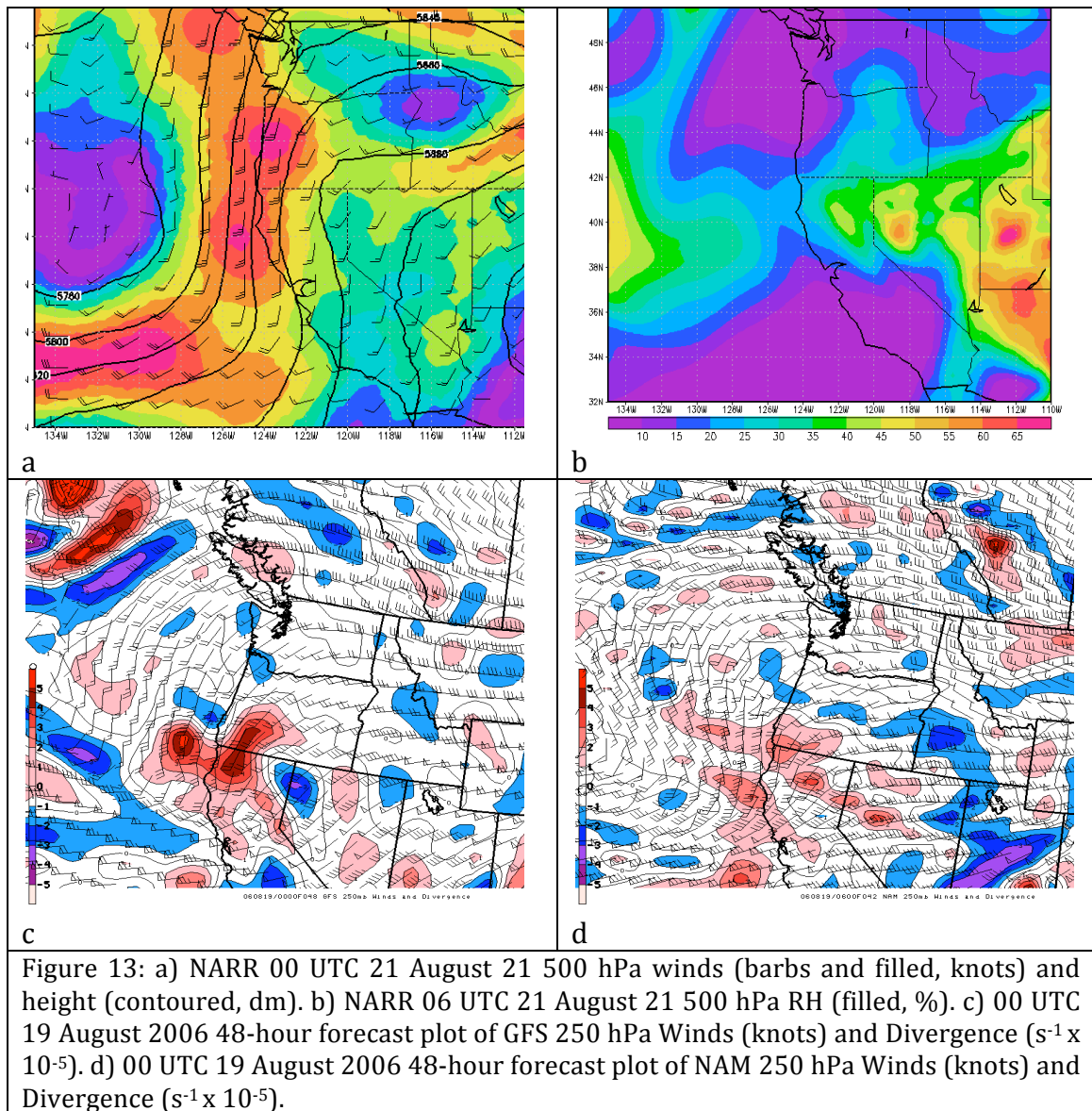
tropopause plots. Due to the lack of dominant upper level features, the ULLR and 250 hPa divergence components mitigated the effectiveness of the DTP.

3.5 Case Study: 20-22 August 2006

Less than 1500 lightning strikes were observed over the Pacific Northwest primarily in Oregon during 20-22 August 2006. Very dry lower atmospheric conditions and receptive fuels led to multiple large fires including 5 IMET deployments. In terms of the shear magnitude of lightning strikes, 20-22 August 2006 represents the least impressive lightning output among the case studies that occurred over two days mostly during the afternoon and evening hours (See Appendix A35). Significant upper-level dynamical support aided thunderstorm development, while just enough moisture at mid-levels and a drier lower atmosphere helped transform the event into the dry category (Figure 13a). A stream of instability stretched across Oregon coinciding with thunderstorm development. Moisture from the Pacific at mid- and upper-levels extended over the Cascades, while the very fringe of a monsoonal surge provided additional moisture (Figure 13b).

A negatively tilted trough approached the Pacific coast along the Oregon and California border on 21 August 2006. Accompanying the 500 hPa trough, a vigorous jet streak impinged on northern California. The jet streak lay south of the main area of convection, but the curved flow of the jet stream wrapped up the coast across

Oregon creating an area of strong 250 hPa divergence in southwestern Oregon (Figures 13c-d). Diffluence aloft generated by the split in the 250 hPa winds aided

Figure 13: a) NARR 00 UTC 21 August 21 500 hPa winds (barbs and filled, knots) and height (contoured, dm). b) NARR 06 UTC 21 August 21 500 hPa RH (filled, %). c) 00 UTC 19 August 2006 48-hour forecast plot of GFS 250 hPa Winds (knots) and Divergence (s^{-1} x 10^{-5}). d) 00 UTC 19 August 2006 48-hour forecast plot of NAM 250 hPa Winds (knots) and Divergence (s^{-1} x 10^{-5}).

upward vertical motion, which destabilized the atmosphere and subsequently triggered and sustained thunderstorms across Oregon. The GFS (Figure 13c) exhibits larger magnitude divergence relative to the NAM (Figure 13d), and the NAM required an extra 6 hours to delineate the area of divergence. Both simulations

did create the area of upward vertical motion and at the correct time of ascent more than 42 hours ahead of the event. The dynamic tropopause plots surprisingly did not indicate a strong tropopause undulation. The only lowering of the tropopause occurred in northern California just south of the main jet streak. Not even a weak gradient appeared over southwestern Oregon as this occurred throughout the first day of convection. The failure of this product represents the largest mis-forecast in any of the case studies examined.
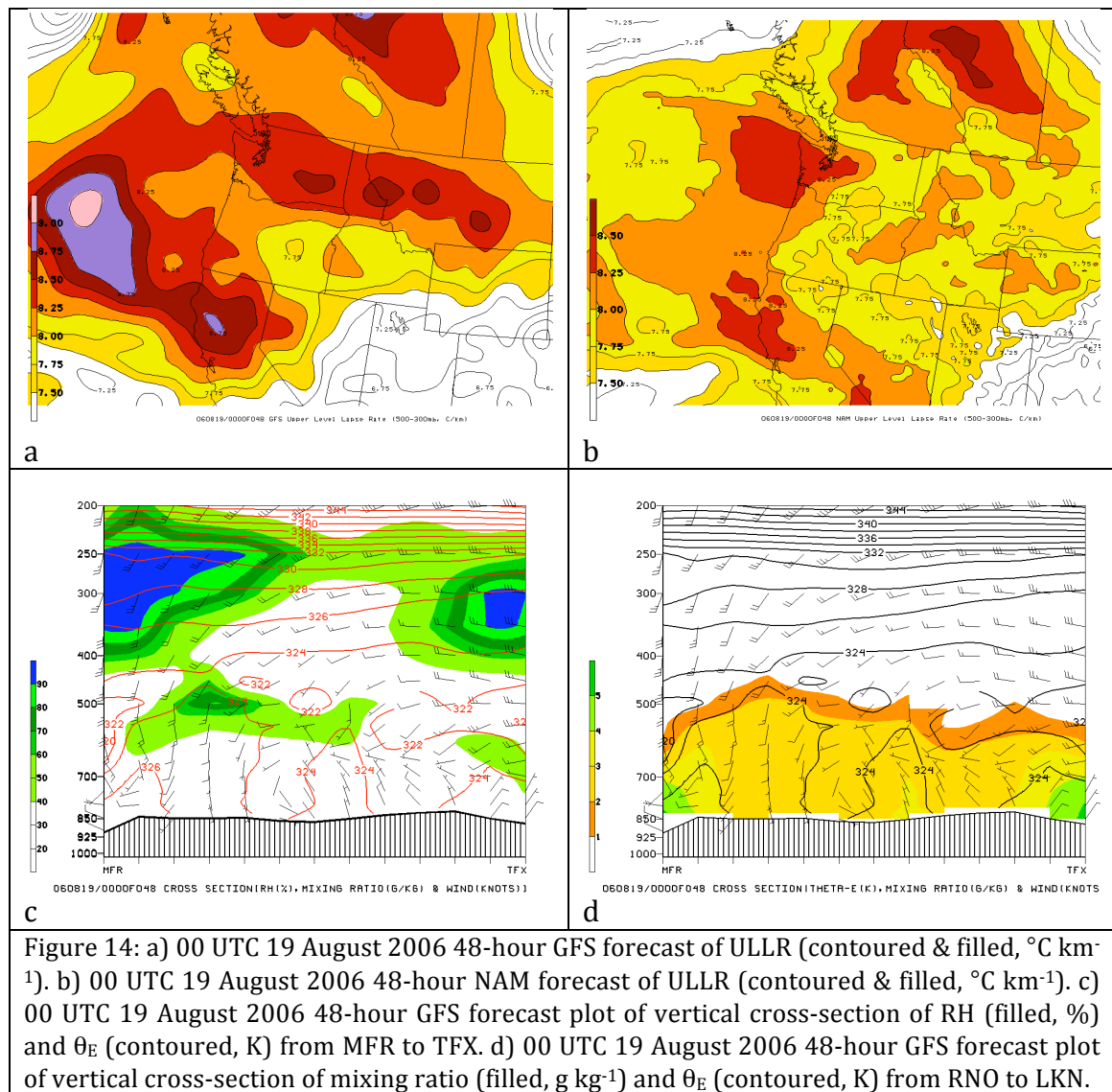
Figure 14: a) 00 UTC 19 August 2006 48-hour GFS forecast of ULLR (contoured & filled, °C km^{-1}). b) 00 UTC 19 August 2006 48-hour NAM forecast of ULLR (contoured & filled, °C km^{-1}). c) 00 UTC 19 August 2006 48-hour GFS forecast plot of vertical cross-section of RH (filled, %) and θ_E (contoured, K) from MFR to TFX. d) 00 UTC 19 August 2006 48-hour GFS forecast plot of vertical cross-section of mixing ratio (filled, g kg^{-1}) and θ_E (contoured, K) from RNO to LKN.

The ULLR showed enhanced instability over southern Oregon with values reaching 8.5°C km^{-1} (Figures 14a-b). The strong trough coupled with the augmented instability aloft explains the high ULLR values. The position of the trough put the most divergent region over southwestern Oregon. This region lies just downstream of the axis of the trough where the ageostrophic flow is directed back upstream just before the divergent region, and then directed downstream just after creating an area where upward vertical motion occurs (Figure 14c). This case offers the strongest quasi-geostrophic (QG) forcing when compared to the five other cases. The NAM (Figure 14b) had values just slightly less than GFS (Figure 14a), but by only fractions of the ULLR. Both accurately simulated the time and area for thunderstorm development during the afternoon of 21 August 2006.

The thermodynamic and moisture cross-sections depict an unstable and mostly dry atmosphere. This case probably contains the least amount of moisture available of all the cases examined, which explains the isolated to scattered lightning strikes. However, due to the dryness of the atmosphere and the storms, the lightning strikes reached the ground with minimal precipitation. Figures 14c and 14d show the instability centered near 500 hPa over central Oregon. Due to the cold trough located at 500 hPa the largest instability should reside at this level of the atmosphere (Figure 14a). In addition, the 250 hPa divergence helped stretched the moist isentropes and helped increase the RH in the upper levels above western Oregon as illustrated in Figure 14c. The negatively tilted system also brought just enough moisture along the leeside of the Sierra Mountain and Cascades. The Pacific

moisture did not make it over the Cascades initially, and the limited fringe monsoonal moisture was just enough to help start dry thunderstorm formation across central Oregon (Figure 14b). The GFS does a better job of locating the moisture available at the mid levels (Figures 14c-d). The increase of RH also represents the thunderstorms developing and moistening the mid levels of the atmosphere. The NAM does not illustrate as much moisture, and shows the potential instability about 100 hPa lower in the atmosphere (See Appendix A36 & A37). However, both the GFS and NAM simulations depict instability right at the top of the moisture flow entering Oregon.

HLTT show values right at and just above the 28°C threshold in a pattern following the path of dry thunderstorm formation across western and Central Oregon (See Appendix A38 & A39). The NAM shows the path better, most likely due to the higher model grid resolution; however, the GFS outlines the same general area. Both predict the area and values correctly 48 hours in advance, thus agreeing with the other DTP components with the exception of the dynamic tropopause plots. The NAM (See Appendix A39) shows a southwest to northeast oriented line of elevated HLTT corresponding to Figure A39 where the instability extended more over eastern Oregon and into Idaho compared to the GFS solution (Figures 14c-d, A38). With the instability and moisture laying in the 700-500 hPa layer the HLTT of 28°C or greater should exist.

This case clearly demonstrates that when strong Q-G forcing exists even with very limited available moisture, dry thunderstorms can still develop. The periphery

of the moisture tongue was several hundred miles southeast of the area, but the strong trough embedded within the jet streak created a low-level return branch flow of water vapor that brought enough of that moisture plume into Oregon. The most substantial jet streak lifting existed just to the south of the dry lightning region, but the bifurcation of the jet stream just off the Oregon coast created diffluence, and with the strong 500 hPa trough, this diffluence existed throughout the upper-levels of the atmosphere stretching moist isentropes and generating divergence aloft. While not as many lightning strikes or fires occurred as the other case studies, 5 IMET's and a number of Type 1-3 incident management teams were deployed across the lightning affected region. The dry lightning on 21-22 August 2006 demonstrates the flexibility of the forecast procedure and how not only the presence, but also the strength of each component of the procedure affects the outcome of the event. The absence of a strong pressure gradient of the dynamic tropopause was noted, but the presence of the four other collocated components showed that an event was possible although maybe not as severe as other cases such as the June 2008 northern California dry lightning bust.

3.6 Case Study: 25-26 June 2006

This two-day dry lightning bust started multiple large fires including several complexes throughout northern Nevada and California. The Sierra-Tahoe Complex (biggest two were Balls Canyon and Linehan fires near Reno/Carson), the Boulder Complex in Plumas County, Observation Complex in Lassen County, and the Suzie Fire in Elko County all were apart of this event. Following a similar lightning path of

the 1 August 2009 case study, dry thunderstorms affected most of the lee side of the northern half of the Sierra Nevada and very southern tier of the Cascades over a 48-hour time period (Figure 15a). The lightning started late in the afternoon on 25 June 2006 with most of the lightning occurring during the next day (26 June). An interesting synoptic pattern prevailed over northern California and Nevada over the course of the event. A strongly negatively tilted and massive elongated trough (almost oriented east to west) was centered over central California (Figure 15b). A small area of weak flow resembling a closed high-pressure system existed just southeast of Lake Tahoe over western Nevada. A swath of high momentum moved east to west just to the south and to the northwest of this closed ridge. The highly accelerative nature of these fine scale features indicates a higher Rossby number for this system consistent with subsynoptic scale circulations. Due to this, the lack of a larger scale vigorous jet aloft was compensated for by rapid subsynoptic scale adjustments accompanying these highly anticyclonically curved, and therefore ageostrophic flows helping induce mesoscale patterns of divergence, which organize the instability aloft.

Figures 15c and 15d illustrate the divergence aloft. Even with a weak jet the highly diffluent and ageostrophic flow along with the 250 hPa jet(let) just south of Lake Tahoe help produce the divergence. The GFS (Figure 15d) does a better job expanding the area under divergence in eastern California and western Nevada; however, throughout all the runs, the NAM (Figure 15c) more accurately depicts the wind flow and divergence at the 250 hPa level. Even a noticeable difference within

the flow structure and speed shows up in the plots when the two simulations are intercompared across eastern California and western Nevada. The higher resolution of the NAM could explain why it more accurately demonstrates the detail of the flow at the 250 hPa level. The 48-hour forecast verifying at 00 UTC 26 June 2006 represents the beginning of the observed dry lightning event. More impressive figures exist during the subsequent afternoon, but the priority of this research is to show how the DTP can predict an event from start to finish, and not just the peak.
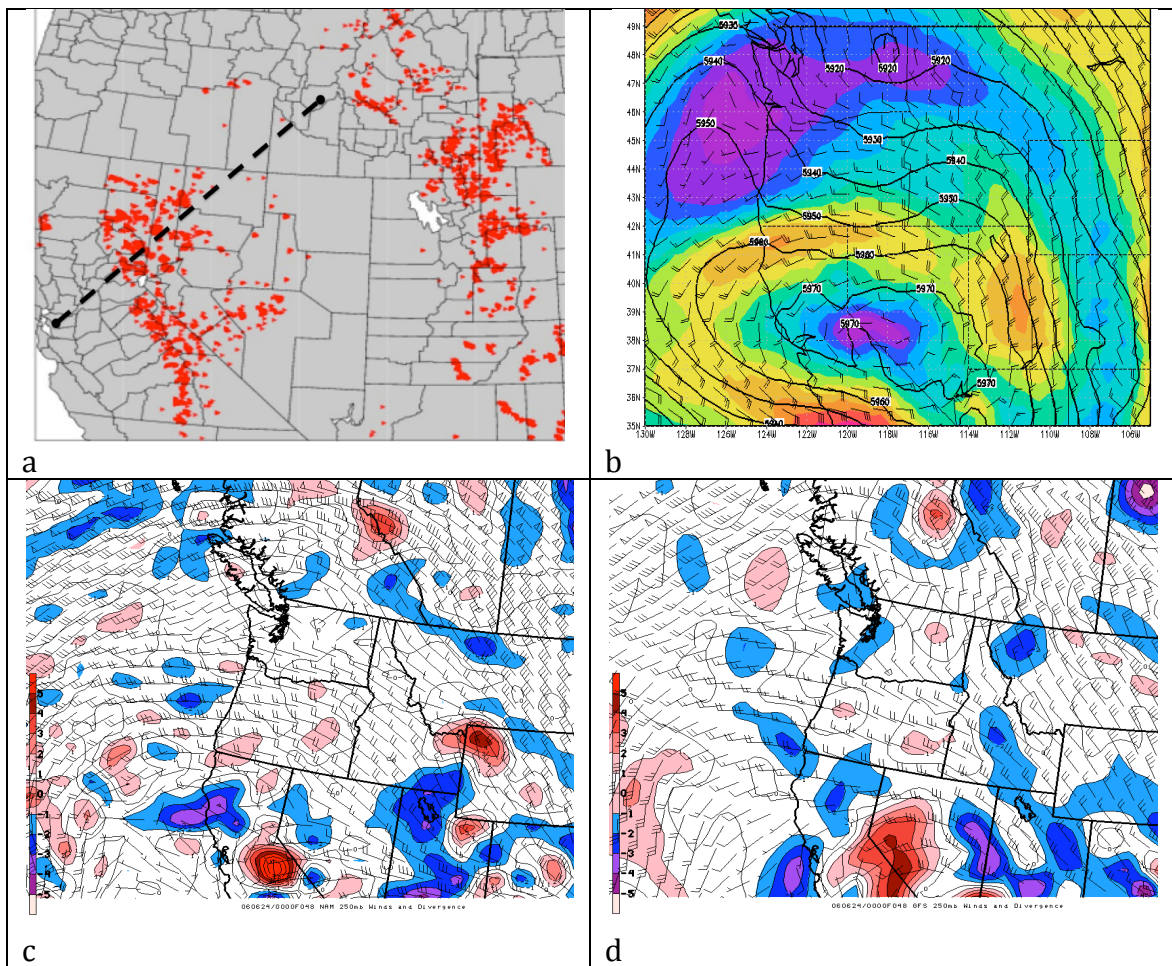
Figure 15: a) Lightning strike plot from 12 UTC 26 June to 00 UTC 27 June 2006. Dotted line OAK-BOI cross-section. b) NARR 00 UTC 26 June 2006 500 hPA winds (barbs & color filled, knots) and height (contoured, dm). c) 00 UTC 24 June 2006 48-hour forecast plot of NAM 250 hPa Winds (knots) and Divergence ($s^{-1} \times 10^{-5}$) d) 00 UTC 24 June 2006 48-hour forecast plot of GFS 250 hPa Winds (knots) and Divergence ($s^{-1} \times 10^{-5}$).

With the extremely negatively tilted trough, the flow over the region of interest becomes nonuniform over a short distance. Residual monsoonal moisture underneath the subsynoptic ridge in western Nevada, monsoonal moisture wrapping around this subsynoptic high, and Pacific moisture all support dry thunderstorm formation. Most of the moisture that triggered this event was observed at the 500 hPa level. Instability also existed between the 600 and 500 hPa levels on the lee side of the mountains, while some lower instability existed on the windward side; however, this did not play much of a role other than helping provide some extra moisture crossing the mountain via convective lifting (Figures 16a-d) (Kaplan 2009). Figures 16a and 16b illustrate the stream of moisture and relatively collocated instability at mid levels through the vertical cross-section from OAK to BOI. Increased mixing ratio and RH values also coexist with pockets of instability over northern California and northwestern Nevada demonstrating an ideal case for the cross-section component of the DTP.

Upper level divergence helped stretch the moist isentropes and increase RH aloft, which is distinctly noted through the 250 hPa level over northern California and northwestern Nevada. As with all the other plots from this event, the next afternoon forecast had better instability and moisture placement, but these 48 hour forecasts for 00 UTC 26 June 2006 demonstrate the accurate simulation of the indices needed to ascertain the commencement of the dry lightning bust. The GFS cross-sections did not entirely show the moisture and instability consistent with observations for the afternoon of 25 June (Figures 16c-d). However, the 42-hour

forecasts verifying at 06 UTC 26 June 2006 exhibit similar signals to the NAM simulation 12 hours earlier and for 6 hours longer duration for use as a forecast. The NAM more accurately predicted this event than the NAM in every component of the DTP.
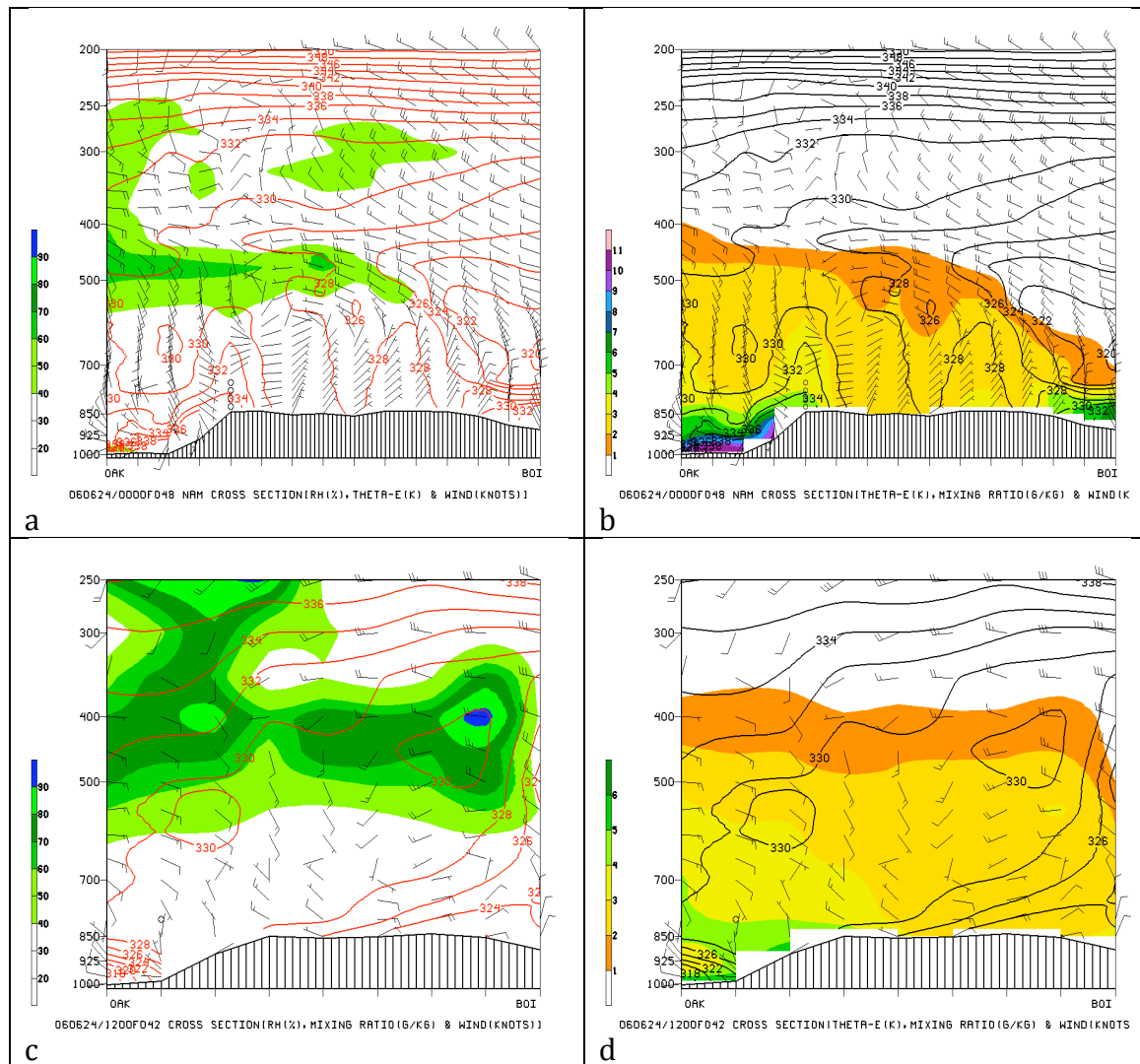
Figure 16: a) 00 UTC 24 June 2006 48-hour NAM forecast plot of vertical cross-section of RH (filled, %) and θ_E (contoured, K) from OAK to BOI. b) 00 UTC 24 June 2006 48-hour NAM forecast plot of vertical cross-section of mixing ratio (filled, g kg^{-1}) and θ_E (contoured, K) from OAK to BOI. c) 12 UTC 24 June 2006 42-hour GFS forecast plot of vertical cross-section of RH (filled, %) and θ_E (contoured, K) from OAK to BOI. d) 12 UTC 24 June 2006 42-hour GFS forecast plot of vertical cross-section of mixing ratio (filled, g kg^{-1}) and θ_E (contoured, K) from OAK to BOI.

The NAM ULLR results exhibit a wide area of values exceeding the 7.5°C km^{-1} threshold including an area of 8°C km^{-1} in western Nevada and northern California with the 48-hour forecast verifying at 00 UTC 26 June (See Appendix A40). With most of the instability near 500 hPa and the divergence at 300 hPa, the elevated ULLR values make physical sense. Examining Figure A41 (See Appendix) and comparing it to Figure A40 the NAM ULLR exceeded the GFS by approximately 0.5°C km^{-1} throughout the forecast period. The GFS approximately outlines a region of 7.5°C km^{-1} that mirrors the area of dry thunderstorm development in western Nevada and northern California. However, it does not perform as well as the NAM and throughout all the runs it underestimates the coverage and magnitude of ULLR.

Examining the HLTT, the NAM once again outperforms the GFS (See Appendix A42 & A43). The NAM (See Appendix A42) illustrates the instability aloft and potential for high-based thunderstorms just on the lee side of the Sierra Nevada and through northeastern California. The GFS (See Appendix A43) generally outlines an area on the lee side; however, this does not occur until the 30-hour forecast verifying at the same time as the rest of the runs. It also underestimates the HLTT throughout all the runs. With the instability and moisture located anywhere from 700-500 hPa, the HLTT should be a key component in deciding the potential for high-based thunderstorms. The NAM exemplifies this by outlining values 28-32°C across the examined area while the GFS falls short. Granted the GFS improves its forecasting for the peak of the event, but it still remains a lesser tool compared to the NAM throughout the whole event.

The dynamic tropopause depicted is elevated 150 hPa over the region of convection. However, the region of tropopause pressure gradient existed in close proximity to dry thunderstorm formation 48 hours in advance (See Appendix A44 & A45). The elevated tropopause pressure values occurred due to the divergence aloft stretching the moist isentropes, thus raising the level of the tropopause as seen by the tight gradient of moist isentropes in Figures 16a-d. The NAM (See Appendix A44) did a better job depicting the dynamic tropopause environment and structure, but the GFS (See Appendix A45) and possibly for the wrong reasons, still placed a gradient of pressure in northwestern Nevada and northeastern California. Both figures show the high frequency nature of this system with many different undulations in around the Great Basin and California.

25-26 June 2006 represents a memorable event for North Ops and the Western Great Basin GACC's since several large complexes emerged throughout the region. The dry lightning bust triggered thousands of lightning strikes over two plus days causing a strain on local and regional resources due to the multiple large fires ignited. Examining the DTP, the NAM outperformed the GFS. The GFS indicated that an event was possible, but without the NAM, the magnitude and coverage of the event would have been missed. The highly curved and high Rossby number associated with the wave structure requires the use of a numerical model with better resolution to have an enhanced chance of determining the atmospheric environment. Disagreements between models perplex forecasters and complicate forecasts. That is why an examination of the whole DTP with both models is

recommended to ensure that each facet of dry thunderstorm formation will be investigated. A trend of negatively-tilted troughs approaching the West Coast is now emerging from this research as 25-26 June 2006 represents the third case in which this occurs, and the second instance in the same geographical area producing nearly an identical location and coverage of lightning strikes and dry thunderstorm formation.

4. Summary, Conclusions, and Future Work

Throughout each event, the DTP accurately depicted the magnitude and location of the dry lightning. Some discrepancies between the models revealed themselves, but by using both the GFS and NAM operational models, the loss of accuracy was minimized. The differences between the models were noted, but the intention of this paper was not to compare how the NAM and GFS compared to each other. The intention was to determine if both operational models could be used to implement the DTP, and the dissimilarities were side notes. The GFS and NAM performed well enough in each case to demonstrate the ability of the DTP to forecast dry thunderstorm formation, and were mere vessels of the DTP.
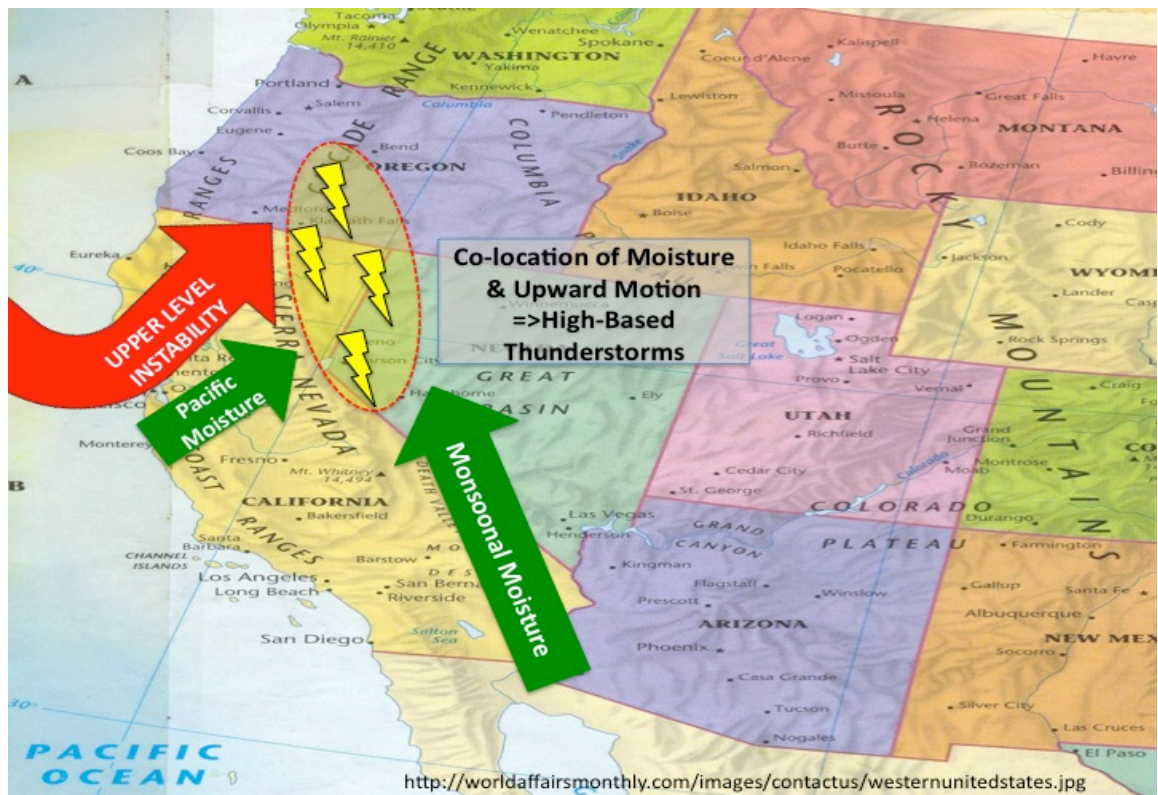
Figure 17: Planar schematic of dry thunderstorm ingredients identifying the collocation of different moisture sources with instability aloft.

The flexibility of the DTP represents its strongest trait. The encompassing components of the DTP form a group of dry thunderstorm formation predictors. Moist isentropic analysis via vertical cross-sections exhibiting θ_E with RH and mixing ratio illustrate moisture and instability otherwise missed by constant pressure plots. 250 hPa wind and divergence plots categorize upper-level support for thunderstorm formation, while the ULLR provide another numerical value of instability just below the 250 hPa level (500-300 hPa layer) and connect the mid-levels to the upper-levels. The HLTT highlights the 700-500 hPa layer where much of the instability and moisture exist in dry lightning events. Finally, the pressure of the dynamic tropopause on the 1.5 IPV surface depict undulations of the tropopause, and present short waves that constant pressure maps underestimate or miss entirely.

Each component measures instability or moisture, and in some instances both instability and moisture. Any thunderstorm formation, whether wet or dry, needs both of these characteristics to develop and be significant. The complex terrain of the West makes forecasting thunderstorms more difficult than east of the Rockies. With upslope flow, the passage of Pacific systems, and monsoonal surges during the summer, thunderstorms can develop in a number of ways. The subtle features that can spawn small to large thunderstorm complexes especially in a dry thunderstorm formation environment can be lost employing traditional forecasting maps and procedures. The unique and diverse components of the DTP bring these features to the forefront, and allow forecasters to determine if thunderstorms will

form, and if they will be dry or wet. A number of different patterns triggered these six case studies; however, a common theme to each event is the collocation of instability and moisture on the periphery of the most favorable instability and moisture (Figures 17-19). Monsoonal surges and approaching Pacific systems interact in complex ways in the western United States. Moisture and instability may come from multiple places making forecasting these dry lightning busts even more difficult.
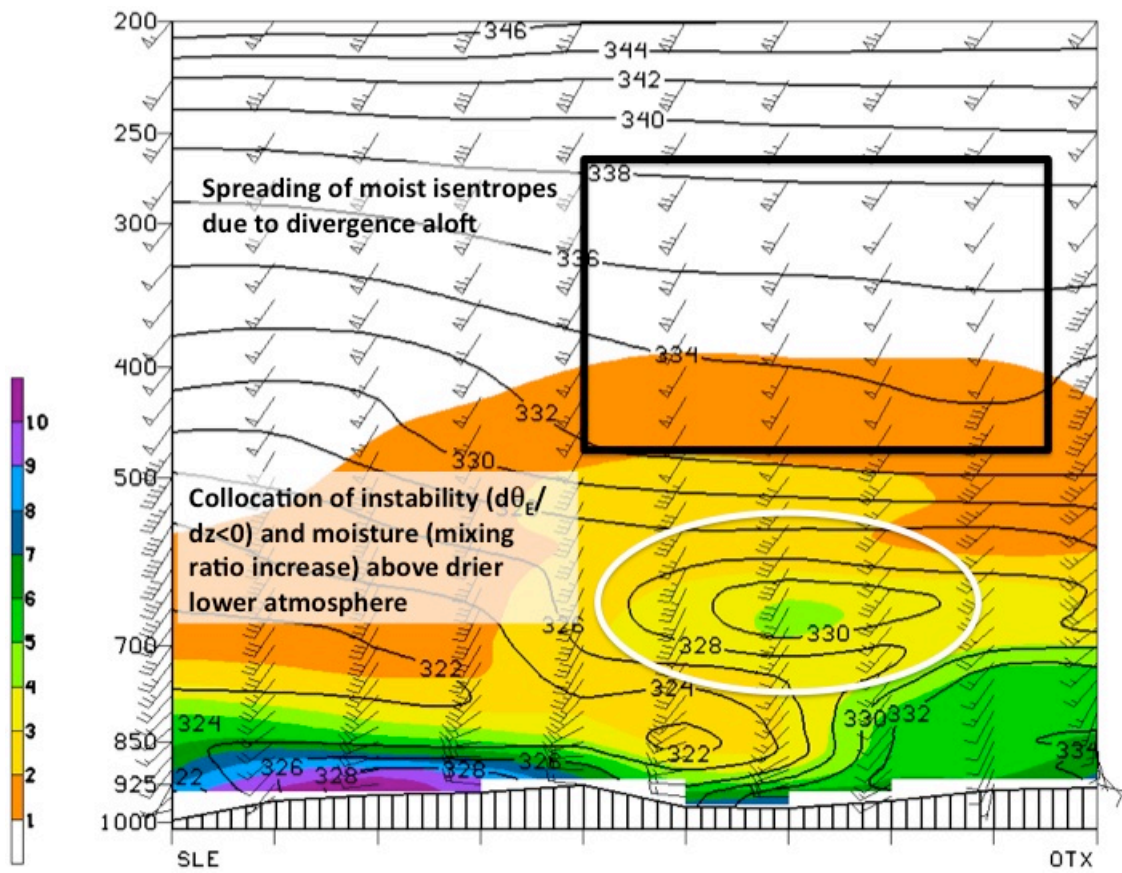
Figure 18: Plot of vertical cross-section of mixing ratio (filled, g kg^{-1}) and θ_E (contoured, K) from SLE to OTX. Denotes important features (collocated instability & moisture, drier lower levels & divergence) within the vertical view of the atmosphere.

The key aspects of DTP are:

- Approaching trough necessary to help provide instability;

- Monsoonal and/or Pacific Moisture in front of and/or entrained with approaching trough at mid–levels;

- Collocation of instability and moisture within the 700-400 hPa layer with drier lower atmosphere underneath the pairing;

- Goldilocks environment: The area conducive for dry thunderstorms resides on the periphery of best moisture and instability, where magnitude location of each allow for thunderstorm development, but not widespread wetting thunderstorms.
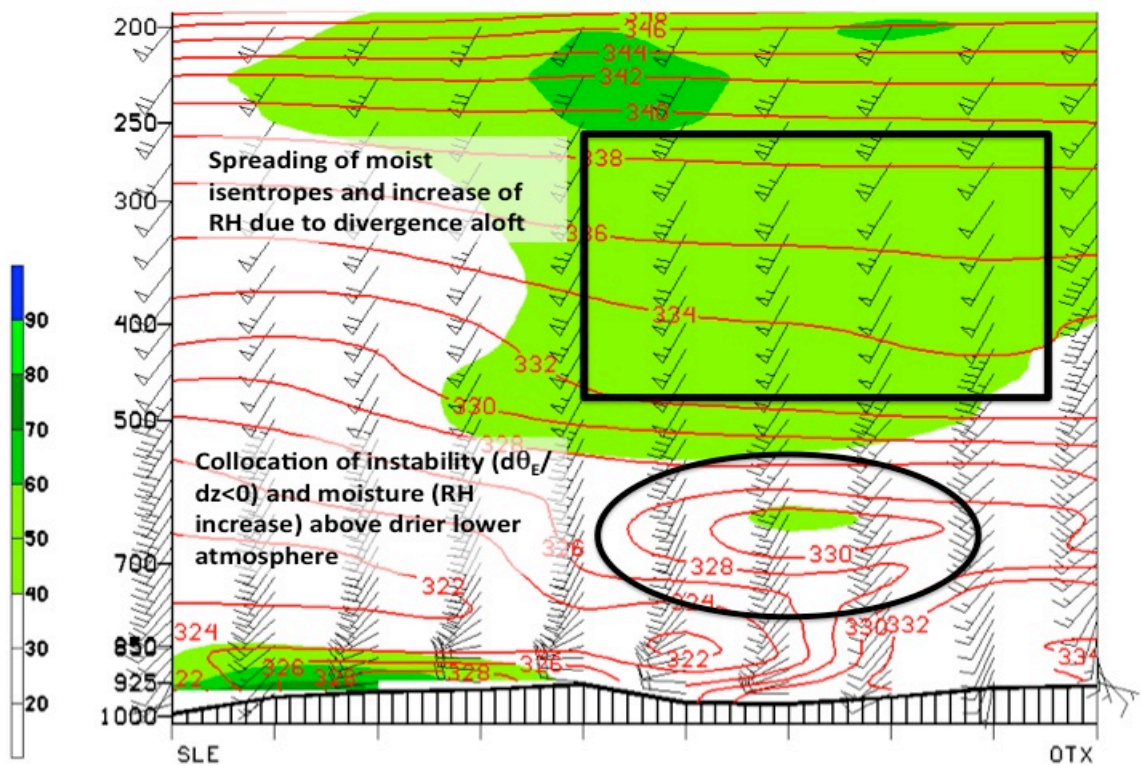
Figure 19: Plot of vertical cross-section of RH (filled, %) and θ_E (contoured, K) from SLE to OTX. Denotes important features (collocated instability & moisture, drier lower levels & divergence) within the vertical view of the atmosphere.

An existing procedure (WA04) was improved upon and made more thorough by adding moist isentropic analysis and enhancing jet streak analysis. This led to an operational checklist that can be implemented by operational fire weather forecasters across the western United States (see DTP summary above). The six case studies examined show a consistency of the procedure, although more research of other cases over a longer time scale would help validate or at least improve the quality of the DTP. The DTP demonstrated that if implemented correctly, it could help fire managers prepare for dry lightning events and the multiple fires that follow.

While the DTP performed well in each one of the cases, improvements and further investigation is warranted. The creation of a moisture threshold in terms of mixing ratio or precipitable water could benefit forecasters. Also, another useful tool coming out of this research is the determination if the lower levels are dry enough to avoid wetting rains by estimating a threshold from the RH and mixing ratio values produced from the cross-section plots. Separate from atmospheric conditions, the status of the fuels potentially ignited by the dry lightning would also help quantify the magnitude of the event. More of these events occur regularly, but were less severe due to the wet fuels at the surface. Additionally, the validity of the DTP and the understanding of dry thunderstorms as a whole would be improved when forecast misses are examined when the DTP shows dry lightning, but dry lightning does not happen.

With the demonstrated ability of the DTP to forecast dry thunderstorm formation 48 hours in advance, these suggestions would only help improve the confidence in forecasting. With the improvements, the DTP could be employed out to 72 hours to determine if the forecasting skill would diminish. Two parts of the procedure that could suffer are HLTT and moist isentropic analysis due to their dependence on moisture. Moisture, especially in the observation sparse western United States and Pacific Ocean, can be hard to monitor and quantify. Due to both temporally and spatially sensitivity of instability and moisture, the DTP would not be a strong candidate to become a mid-range model, and even 72 hours could diminish the forecast skill. A more objective DTP that quantifies certain moisture and instability thresholds would improve the viability and increase the diversity of the DTP even across the varied regions of the western United States.

5. References

AirFire. The AirFire Team: Understanding weather and climate as they relate to forests and fire. http://www.airfire.org/. Last date accessed 14 October 2010.

Baughman, R. G., and D.M. Fuquay, 1970. Hail and Lightning Occurrence in Mountain Thunderstorms. *Journal of Applied Meteorology*, **9**, 657-660.

Bothwell, P. D., 2002a. Prediction of Cloud-to-Ground Lightning in the Western United States, Ph. D., University of Oklahoma, 178 pp.

Bothwell, P. D., 2005. Development of an Operational Statistical Scheme to Predict the Location and Intensity of Lightning. *85th Annual American Meteorological Meeting: Conference on Meteorological Applications of Lightning Data*, San Diego, CA, January 2005.

Bothwell, P. D., 2009. Development, Operational Use, and Evaluation of the Perfect Prog National Lightning Prediction System at the Storm Prediction Center. *89th Annual American Meteorological Meeting: 4th Conference on Meteorological Applications of Lightning Data*, Phoenix, AZ, January 2009.

Bright, D. R., Wandishin, M. S., Jewell, E. Ryan, and S. J. Weiss, 2004. A Physically Based Parameter for Lightning Prediction and its Calibration in Ensemble Forecasts. *85th Annual American Meteorological Meeting: Conference on Meteorological Applications of Lightning Data*, San Diego, CA, January 2005.

Crimmins, M. A., 2006. Synoptic Climatology of Extreme Fire-Weather Conditions Across the Southwest United States. *International Journal of Climatology,* **26**, 1001-1016.

Fuquay, D. M., R. G. Baugman, and D. J. Latham, 1979. A Model for Predicting Lightning Fire Ignition in Wildland Fuels. *USDA Forest Service Research Paper INT-217*, Intermountain Forest and Range Experiment Station, Ogden, UT 22 pp.

Fuquay, D. M., 1980. Lightning that Ignites Forest Fires. *Proc. Sixth Conference on Fire and Forest Meteorology*, Seattle, WA, Society of American Foresters, 119-112.

Fuquay, D. M., 1982. Positive Cloud-to-Ground Lightning in Summer Thunderstorms. *Journal of Geophysics Research*, **97**, 7131-7140.

Hamilton, D. W., Y.-L. Lin, R. P. Weglarz, and M. L. Kaplan, 1998. Jetlet Formation from Diabatic Forcing with Applications to the 1994 Palm Sunday Tornado Outbreak. *Monthly Weather Review*, **126**, 2061-2089.

Hirschberg, P. and J. M. Fristch, 1991. Tropopause Undulations and the Development of Extratropical Cyclones. Part I: Overview and Observations of a Cyclone Event. *Monthly Weather Review,* **119,** 496-517.

Hirschberg, P. and J. M. Fristch, 1991. Tropopause Undulations and the Development of Extratropical Cyclones. Part II: Diagnostic Analysis and Conceptual Model. *MWR,* **119,** 518-550.

Houze, R. A., Jr., 1993. Cloud Dynamics. Academic Press, 573 pp.

Kaplan, M. L., Y.-L. Lin, D. W. Hamilton, and R. A. Rozumalski, 1998. The Numerical Simulation of an Unbalanced Jetlet and Its Role in the Palm Sunday 1994 Tornado Outbreak in Alabama and Georgia. *Monthly Weather Review*, **126**, 2133-2165.

Kaplan, M. L., C. S. Adaniya, ., P. J. Marzette, K. C. King, S. J. Underwood, and J. M. Lewis, 2009. The Role of Upstream Midtropospheric Circulations in the Sierra Nevada Enabling Leeside (Spillover) Precipitation – Part II – A Secondary Atmospheric River Accompanying a Mid-level Jet. *Journal of Hydrometeorology,* **10**, 1327-1354.

MacGorman, D. R., and W. D. Rust, 1998. The Electrical Nature of Storms. Oxford University Press, 422 pp.

Meisner, B. N. and Coauthor, 1993. A Lightning Fire Ignition Assessment Model. *Proc. 12th Conference on Fire and Forest Meteorology*, Jekyll Island, GA, Society of American Foresters. 172-178.

Milne, R. M., 2004. A Modified Total Totals Index for Thunderstorm Potential over the Intermountain West. *WR Technical Attachment No. 04-04.*

Moore, J.T. COMET: Isentropic Analysis. http://www.meted.ucar.edu/isen_ana/navmenu0.htm. Last date accessed 28 November 2010.

Nauslar, N. J., J. Wallmann, and T. J. Brown, 2009. A Forecast Procedure for Dry Lightning Busts. *American Meteorological Society 8th Symposium on Fire and Forest Meteorology*, Kalispell, MT, October 2009.

NICC Predictive Services. Incident Management Situation Report. http://www.predictiveservices.nifc.gov/IMSR/2007/20070717IMSR.pdf. Last date accessed 19 November 2010.

NICC Predictive Services. Incident Management Situation Report. http://www.predictiveservices.nifc.gov/IMSR/2006/20060822IMSR.pdf. Last date accessed 19 November 2010.

NICC Predictive Services. Incident Management Situation Report. http://www.predictiveservices.nifc.gov/IMSR/2006/20060627IMSR.pdf. Last date accessed 19 November 2010.

Reap, R. M., 1985. Evaluation of Cloud-to-Ground Lightning Data from the Western United States for the 1983-1984 Summer Seasons. *Journal of Climate and Applied Meteorology*, **25**, 785-789.

Rorig, M. L. and S. A. Ferguson, 1999. Characteristics of Lightning and Wildland Fire Ignition in the Pacific Northwest. *Journal of Applied Meteorology*, **38**, 1565-1575.

Rorig, M. L. and S. A. Ferguson, 2002. The 2000 Fire Season: Lightning-Caused Fires. *Journal of Applied Meteorology*, **41,** 786-791.

Rorig, M. L., S. L. Mckay,, S. A. Ferguson, and P. Werth, 2007. Model-Generated Predictions of Dry Thunderstorm Potential. *Journal of Applied Meteorology and Climatology*, **46**, 605-614.

Staley, D. O., 1988. Baroclinic Instability and Isentropic Slope. *Journal of Atmospheric Science*, **45**, 3298-3304.

Staley, D. O., 1991. Baroclinic Instability in the Upper Troposphere. *Journal of Atmospheric Science*, **48**, 1133-1140.

Uccellini, L. W. and D. R. Johnson, 1979. The Coupling of Upper and Lower Tropospheric Jet Streaks and Implications for the Development of Severe Convective Storms. *Monthly Weather Review*, **107**, 682-703.

Wallace, J. M., and P. V. Hobbs, 2006. Atmospheric Science: An Introductory Survey 2nd Edition. San Diego, CA: Academic Press. 483 pp.

Wallmann, J., 2004. A Procedure for Forecasting Dry Thunderstorms in the Great Basin using the Dynamic Tropopause and Alternate Tools for Assessing Instability. *WR Technical Attachment No. 04-04. August 3, 2004.*

Wallmann, J., R. Milne, C. Smallcomb, and M. Mehle, 2010. Using the 21 June 2008 California Lightning Outbreak to Improve Dry Lightning Forecast Procedures. *Weather and Forecasting*, **25**, 1447-1462.

APPENDIX

Additional figures that provide support and enhance the understanding of the DTP for each case study.

Figure A1: Map of large fires on 25 June 2008 after the 20-21 June lightning bust. http://www.thedailygreen.com/environmental-news/latest/california-wildfires-47062602.

Figure A2: 25 June 2008 NASA Satellite Imagery of fire in northern California.
http://www.thedailygreen.com/environmental-news/latest/california-wildfires-47062602.

Case Study: 20-21 August 2009
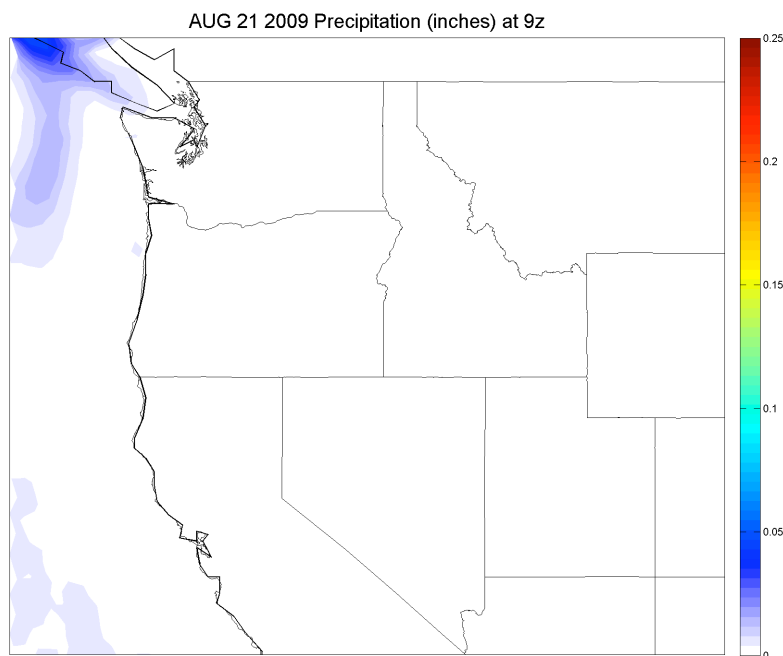
Figure A3: NARR precipitation (inches) from 06-09 UTC 21 August 2009.
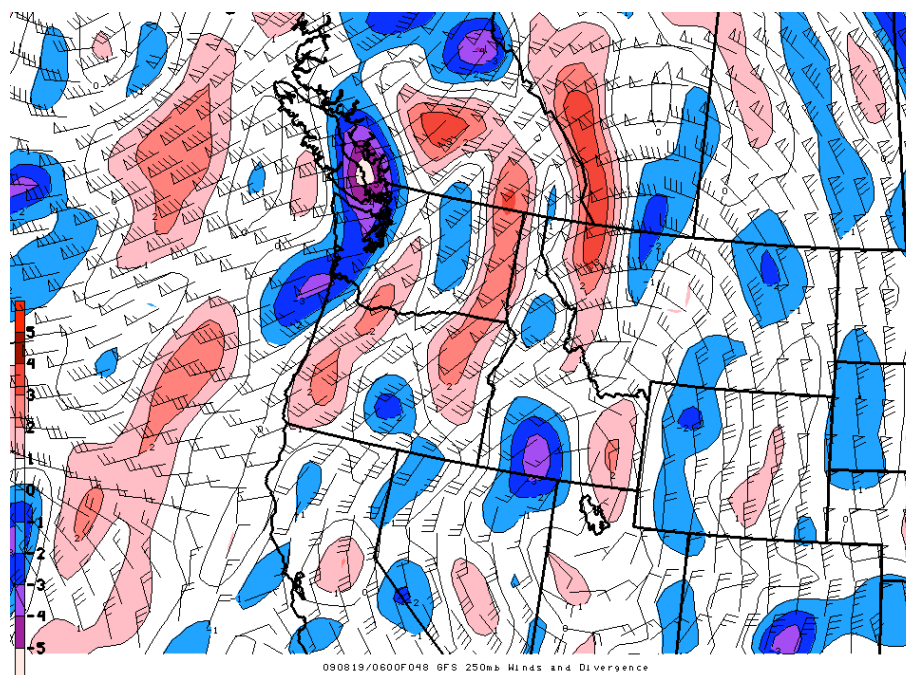
Figure A4: 06 UTC 19 August 2009 48-hour forecast plot of GFS 250 hPa Winds (knots) and Divergence (s^{-1} x 10^{-5}).
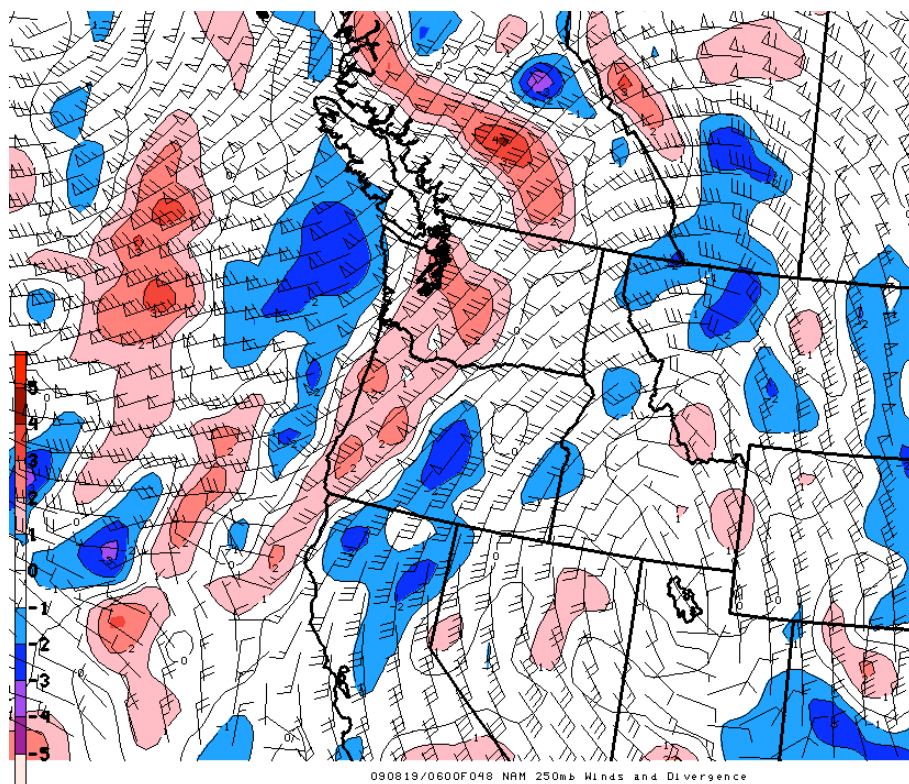
Figure A5: 06 UTC 19 August 2009 48-hour forecast plot of NAM 250 hPa Winds (knots) and Divergence (s^{-1} x 10^{-5}).
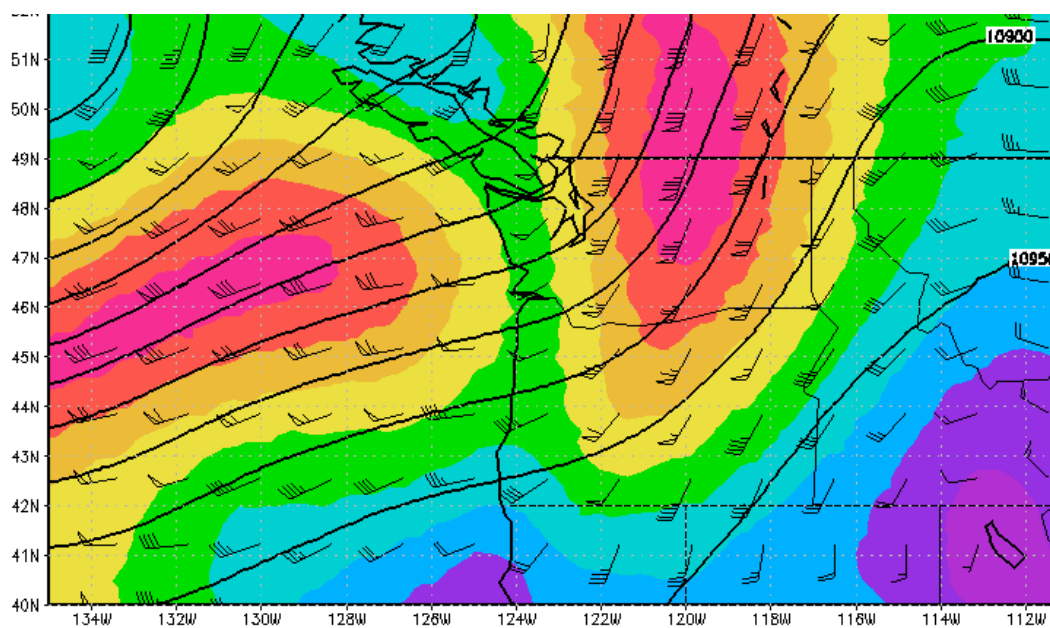
Figure A6: NARR 06 UTC 21 August 2009 250 hPa winds (barbs and filled, knots) and height (contoured, dm).
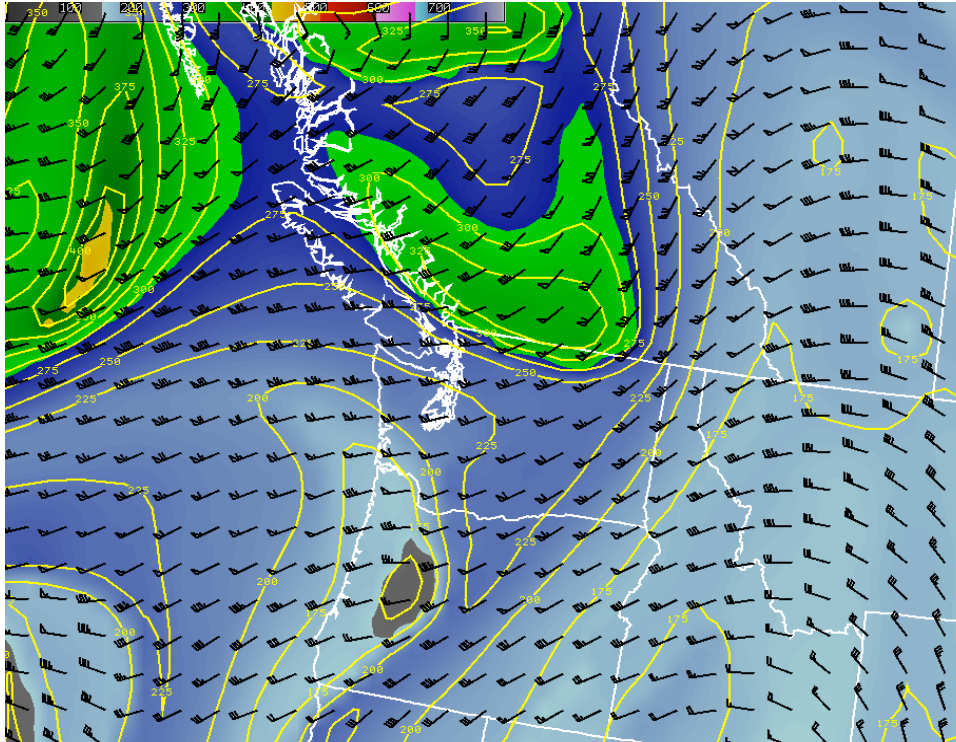
Figure A7: 00 UTC 20 August 2009 30-hour GFS forecast of dynamic tropopause pressure (contoured & filled, hPa) and winds (knots) plotted on 1.5 potential vorticity surface.
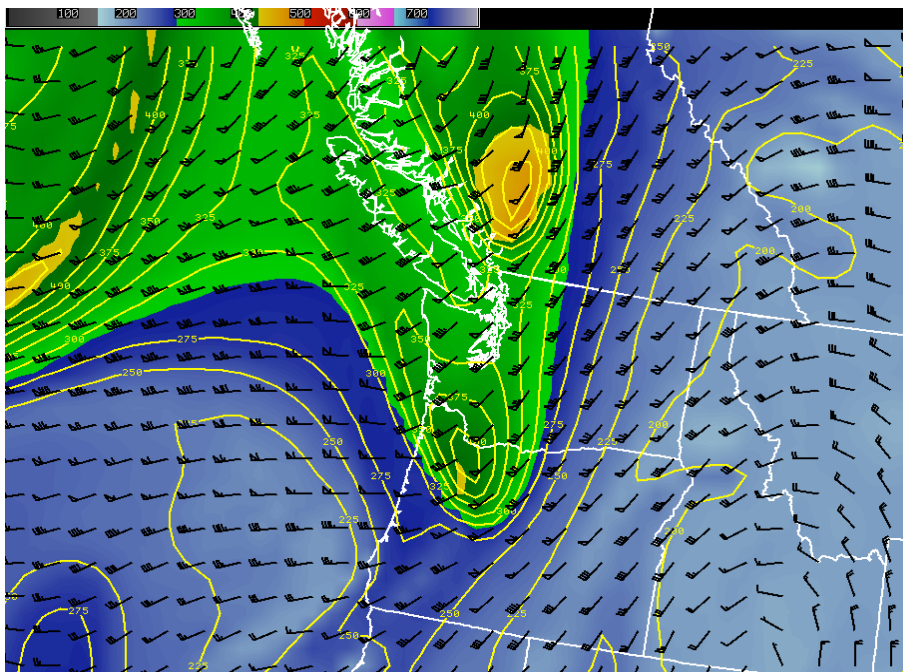

Figure A8: 00 UTC 20 August 2009 30-hour NAM forecast of dynamic tropopause pressure (contoured & filled, hPa) and winds (knots) plotted on 1.5 potential vorticity surface.
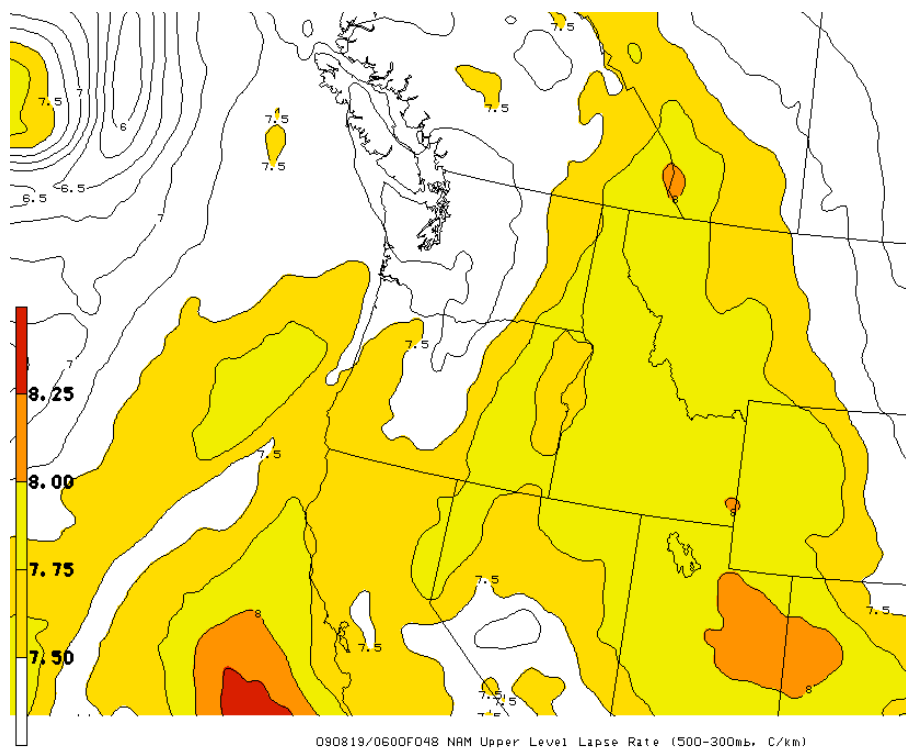
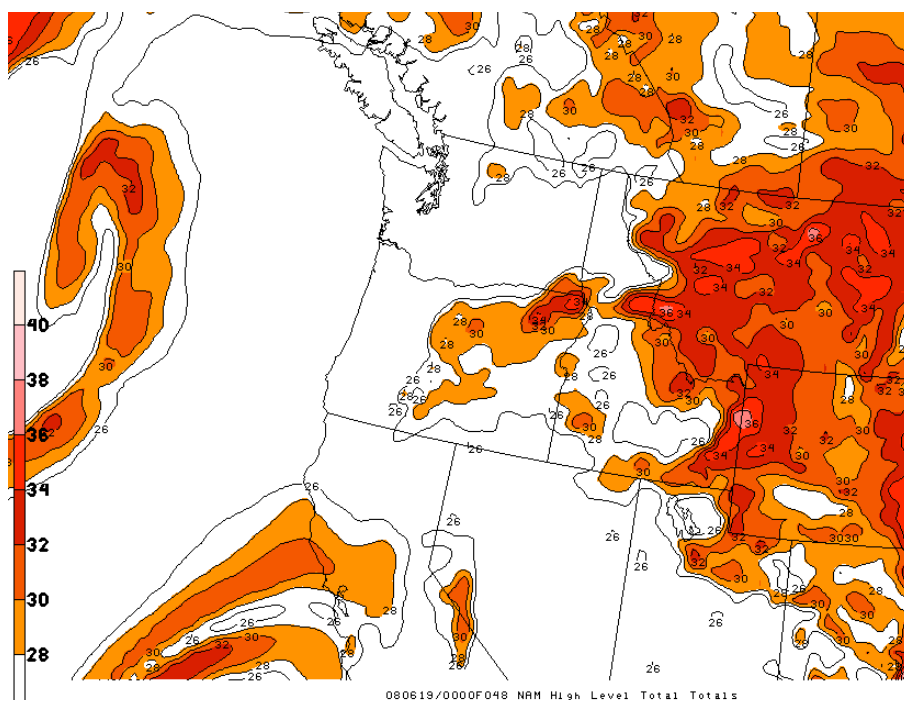Figure A9: 06 UTC 19 August 2009 48-hour NAM forecast of ULLR (contoured & filled, °C km^{-1}).
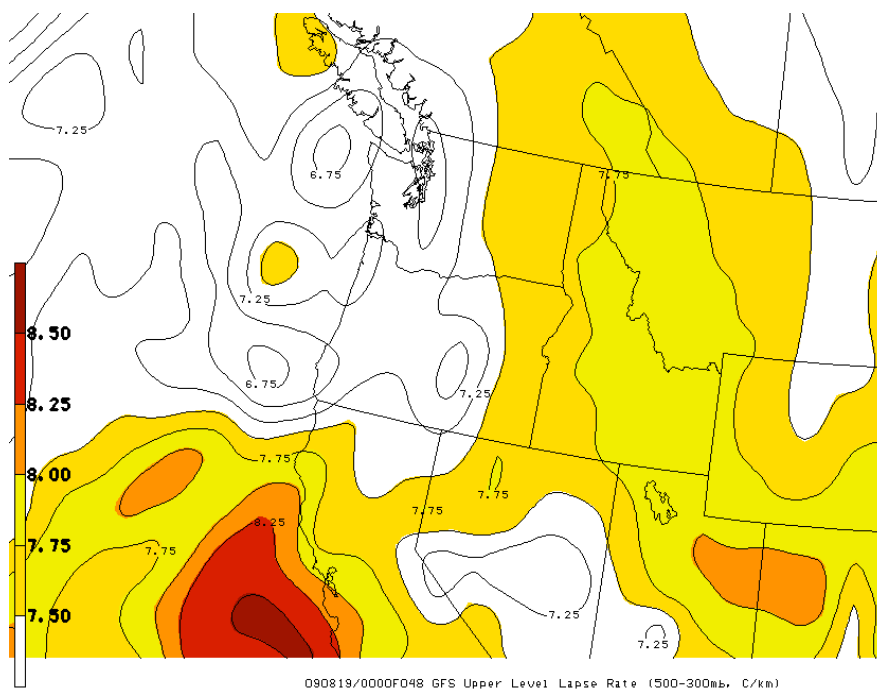
Figure A10: 06 UTC 19 August 2009 48-hour GFS forecast of ULLR (contoured & filled, °C km^{-1}).
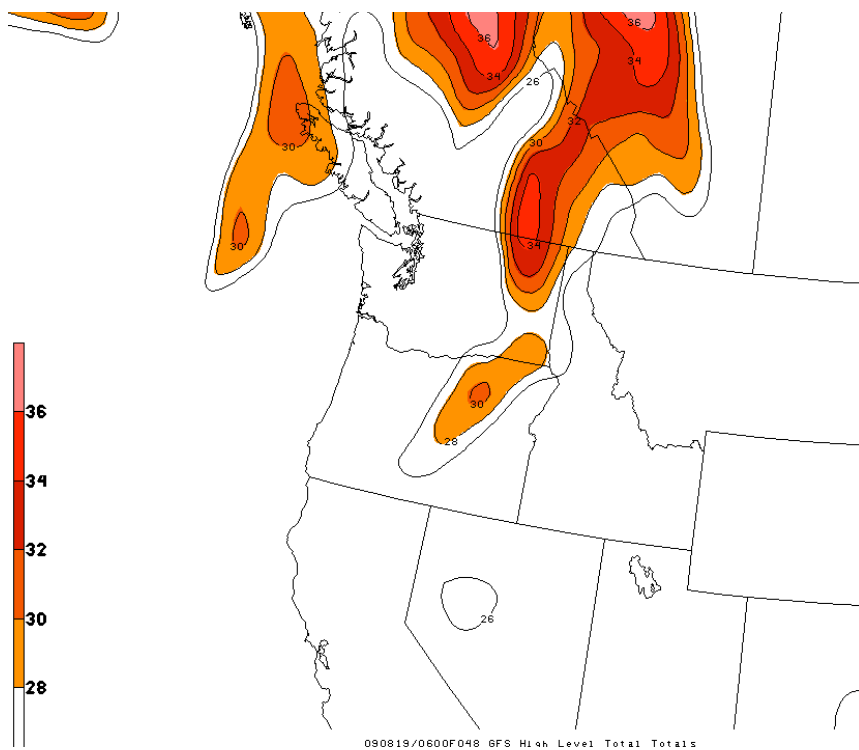
Figure A11: 06 UTC 19 August 2009 48-hour GFS forecast of HLTT (contoured & filled, °C).
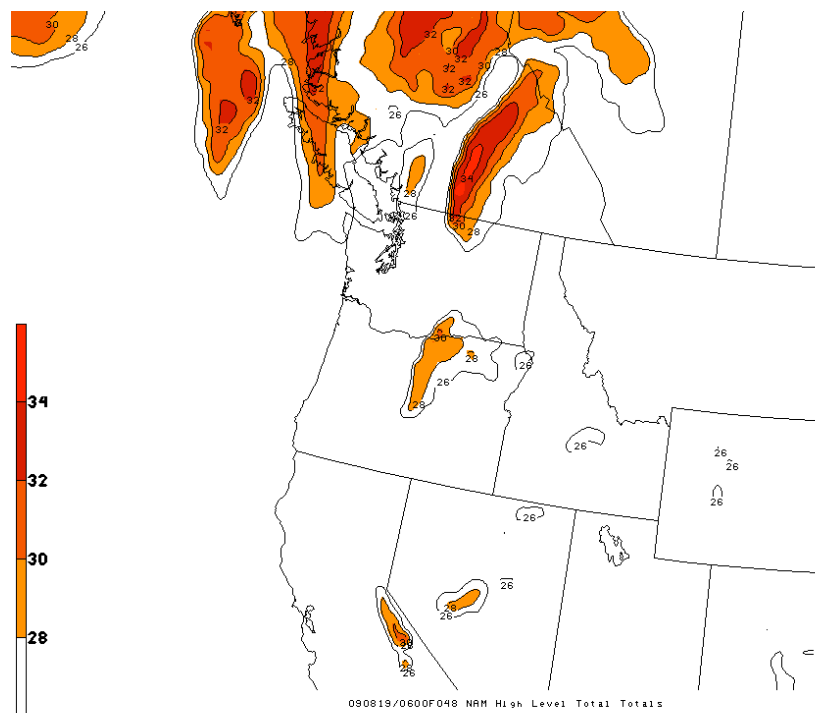
Figure A12: 06 UTC 19 August 2009 48-hour GFS forecast of HLTT (contoured & filled, °C).

Case Study: 1 August 2009
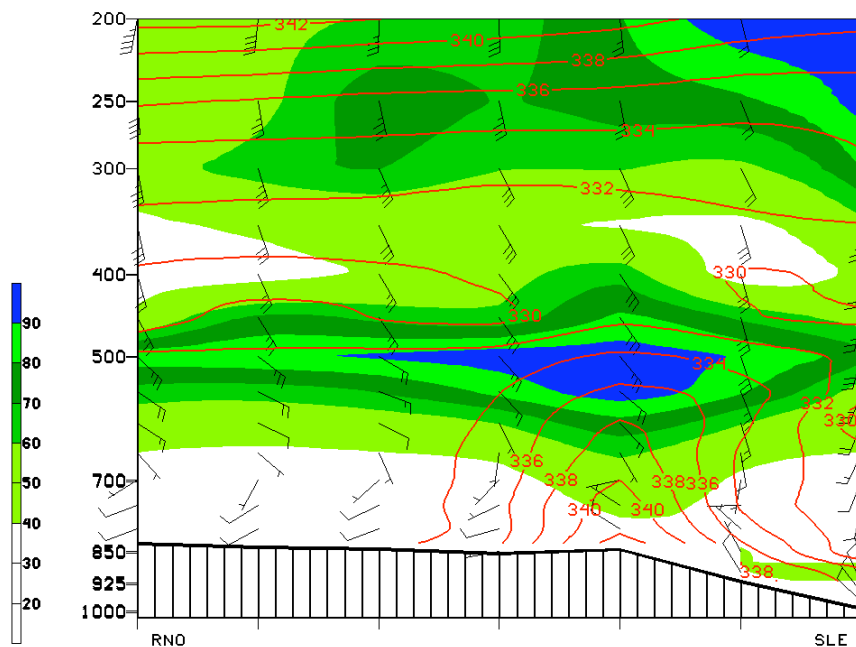
090731/0000F048 CROSS SECTION(RH(%),MIXING RATIO(G/KG) & WIND(KNOTS))

Figure A13: 00 UTC 31 July 2009 48-hour GFS forecast plot of vertical cross-section of RH (filled, %) and θ_E (contoured, K) from RNO to SLE.
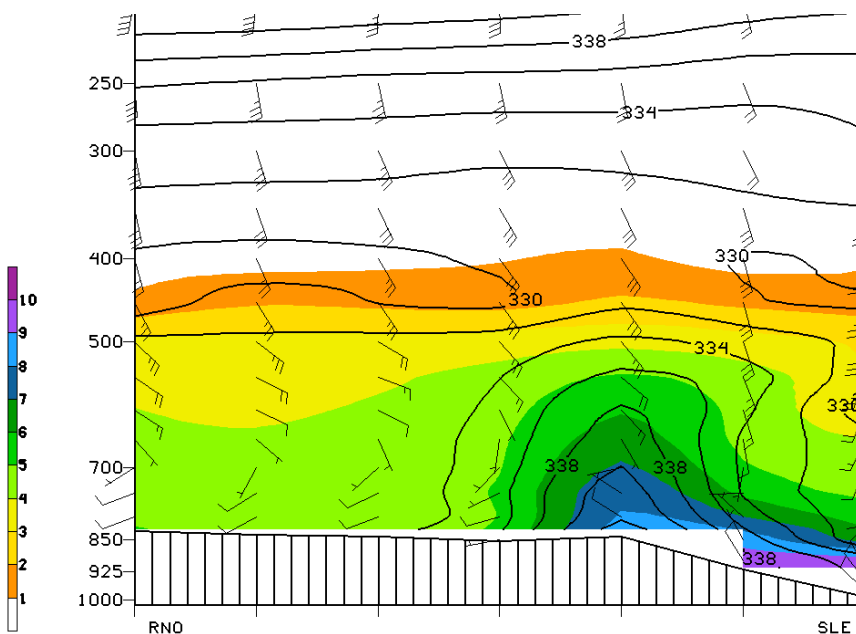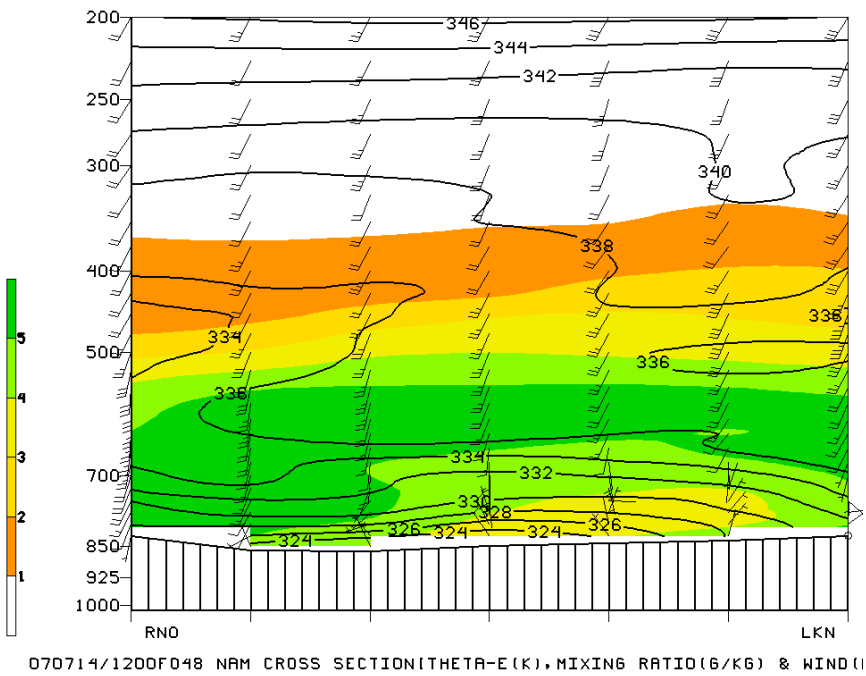

090731/0000F048 CROSS SECTION(THETA-E(K),MIXING RATIO(G/KG) & WIND(KNO

Figure A14: 00 UTC 31 July 2009 48-hour GFS forecast plot of vertical cross-section of mixing ratio (filled, g kg^{-1}) and θ_E (contoured, K) from RNO to SLE.
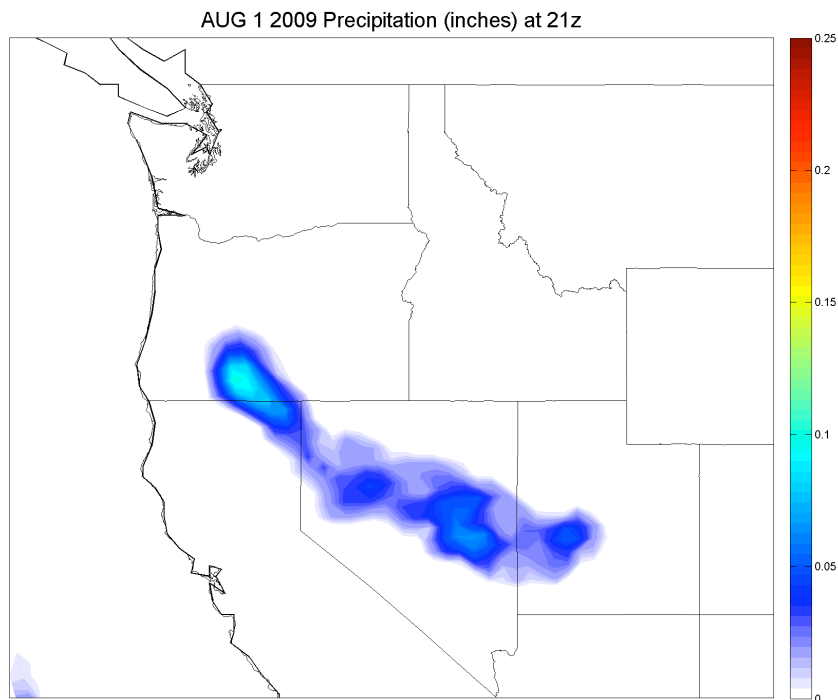
Figure A15: NARR precipitation (inches) from 18-21 UTC 1 August 2009.
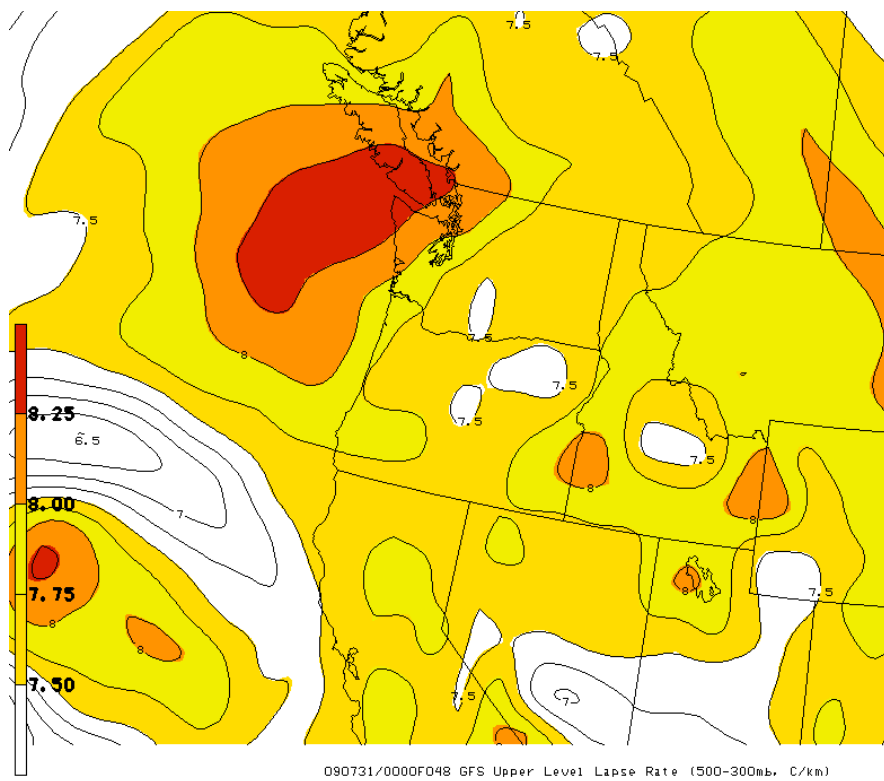
Figure A16: 00 UTC 31 July 2009 48-hour GFS forecast of ULLR (contoured & filled, °C km^{-1}).
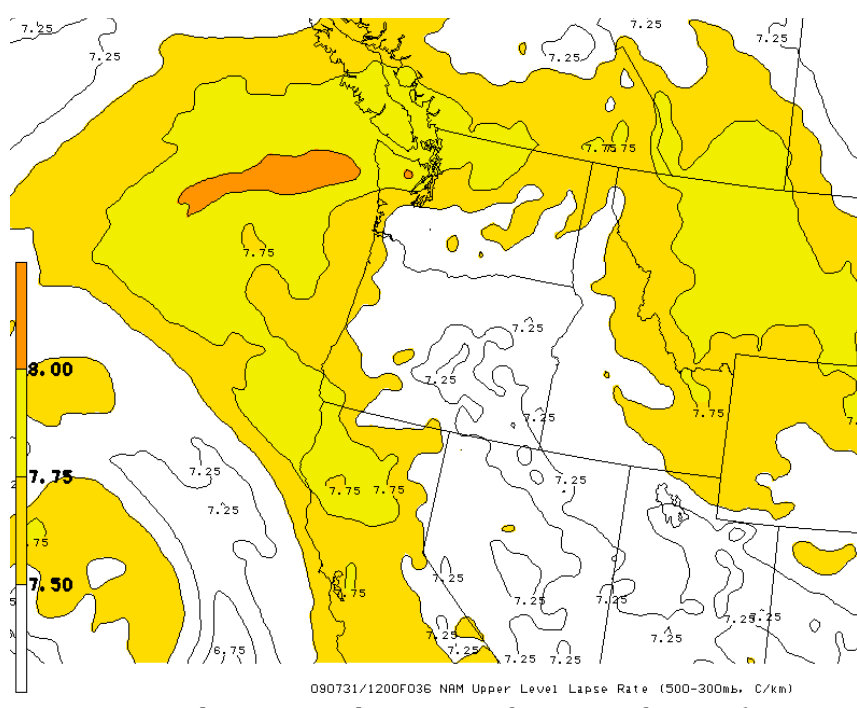
Figure A17: 12 UTC 31 July 2009 36-hour NAM forecast of ULLR (contoured & filled, °C km^{-1}).
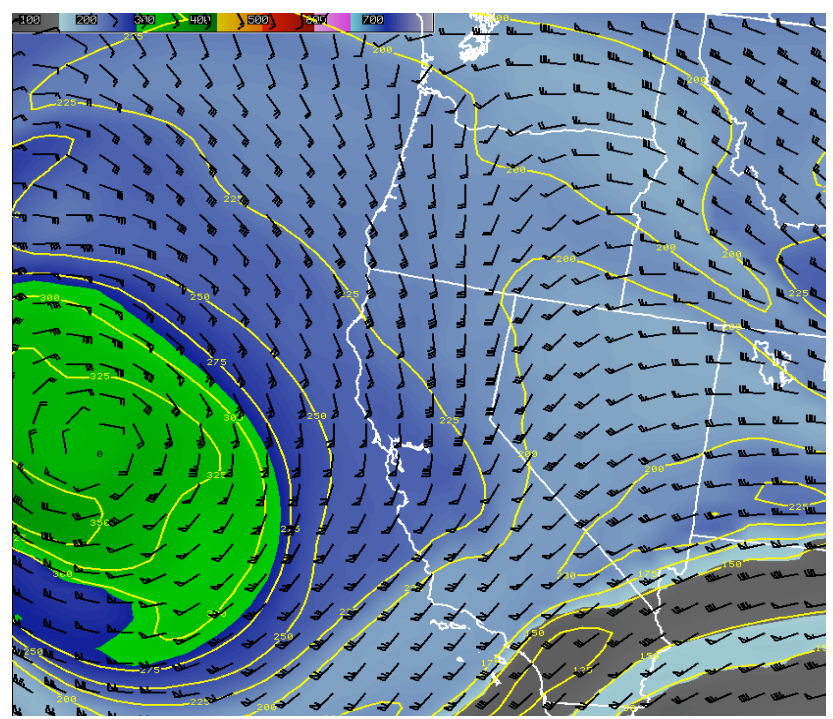

Figure A18: 00 UTC 31 July 2009 48-hour GFS forecast of dynamic tropopause pressure (contoured & filled, hPa) and winds (knots) plotted on 1.5 potential vorticity surface.
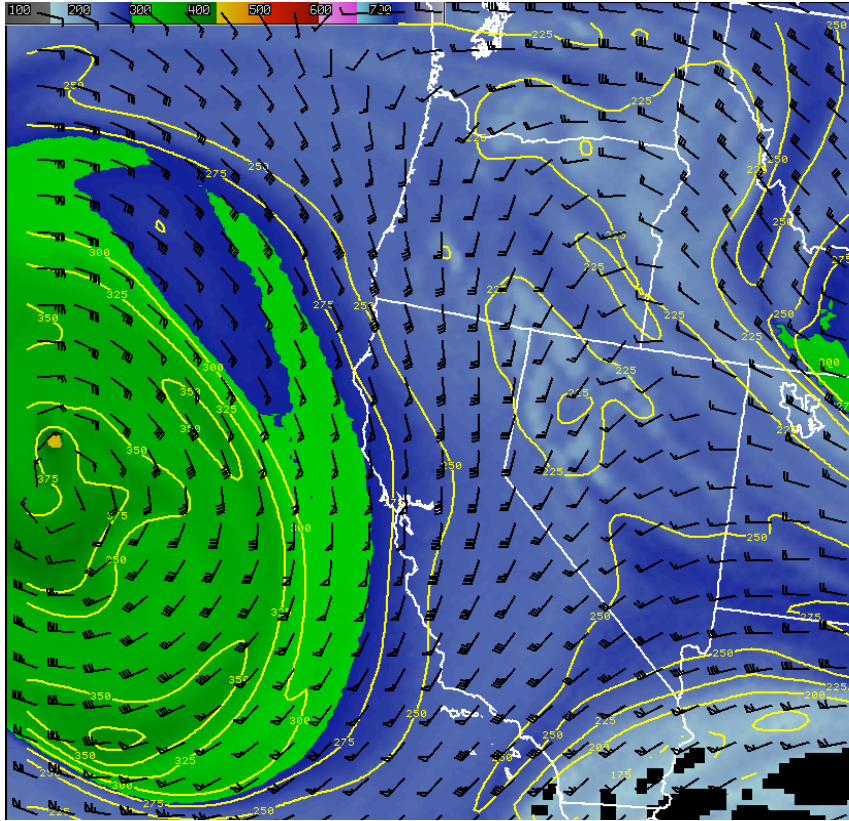
Figure A19: 00 UTC 31 July 2009 48-hour NAM forecast of dynamic tropopause pressure (contoured & filled, hPa) and winds (knots) plotted on 1.5 potential vorticity surface.

Case Study: 20-21 June 2008
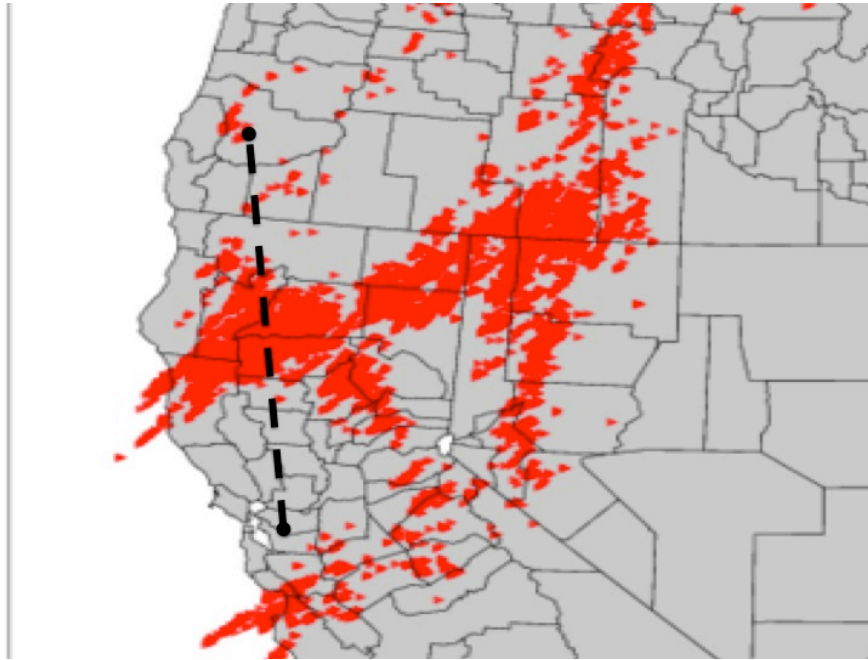
Figure A20: Lightning strike plot 12 UTC 21 June to 00 UTC 22 June 2008. Dotted Line: OAK-MFR cross-section.
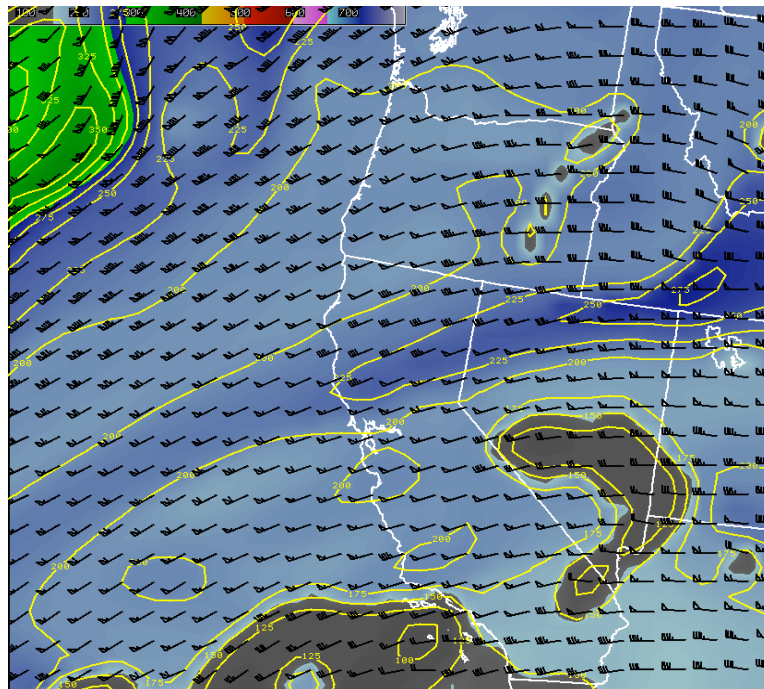
Figure A21: 00 UTC 19 June 2008 48-hour GFS forecast of dynamic tropopause pressure (contoured & filled, hPa) and winds (knots) plotted on 1.5 potential vorticity surface.
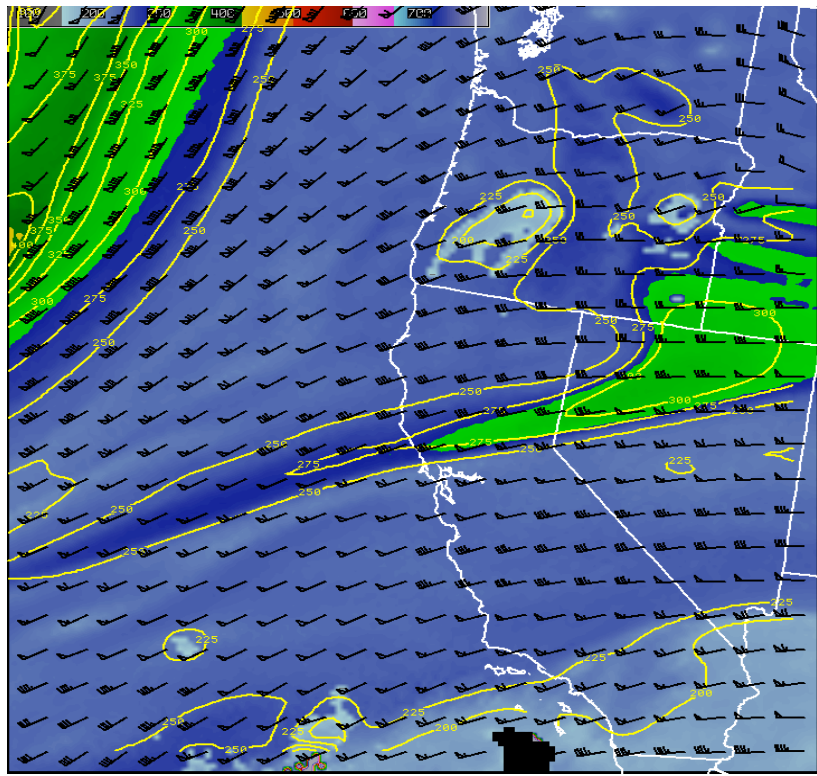
Figure A22: 00 UTC 19 June 2008 48-hour NAM forecast of dynamic tropopause pressure (contoured & filled, hPa) and winds (knots) plotted on 1.5 potential vorticity surface.
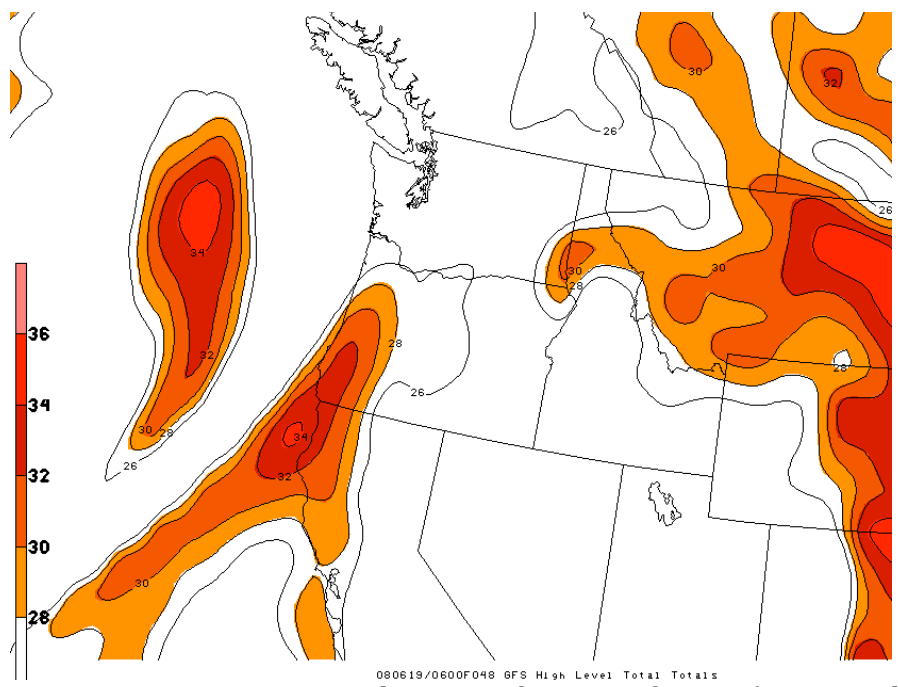
Figure A23: 06 UTC 19 June 2008 48-hour GFS forecast of HLTT (contoured & filled, °C).

Figure A24: 00 UTC 19 June 2008 48-hour NAM forecast of HLTT (contoured & filled, °C).
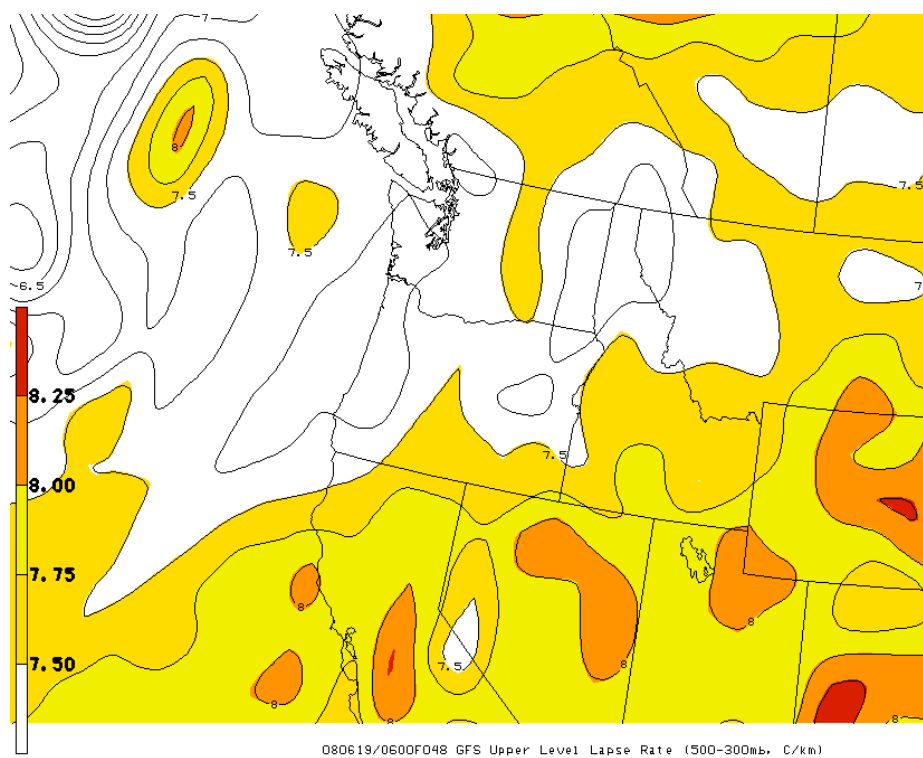
Figure A25: 06 UTC 19 June 2008 48-hour GFS forecast of ULLR (contoured & filled, °C km^{-1}).
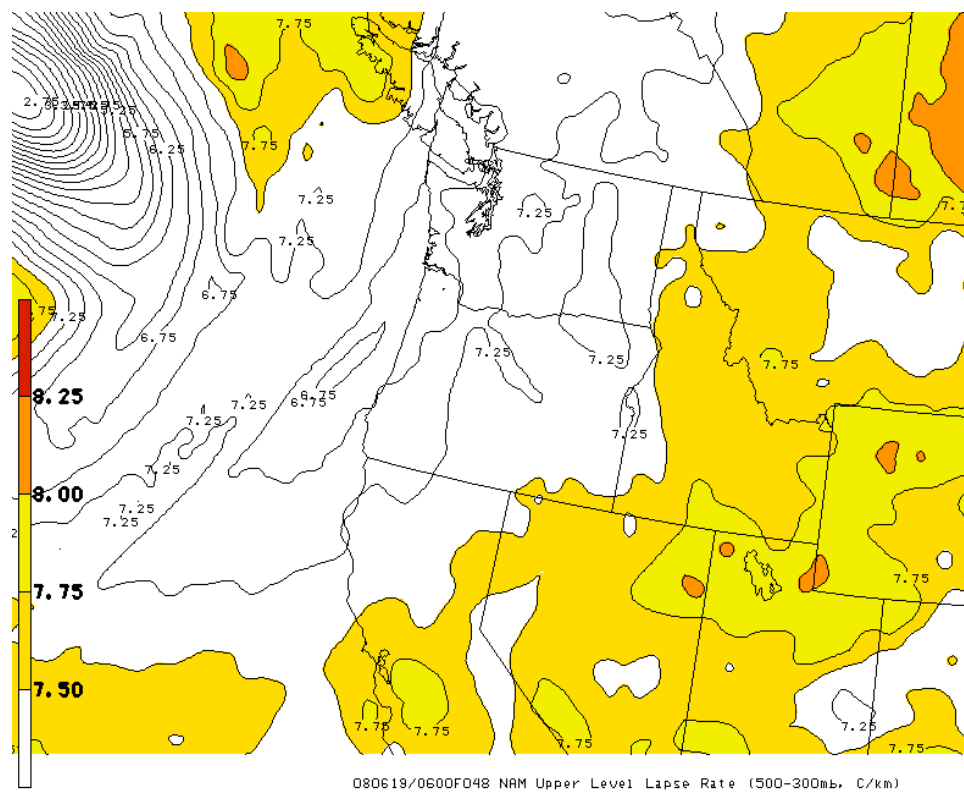
Figure A26: 06 UTC 19 June 2008 48-hour NAM forecast of ULLR (contoured & filled, °C km^{-1}).

Case Study: 16-17 July 2007

070714/1200F048 NAM CROSS SECTION[RH(%),THETA-E(K) & WIND(KNOTS)]
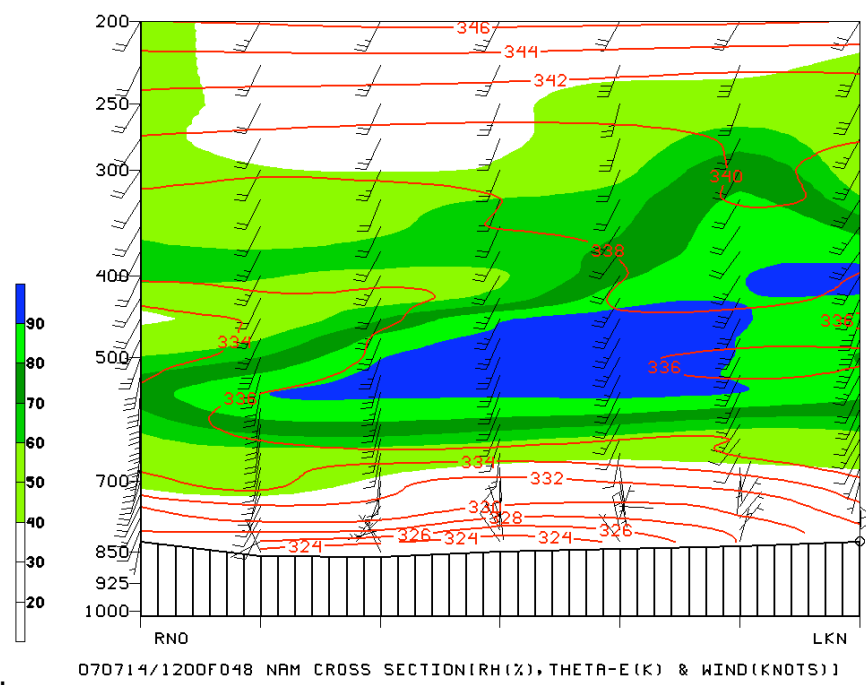
Figure A27: 12 UTC 14 July 2007 48-hour NAM forecast plot of vertical cross-section of RH (filled, %) and θ_E (contoured, K) from RNO to LKN.

070714/1200F048 NAM CROSS SECTION[THETA-E(K),MIXING RATIO(G/KG) & WIND(I

Figure A28: 12 UTC 14 July 2007 48-hour NAM forecast plot of vertical cross-section of mixing ratio (filled, g kg^{-1}) and θ_E (contoured, K) from RNO to LKN.
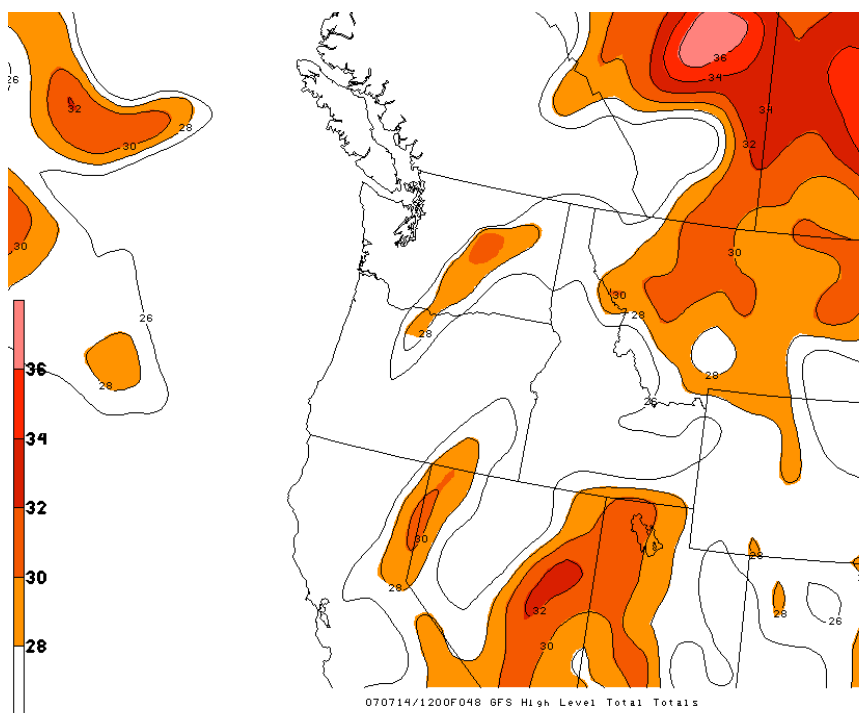
Figure A29: 12 UTC 14 July 2007 48-hour GFS forecast of HLTT (contoured & filled, °C).
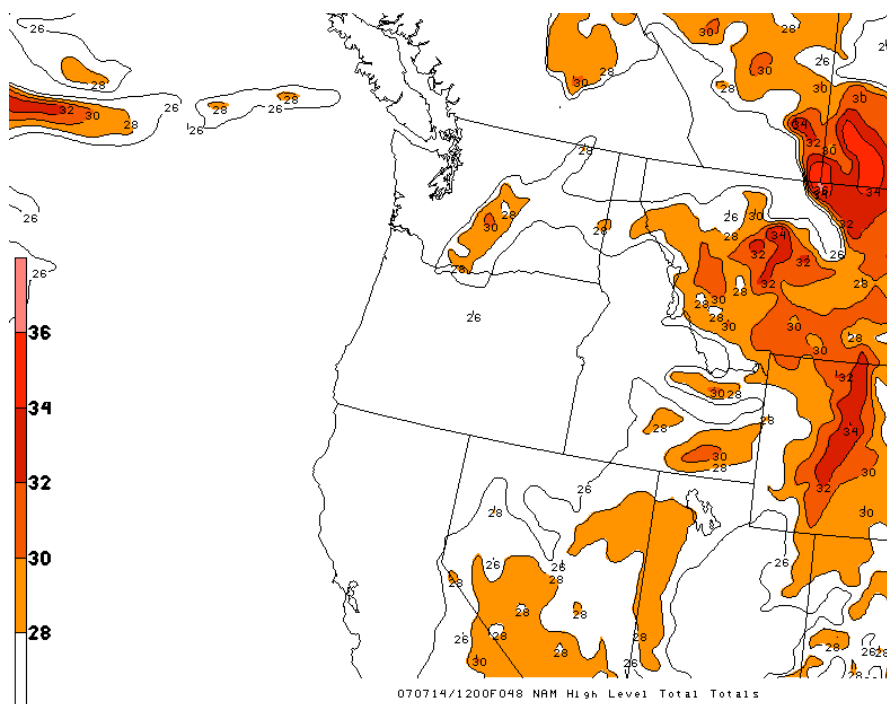
Figure A30: 12 UTC 14 July 2007 48-hour NAM forecast of HLTT (contoured & filled, °C).
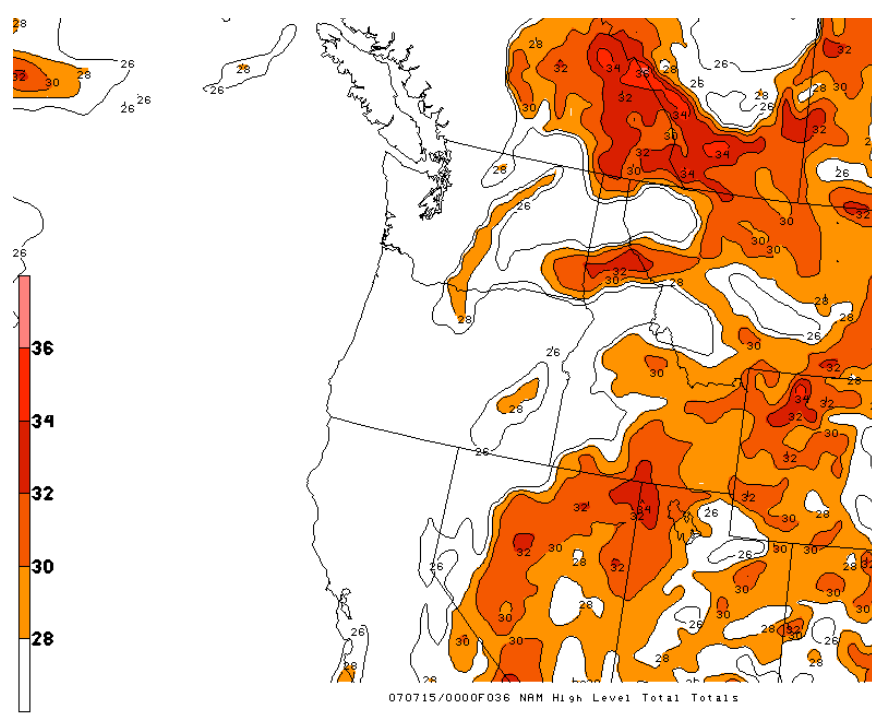
Figure A31: 12 UTC 14 July 2007 36-hour NAM forecast of HLTT (contoured & filled, °C).
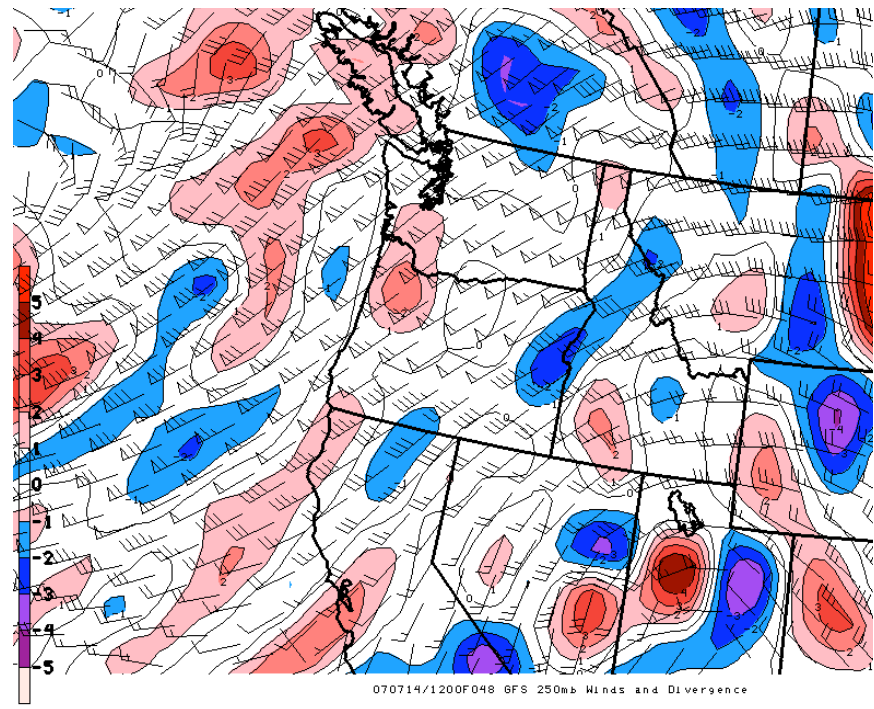
Figure A32: 12 UTC 14 July 2007 48-hour forecast plot of GFS 250 hPa Winds (knots) and Divergence (s^{-1} x 10^{-5}).
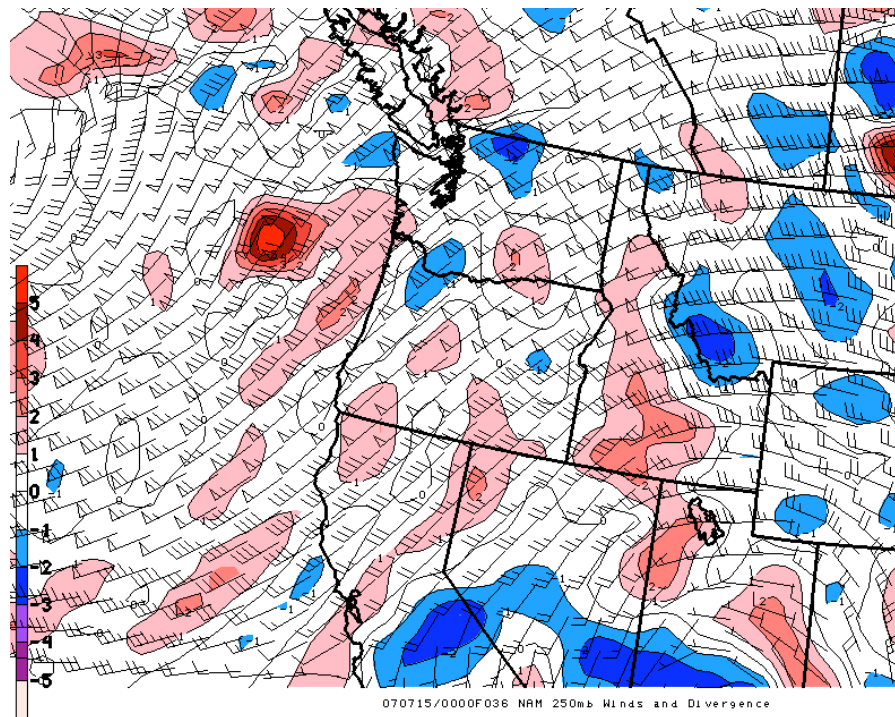
Figure A33: 12 UTC 14 July 2007 36-hour forecast plot of NAM 250 hPa Winds (knots) and Divergence (s^{-1} x 10^{-5}).
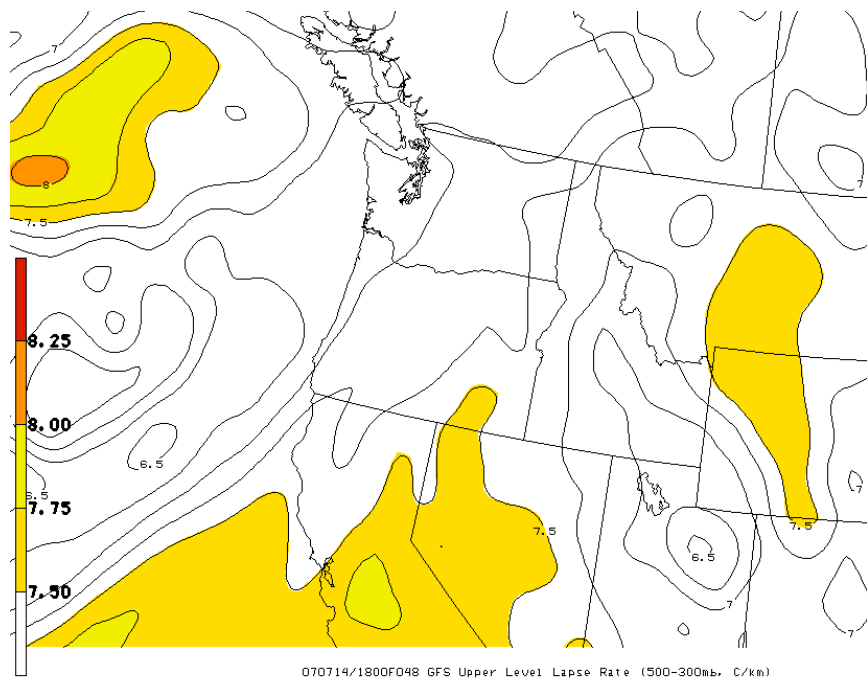
Figure A34: 18 UTC 14 July 2007 48-hour GFS forecast of ULLR (contoured & filled, °C km^{-1}).

Case Study: 20-22 August 2006
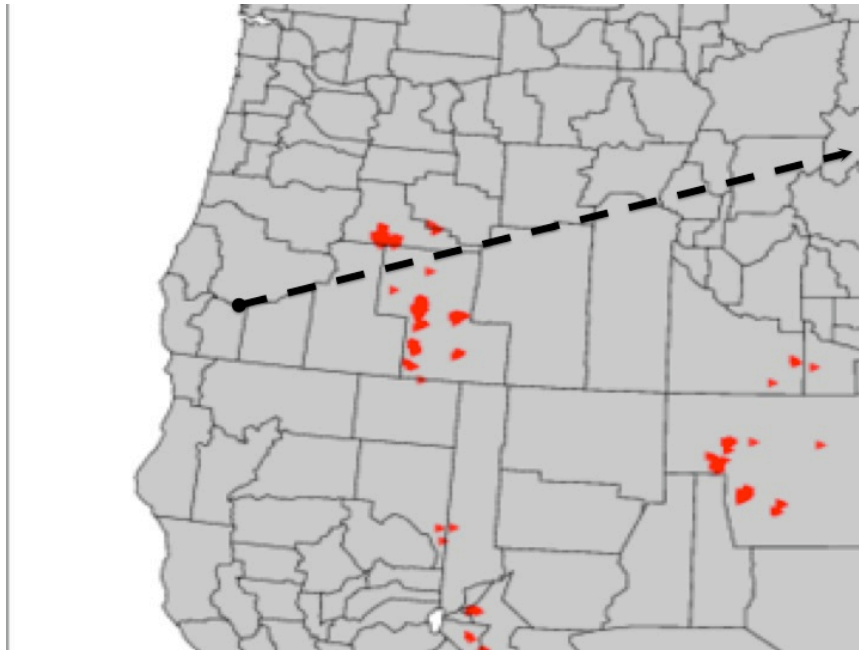
Figure A35: Lightning strike plot 00-12 UTC 21 August 2006. Dotted line: MFR-TFX cross-section.
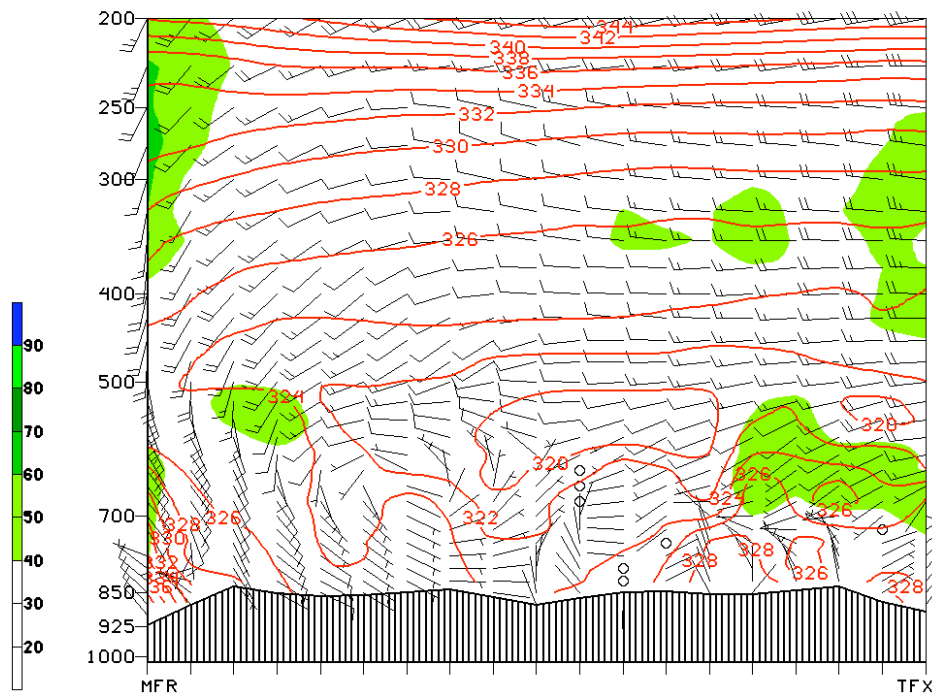
060819/0000F048 NAM CROSS SECTION(RH(%),THETA-E(K) & WIND(KNOTS))

Figure A36: 00 UTC 19 August 2006 48-hour NAM forecast plot of vertical cross-section of RH (filled, %) and θ_E (contoured, K) from MFR to TFX.

Figure A37: 00 UTC 19 August 2006 48-hour NAM forecast plot of vertical cross-section of mixing ratio (filled, g kg^{-1}) and θ_E (contoured, K) from MFR to TFX.

Figure A38: 00 UTC 19 August 2006 48-hour GFS forecast of HLTT (contoured & filled, °C).
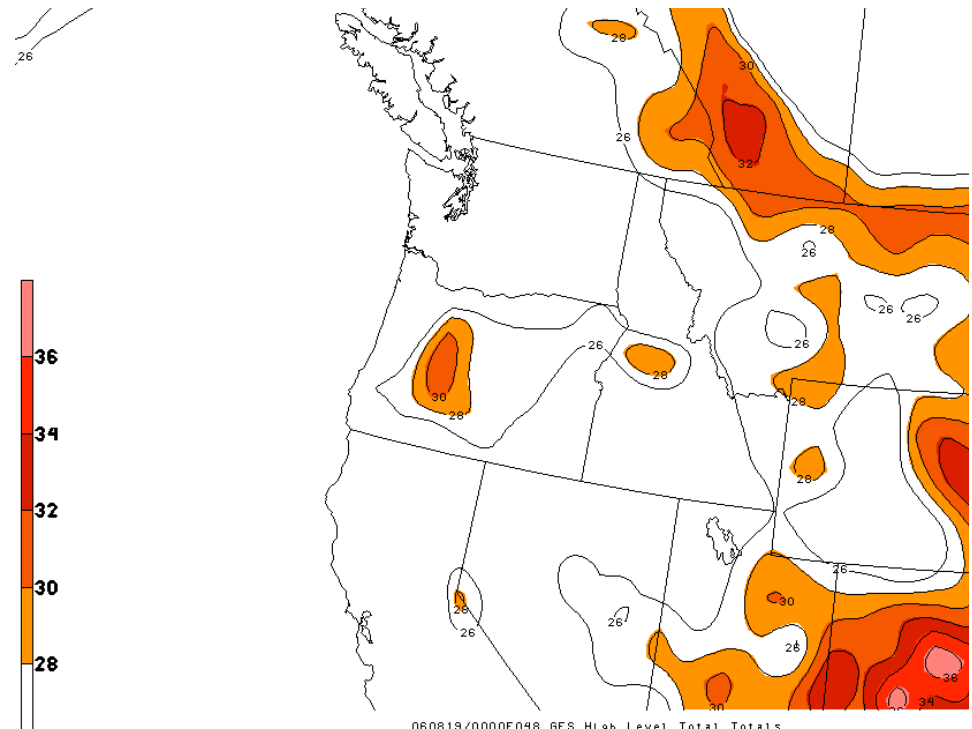
060819/0000F048 NAM High Level Total Totals
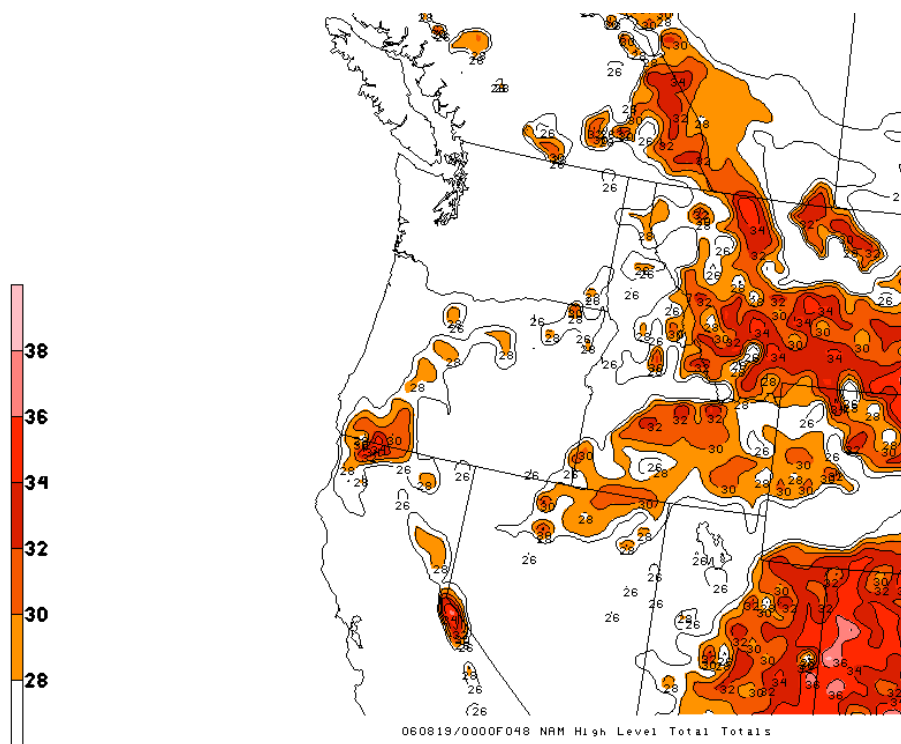
Figure A39: 00 UTC 19 August 2006 48-hour NAM forecast of HLTT (contoured & filled, °C).

Case Study: 25-26 June 2006

060624/0000F048 NAM Upper Level Lapse Rate (500-300mb, C/km)
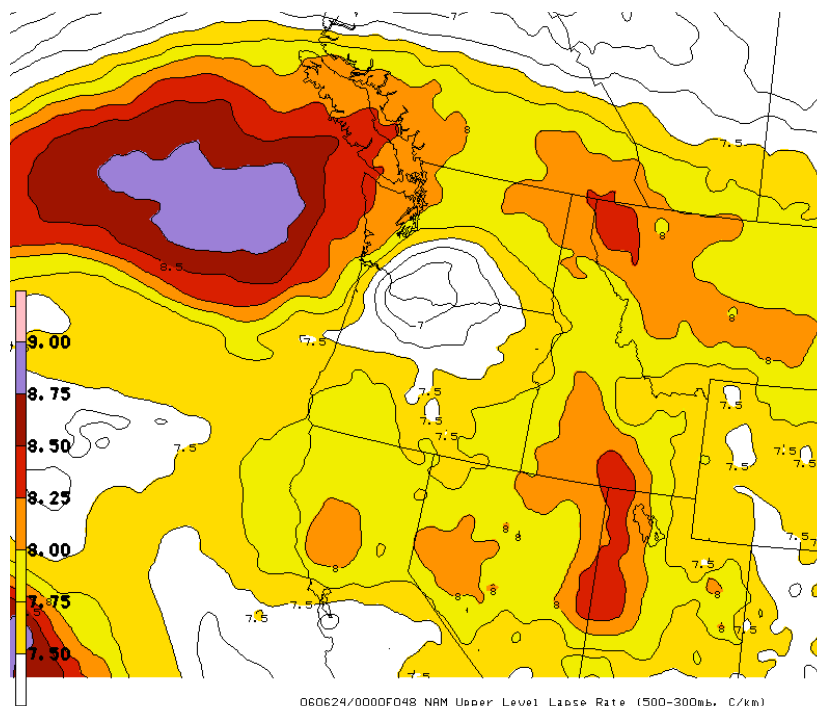
Figure A40: 00 UTC 24 June 2006 48-hour NAM forecast of ULLR (contoured & filled, °C km^{-1}).

060624/0000F048 GFS Upper Level Lapse Rate (500-300mb, C/km)
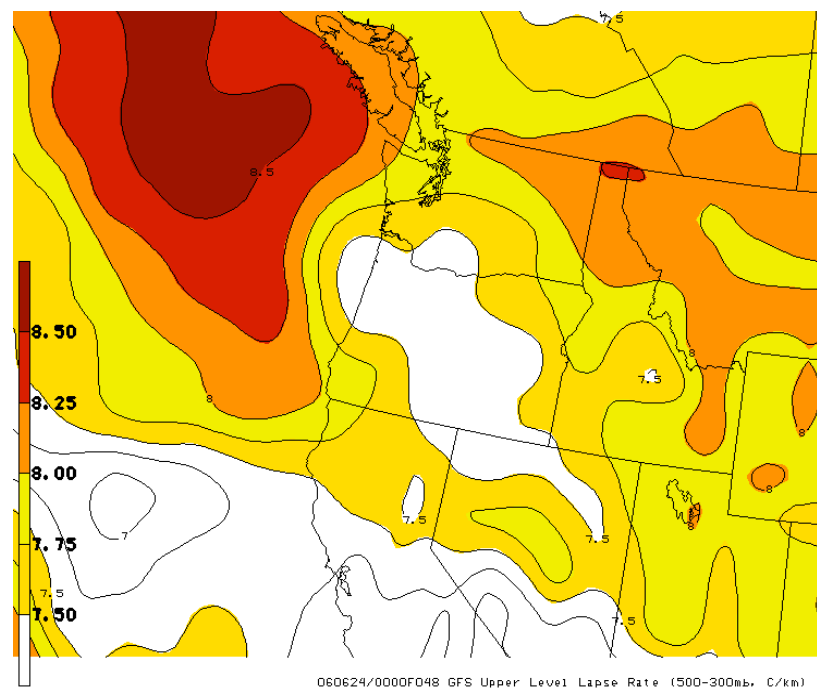
Figure A41: 00 UTC 24 June 2006 48-hour GFS forecast of ULLR (contoured & filled, °C km^{-1}).
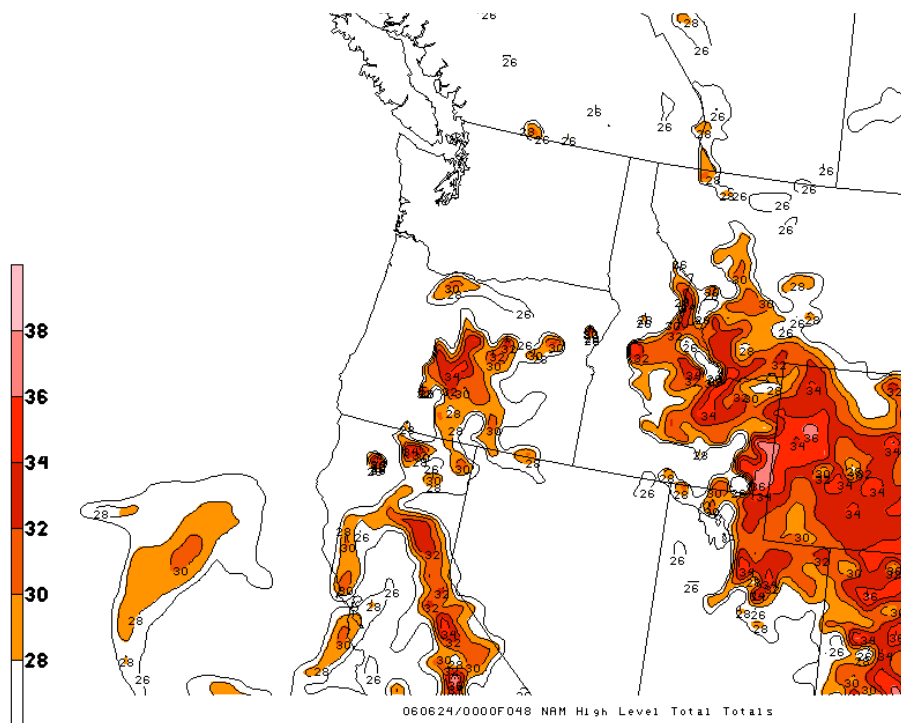
Figure A42: 00 UTC 24 June 2006 48-hour NAM forecast of HLTT (contoured & filled, °C).
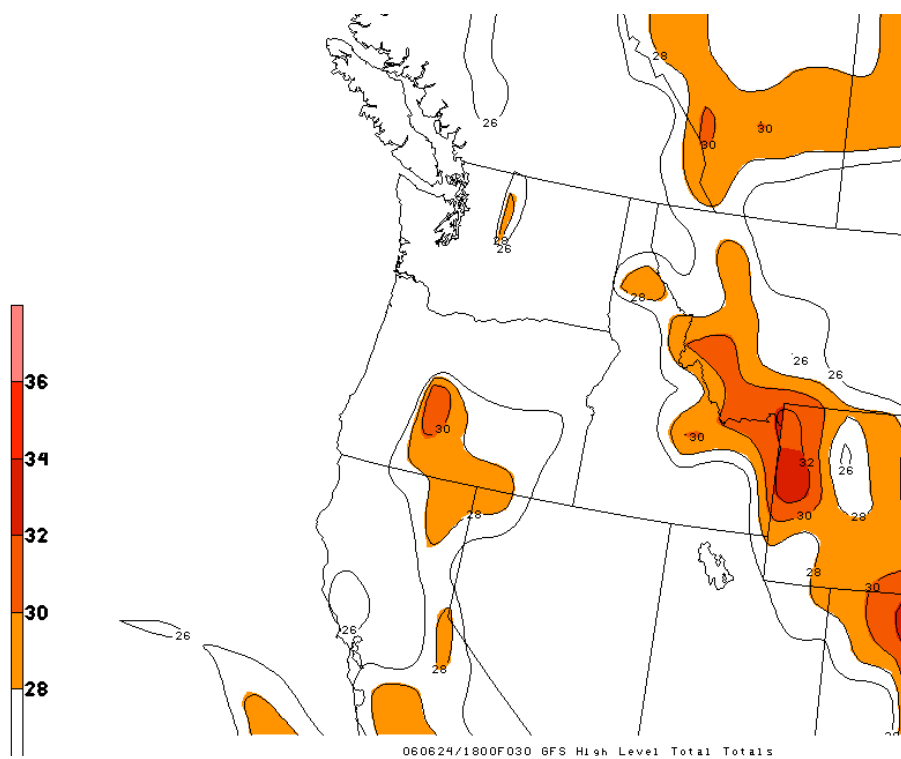

Figure A43: 18 UTC 24 August 2006 30-hour GFS forecast of HLTT (contoured & filled, °C).
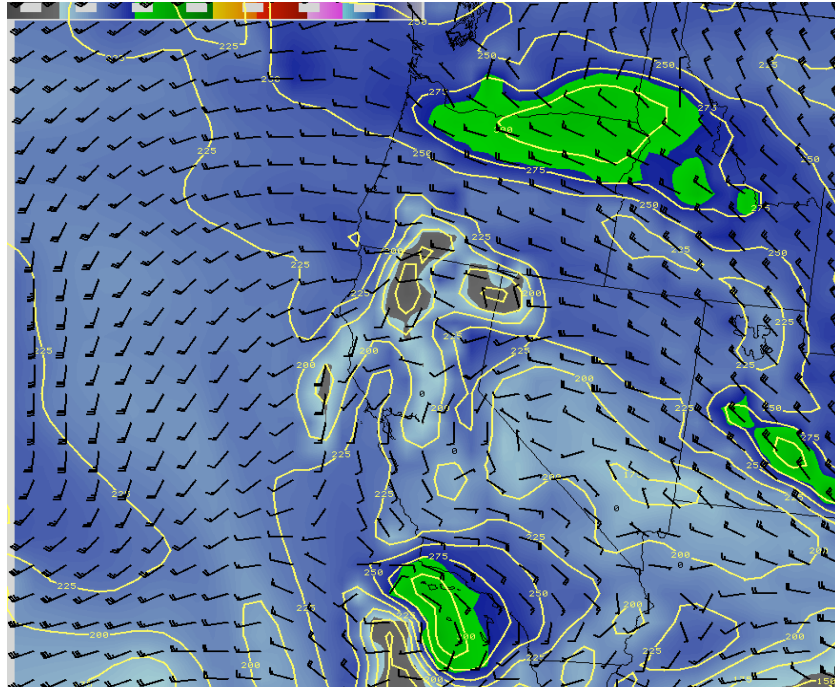
Figure A44: 00 UTC 24 June 2006 48-hour GFS forecast of dynamic tropopause pressure (contoured & filled, hPa) and winds (knots) plotted on 1.5 potential vorticity surface.
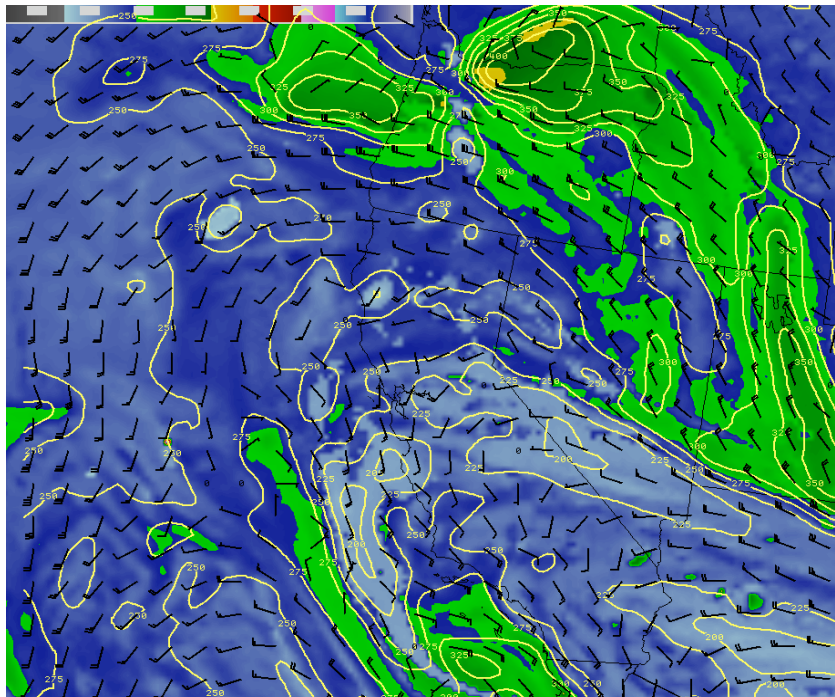

Figure A45: 00 UTC 24 June 2006 48-hour NAM forecast of dynamic tropopause pressure (contoured & filled, hPa) and winds (knots) plotted on 1.5 potential vorticity surface.